DOCTORAL (Ph.D.) DISSERTATION

REMOVAL OF PHARMACEUTICAL RESIDUE FROM WATER AND REAL WASTEWATER USING ACTIVATED CARBON DERIVED FROM AGRO-INDUSTRIAL WASTES

DOI:10.18136/PE.2025.931

Written by:
Osamah Jaber Oudah Al-Sareji
MEngSc UNSW, Sydney in Environmental Engineering

Supervisors:
Dr. Mónika Meiczinger & Dr. Viola Somogyi
Sustainability Solutions Research Lab
Faculty of Engineering
University of Pannonia

Veszprém, Hungary
2025

REMOVAL OF PHARMACEUTICAL RESIDUE FROM WATER AND REAL WASTEWATER USING ACTIVATED CARBON DERIVED FROM AGRO-INDUSTRIAL WASTES

Thesis submitted for obtaining a Ph.D. degree in the Biochemical, Environmental and Chemical Engineering
Doctoral School of Chemical Engineering and Material Science

Faculty of Engineering
University of Pannonia

Written by: Osamah Jaber Oudah Al-Sareji

Supervisors: Dr. Mónika Meiczinger & Dr. Viola Somogyi

Propose acceptance (yes / no) ……. ……

Dr. Mónika Meiczinger Dr. Viola Somogyi
(Supervisors)

As reviewer, I propose acceptance of the thesis:

Name of Reviewer:

..... yes / no .....
(Reviewer)

Name of Reviewer:

..... yes / no .....
(Reviewer)

The PhD-candidate has achieved .....% at the public discussion.

Veszprém

.....
(Chairman of the Committee)

The grade of the PhD Diploma ..... (.....%)

Veszprém

.....
(Chairman of UDHC)

Publications related to this dissertation

1- Al-sareji, Osamah J., Ruqayah Ali Grmasha, Mónika Meiczinger, Raed A. Al-Juboori, Miklós Jakab, Adrienn Boros, Hasan Sh Majdi, Norbert Miskolczi, and Khalid S. Hashim. "A novel two stages chemical activation of pinewood waste for removing organic micropollutants from water and wastewater." Chemosphere 363 (2024): 142974. **D1, IF=8.1**

2- Al-sareji, Osamah J., Ruqayah Ali Grmasha, Mónika Meiczinger, Raed A. Al-Juboori, Viola Somogyi, Csilla Stenger-Kovács, and Khalid S. Hashim. "A sustainable and highly efficient fossil-free carbon from olive stones for emerging contaminants removal from different water matrices." Chemosphere 351 (2024): 141189. **D1, IF=8.8**

3- Al-sareji, Osamah J., Ruqayah Ali Grmasha, Mónika Meiczinger, Raed A. Al-Juboori, Viola Somogyi, and Khalid S. Hashim. "A Sustainable Banana Peel Activated Carbon for Removing Pharmaceutical Pollutants from Different Waters: Production, Characterization, and Application." Materials 17, no. 5 (2024): 1032. **Q2, IF=3.1**

Abstract

The widespread presence of pharmaceutical pollutants in water necessitates cost-effective removal methods. Activated carbon (AC) is an efficient adsorbent for contaminants, but its high cost limits industrial use. Thus, finding affordable precursors to produce competitive AC remains a persistent challenge. This thesis is dedicated to developing sustainable, cost-effective, and environmentally friendly adsorbents from agro-industrial wastes to remove pharmaceutical compounds from Milli-Q water, wastewater, and lake water. ACs derived from agro-industrial waste, specifically from olive stone waste (OSAC), banana peel (BPAC), and pinewood (FPWAC), were investigated. The application of these derived carbons was evaluated for the removal of pharmaceutical compounds such as diclofenac, ciprofloxacin, amoxicillin, and carbamazepine. Each AC was subjected to different chemical treatments to remove at least two pharmaceuticals as a mixture. The removal of pharmaceuticals was assessed in terms of long-term performance in real wastewater, lake water, and synthetic Milli-Q water. Optimal adsorption parameters, Langmuir and Freundlich isotherms, pseudo-first-order and pseudo-second-order kinetics, as well as desorption studies, were investigated. The raw wastes and ACs were analyzed using various analytical techniques, including FTIR, XRD, Boehm titration, SEM-EDS, S_{BET}, TGA, and pHpzc. The ACs demonstrated excellent performance in removing a mixture of pharmaceuticals from wastewater, lake water, and Milli-Q water, with OSAC and BPAC achieving over seven successful removal cycles, while FPWAC completed six cycles. OSAC was effective across a broad pH range (2–11), efficiently removing diclofenac and ciprofloxacin in 75 minutes. In contrast, BPAC performed best at pH 5, while FPWAC showed optimal performance at pH 6, both requiring a longer saturation time of 120 minutes. The production costs for BPAC and FPWAC were $4.27/kg and $4.53/kg, respectively, due to high chemical input during activation. OSAC, with a lower cost of $3.77/kg, benefits from reduced chemical use, improving scalability, environmental impact, and procurement ease. Compared to commercial activated carbon priced at $135/kg, the synthesized ACs are 10 to 36 times more cost-effective, offering a highly economical alternative. The results demonstrate the potential of agro-industrial waste for removing organic micropollutants from complex water sources while promoting sustainable waste management.

Keywords: reusability; wastewater treatment; organic micropollutants; removal, waste.

الملخص

الوجود الواسع للملوثات الدوائية في المياه يستلزم تطوير طرق فعالة من حيث التكلفة لإزالتها. يُعد الكربون المنشط (AC) ممتصًا فعالًا للملوثات، لكن تكلفته العالية تحد من استخدامه الصناعي. لذا، يظل العثور على مواد أولية ميسورة التكلفة لإنتاج كربون منشط تنافسي تحديًا مستمرًا. تكرس هذه الأطروحة جهودها لتطوير مواد ممتصة مستدامة ومنخفضة التكلفة وصديقة للبيئة، مشتقة من نفايات الصناعات الزراعية، لإزالة المركبات الدوائية من مياهMilli-Q ، ومياه الصرف الصحي، ومياه البحيرات. تم دراسة الكربون المنشط المستخلص من نفايات الصناعات الزراعية، وتحديدًا من نفايات نوى الزيتون(OSAC) ، وقشور الموز(BPAC) ، وخشب الصنوبر .(FPWAC) تم تقييم تطبيق هذه المواد في إزالة المركبات الدوائية مثل ديكلوفيناك، وسيبروفلوكساسين، وأموكسيسيلين، وكاربامازيبين .خضعت كل من هذه الأنواع من الكربون المنشط لمعالجات كيميائية مختلفة لإزالة ما لا يقل عن دوائين كمزيج. تم تقييم إزالة الأدوية من حيث الأداء طويل الأمد في مياه الصرف الصحي الحقيقية، ومياه البحيرات، والمياه الاصطناعية Milli-Q .كما تم التحقيق في معايير الامتزاز المثلى، ونماذج لانجموير وفرويدليش، وحركيات التفاعل من الدرجة الأولى والثانية، بالإضافة إلى دراسات إزالة الامتزاز .تم تحليل النفايات الخام والكربونات المنشطة باستخدام تقنيات تحليلية متعددة، بما في ذلك مطيافية الأشعة تحت الحمراء(FTIR) ، وحيود الأشعة السينية(XRD) ، ومعايرة بوهيم، والمجهر الإلكتروني الماسح المزود بتحليل الطاقة المشتتة(SEM-EDS) ، ومساحة السطح(S_{BET}) ، والتحليل الحراري الوزني (TGA)، وقياس نقطة الشحن الصفرية (pHpzc) .

أظهرت الكربونات المنشطة أداءً ممتازًا في إزالة مزيج من المركبات الدوائية من مياه الصرف الصحي ومياه البحيرات ومياه Milli-Q، حيث حقق OSAC و BPACأكثر من سبع دورات إزالة ناجحة، بينما أكمل FPWAC ست دورات. كان OSAC فعالًا عبر نطاق واسع من الأس الهيدروجيني (2-11)، حيث أزال ديكلوفيناك وسيبروفلوكساسين بكفاءة خلال 75 دقيقة. في المقابل، كان BPAC الأفضل عند درجة حموضة 5، بينما أظهر FPWAC أداءً مثاليًا عند درجة حموضة 6، مع حاجة كل منهما إلى وقت إشباع أطول بلغ 120 دقيقة .بلغت تكاليف الإنتاج لـ BPAC و FPWACحوالي 4.27 دولار/كجم و4.53 دولار/كجم على التوالي، نظرًا للاستهلاك العالي للمواد الكيميائية أثناء عملية التنشيط. أماOSAC ، فكانت تكلفته أقل (3.77 دولار/كجم) بسبب انخفاض استهلاك المواد الكيميائية، مما يعزز من قابليته للتوسع وتقليل أثره البيئي وسهولة الحصول عليه. بالمقارنة مع الكربون المنشط التجاري الذي يبلغ سعره 135 دولارًا/كجم، فإن الكربون المنشط المصنع يُعد أكثر كفاءة من حيث التكلفة بمقدار 10 إلى 36 مرة، مما يجعله بديلاً اقتصاديًا للغاية .تظهر النتائج إمكانات نفايات الصناعات الزراعية في إزالة الملوثات العضوية الدقيقة من مصادر المياه المعقدة، مع تعزيز الإدارة المستدامة للنفايات.

الكلمات المفتاحية: إعادة الاستخدام؛ معالجة مياه الصرف الصحي؛ الملوثات العضوية الدقيقة؛ الإزالة؛ النفايات.

Table of Contents

List of Figures

List of Tables

List of abbreviations

ACs	Activated carbons
AMO	Amoxicillin
AOPs	Advanced oxidation processes
BP	Banana peels
BPAC	Activated carbon from banana peel
CBZ	Carbamazepine
CIP	Ciprofloxacin
DCF	Diclofenac
ECs	Emerging contaminants
EU	European Union
FAO	Food and Agriculture Organization
FPWAC	Final Pinewood Activated Carbon
FTIR	Fourier Transform Infrared Spectroscopy
HPLC	High-Performance Liquid Chromatography
MQ water	Milli-Q water
NSAID	Nonsteroidal anti-inflammatory medication
OSAC	Activated carbon from olive stone waste
OSW	Olive stone waste
PCs	Pharmaceutical compounds
PFO	Pseudo-first-order kinetic
pH_{PZC}	Point of zero charge
pKa	Acid dissociation constant
PSO	Pseudo-second-order kinetic
PW	Pinewood
S_{BET}	Specific surface area (m^2/g)
SEM-EDS	Scanning Electron Microscopy with Energy Dispersive X-ray analysis
TGA	Thermogravimetric Analysis
WFD	Water Framework Directive
XRD	X-ray Powder Diffraction

1. Introduction

Ensuring access to potable and uncontaminated water has emerged as a formidable challenge across various regions worldwide. The exponential growth of the global population, urbanization, agricultural activities, escalating industrialization, and advancements in technocratic societies, alongside geological, environmental, and overarching global shifts, collectively contribute to a gradual escalation in water pollution. Recently, the existence of hazardous substances such as micro-contaminants, endocrine-disrupting phthalate compounds, personal care products, pesticides, and inorganic anions has been identified at alarming concentrations in potable water sources globally [1]. Polluted water stands as a formidable quandary, posing significant hazards to both human well-being and the delicate interplay between humanity and the environment [2]. Consequently, various health afflictions in human populations have been documented because of water pollution [3].

On an industrial scale, advancements have been made in water and wastewater treatment technologies over recent years to combat the diverse array of aquatic pollutants. The spectrum of water purification techniques includes, but is not limited to, filtration, ultrafiltration, dialysis [4], reverse osmosis [5], solvent extraction [6], advanced oxidation [7], coagulation [8], microbial reduction [9], adsorption [10], biodegradation [11], and ion exchange [12]. Among them, adsorption stands as a well-established separation method with a rich history in scientific inquiry, recognized for its efficacy and ease of use in removing a diverse array of hazardous contaminants from both water and wastewater. It has a simple design, affordable initial investment, and convenient operations, along with the ability to selectively remove more toxic pollutants. Activated carbons (ACs) are carbonaceous substances distinguished by a substantial internal pore structure. ACs have large surface areas and exhibit macroscopic, mesoscopic, and microscopic pores. Additionally, they are enriched with different chemical functional groups on their surfaces, enabling them to be customized for a wide range of applications. Their extensive utility encompasses the elimination of odor, color, as well as other inorganic and organic impurities from industrial and municipal wastewater, solvent recovery processes, and air pollution control measures in urban areas [13]. The primary obstacles to the wider implementation of activated carbons in industrial environments are the high production costs and the unclear methodology involved in both production and regeneration procedures. Utilizing renewable resources, biomass, or waste high in carbon content to synthesize activated carbon is an option to solve these

constraints. Agricultural waste biomasses, with their carbon-rich chemical composition, are suitable candidates for synthesizing activated carbon [14].

The untreated and substantial quantities of agro-industrial waste pose a significant hazard in every nation, and the situation is worse annually [15]. Agro-industrial waste and effluents are typically released onto land or into aquatic systems. These possess have variable chemical properties and metal concentrations that may be detrimental to the environment. The uncontrolled incineration of agro-industrial waste emits toxic substances (nitrogen oxides, respirable particulate matter, sulfur dioxide,), carcinogens (polycyclic aromatic hydrocarbons, dioxins, furans), and greenhouse gases (methane, nitrous oxide), along with smoke, leading to considerable haze, global warming, and adverse effects on human health [16].Certain agro-industrial wastes, like those from pulp and paper mills and textile mills, contain harmful contaminants that can damage air, water, and soil [16]. Organic and inorganic substances found in waste from the pulp and paper sector have demonstrated detrimental impacts on aquatic ecosystems, including mutagenicity, carcinogenicity, and endocrine disruption [17]. Agro-industrial waste is typically nutrient-rich; but, if not properly managed, it may serve as a reservoir for pathogenic diseases [18], herbicide or pesticide residues, and detrimental fecal coliform bacteria [19]. The continual use of untreated wastes accumulates pesticide and herbicide residues in the soil, which can be detrimental to beneficial soil bacteria [20]. Runoff from nutrient-laden waste, including that generated by the fertilizer industry, poultry, and aquaculture, can trigger eutrophication, leading to extensive algal blooms and disruption of the aquatic ecology [16]. These pollutants can occasionally be water-soluble, contaminating drinking water and then entering the food chain, resulting in significant health issues in people, including Parkinson's disease, cancer, birth defects, Alzheimer's disease, and reproductive disorders [21].Antibiotic residues in animal-derived waste, including milk, meat, and eggs, adversely impact community health and food safety, contributing to carcinogenicity, drug toxicity, allergic reactions, and immunopathological disorders [22]. The keys to waste management and associated environmental issues lie in transforming waste into valuable products. Consequently, efficient disposal and economic utilization of agricultural waste not only reduces pollution but also promotes long-term sustainability.

1.1. Pharmaceuticals Occurrence in the Environment

In recent years, the concept of Emerging Contaminants (ECs) has garnered increasing environmental concern and attracted global public attention due to the presence of highly toxic pollutants in various environmental matrices [23], [24]. These ECs encompass a range of industrial chemicals, including pesticides, dyes, plasticizers, pharmaceuticals, endocrine disruptors, synthetic compounds, and hormones [25]. Characterized by their low biodegradability, ECs tend to persist for extended periods within different environmental compartments such as air, soil, and water, resulting in significant adverse effects on both ecosystem biodiversity and human health [26]. Among these media, aquatic environments are particularly susceptible to contamination from these pollutants. In 2000, the European Union (EU) introduced the "Water Framework Directive" (WFD) as a central legislative tool for safeguarding water quality across Europe. Its primary objective is to address surface water pollutants of significant concern at the EU level, designating them as priority substances, which includes a subgroup of priority hazardous substances, and fostering a comprehensive water management strategy [27]. In recent years, water contamination by pharmaceutical compounds (PCs) has emerged as a growing global issue, posing a significant challenge to contemporary scientific efforts [28]. These pollutants, classified as emerging contaminants, are commonly found in various aquatic systems, including wastewater and natural water bodies [24]. The principal sources of PCs in aquatic environments include inadequately treated effluents from pharmaceutical industries, healthcare facilities, and direct discharges from sewage treatment plants where treatment processes prove insufficient [29]. Additional sources of PCs contamination are municipal wastewater and veterinary practices (Figure 1) [24]. Specifically, the excretion of PCs and their metabolites by humans during therapeutic use, as well as by livestock, contributes to the contamination of surface waters, thereby disturbing aquatic ecosystems (Figure 1). Research indicates that PC concentrations in aquatic environments are typically found at ultra-trace levels, ranging from a few nanograms per liter to a few micrograms per liter [30]. Furthermore, transformation products and metabolites of PCs are noted for their high stability, allowing them to evade conventional treatment methods and ultimately reach drinking water supplies [31].

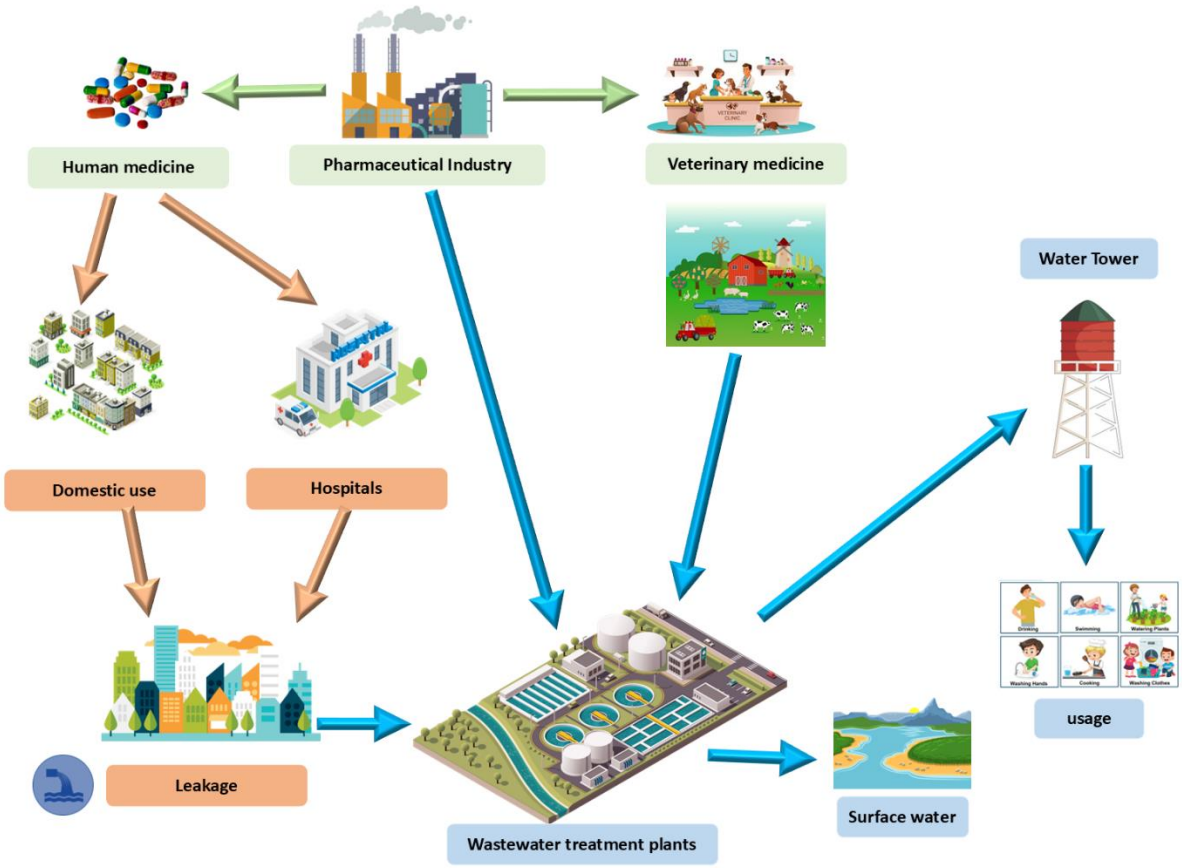

Figure 1 Schematic illustration of potential origins of waters contaminated with pharmaceuticals (redrawn from [24]).

1.2. Properties of Selected Pharmaceuticals

Pharmaceuticals were selected for this work due to their pervasive presence in aquatic environments globally and their significant environmental and public health implications [32]. Among the selected pharmaceuticals, amoxicillin and ciprofloxacin are prominently featured on the updated watch list of the European Water Framework Directive [33]. Moreover, the European Union recently issued a comprehensive directive addressing the management of urban wastewater [34]. The directive mandates that Member States ensure wastewater treatment facilities handling urban effluents with a capacity exceeding 150,000 population equivalent (PE) achieve compliance with specific pharmaceutical removal standards. The directive emphasizes that for compounds

such as carbamazepine and diclofenac, the minimum removal efficiency must reach at least 80% of the influent load prior to discharge into receiving water bodies.

1.2.1. Carbamazepine

Carbamazepine is extensively utilized for managing different seizure types and discomfort associated with trigeminal neuralgia [35]. It is utilized for the treatment of patients with acute mania, partial onset seizure epilepsy, restless legs syndrome, partial seizures with secondary generalization, generalized tonic alcohol withdrawal syndrome, and mixed manic-depressive episodes. It is classified as a dibenzazepine, characterized by a molecular structure in which two benzene rings are linked by an azepine ring. In addition, the molecular weight of carbamazepine is 236.269 g/mol. Carbamazepine is a white to off-white powdery substance. It has extremely low solubility in water, with reported solubility values in the literature ranging from 0.112 mg/L to 35 mg/L. This is an apolar molecule with an acid dissociation constant of pKa = 7.0. It does not undergo hydrolysis under environmental conditions. This chemical exhibit minimal solubility in ethanol and glacial acetic acid, although it is soluble in chloroform, dimethylformamide, methanol, and ethylene glycol monomethyl ether. It is presumed that carbamazepine blocks the voltage-dependent Na^+ channels in the membranes of nerve cells [35]. In instances of overdose, neuromuscular problems, minor cardiovascular issues, vomiting and respiratory depression may be observed [35].

1.2.2. Diclofenac

Diclofenac is a nonsteroidal anti-inflammatory medication (NSAID). It is utilized for the management of chronic and acute pain and inflammation. It possesses antipyretic, analgesic, and platelet-inhibitory properties [36]. It is also utilized to treat patients with inflammatory reactions, inflammatory diseases of the oral cavity or throat, acute musculoskeletal injuries, localized soft tissue rheumatism, postoperative inflammation, ocular inflammatory conditions, conjunctivitis, rheumatoid arthritis, acute gouty arthritis, and acute migraines. Diclofenac is a derivative of phenyl acetic acid. It is classified as a dichlorobenzene. The molecular weight of diclofenac is 296.148 g/mol and pKa of 4.0. It is marketed under various brand names including Diclofenaco, Diclofenacum, Orthophen, Ortofen, Feloran, Novapirina, Orthofen, Voltaren, and Voltarol. Overdose symptoms include vomiting, chest pain, respiratory depression, gastrointestinal bleeding, and, infrequently, hypertension and severe renal failure [37].

1.2.3. Ciprofloxacin

Ciprofloxacin is classified as a second-generation fluoroquinolone (FQ) antibiotic. It is a bactericidal antibiotic and one of the most extensively utilized fluoroquinolone antibiotics globally, with a solubility of 30 g/L. Ciprofloxacin was first commercially released in 1987 and has demonstrated extensive antibacterial efficacy [38]. The International Union of Pure and Applied Chemistry (IUPAC) designates the complete chemical name of ciprofloxacin as 1-cyclopropyl-6-fluoro-1,4-dihydro-4-oxo-7-(1-piperazinyl)-3-quinoline carboxylic acid. The molecular weight is 331.4 g/mol, and the empirical formula is $C_{17}H_{18}FN_3O_3$. The pKa values for ciprofloxacin are approximately 6.1 and 8.7. Ciprofloxacin functions as a broad-spectrum antibiotic for the treatment of Gram-negative and Gram-positive bacterial infections[38].

1.2.4. Amoxicillin

Amoxicillin is a commonly prescribed antibiotic belonging to the beta-lactam class, specifically the penicillin group, and has the molecular formula $C_{16}H_{19}N_3O_5S$. The molecular weight of amoxicillin is approximately 365.4 g/mol and the pKa values for amoxicillin are 2.4 and 7.4. It is a semi-synthetic derivative of penicillin, designed to offer broader antibacterial coverage and greater resistance to stomach acid, allowing it to be effective when taken orally. Amoxicillin works by inhibiting the bacterial enzyme transpeptidase, which is critical for synthesizing the bacterial cell wall. By disrupting the formation of peptidoglycan, a key structural component of the cell wall, it leads to bacterial cell lysis and death, making it effective against a wide range of Gram-positive and some Gram-negative bacteria [39].In clinical use, amoxicillin is frequently prescribed for bacterial infections such as middle ear infections (otitis media), sinusitis, skin infections, bronchitis, pneumonia, and urinary tract infections. It is also used in combination with other drugs to treat more complex infections, such as Helicobacter pylori in peptic ulcers. Amoxicillin is generally well-tolerated in most patients, with common side effects including gastrointestinal disturbances such as nausea, diarrhea, and abdominal pain. Allergic reactions, such as rash or, in rare cases, anaphylaxis, can occur in individuals with penicillin allergies. Additionally, overuse or inappropriate use of amoxicillin can contribute to the development of antibiotic-resistant bacteria, a growing public health concern [39].

1.3. Current Methods for Pharmaceutical Removal

1.3.1 Advanced oxidation processes (AOPs)

1.3.1.1 Photocatalysis

The name photocatalyst combines two concepts: "photo," pertaining to photons, and "catalyst," which refers to a chemical that modifies the reaction rate in its presence. Photocatalysts are substances that alter the rate of a chemical process when exposed to light [40]. This occurrence is referred to as photocatalysis. Photocatalysis encompasses reactions that occur through the use of light and a semiconductor. A photocatalyst is a substrate that absorbs light and facilitates chemical reactions. Photocatalysis is a phenomena wherein an electron-hole pair is produced when a semiconducting substance is exposed to light. Photocatalytic reactions can be classified into two categories based on the physical condition of the reactants [40].

- Homogeneous photocatalysis occurs when both the semiconductor and reactant exist in the same phase, whether gas, solid, or liquid, characterizing these photocatalytic processes as homogeneous.
-Heterogeneous photocatalysis occurs when the semiconductor and reactant exist in distinct phases, categorizing such photocatalytic processes as heterogeneous.

1.3.1.2 Photo-Fenton or Fenton or electro-Fenton

The Photo-Fenton process is an advanced oxidation process (AOP) used in environmental engineering, particularly for treating wastewater. It combines Fenton's reagent (a mixture of hydrogen peroxide and iron salts) with ultraviolet (UV) light to enhance the generation of hydroxyl radicals. These highly reactive radicals effectively degrade various organic pollutants, converting them into less harmful compounds like water and carbon dioxide [41]. The addition of UV light in the Photo-Fenton process speeds up the decomposition of hydrogen peroxide, generating more radicals and making it more efficient for breaking down persistent pollutants compared to the standard Fenton reaction [42].

1.3.1.3 Ozonation

Ozonation is a chemical water treatment procedure that involves the introduction of ozone (O_3) into water. Ozone, being a vigorous oxidant with a significant oxidation potential, is ideal for oxidizing and dissolving sludge slurry [43]. The oxidative capability of ozone operates via the

sequential disintegration of microbial flocs, the oxidation of liberated organic constituents, and the solubilization of sludge. The ozone treatment of sludge eliminates persistent and hazardous chemicals in the sludge slurry by rapidly decomposing them into radicals that oxidize materials via both structure-specific and non-structure-specific processes. Ozonation of organic molecules facilitates solubilization and mineralization, leading to reduced digestion time and enhanced biogas production [43].

1.3.1.4 Ultrasonication

It is an advanced treatment approach that utilizes sonochemical cavitation locally inside the medium. Ultrasonication, when used at high frequency and low intensity, does not cause physicochemical alterations to the medium, hence facilitating the effective destruction of developing pollutants in wastewater. The primary function of ultrasonication treatment involves continuous cycles of compression and expansion, producing waves at a specified frequency as well as subsequently generating cavitation bubbles [44]. The bubbles experience implosion, producing temperatures ranging from 4200 to 5273 K and pressures between 97.5 MPa and 100 MPa, respectively [44]. This creates hotspots within the local region that disintegrate water molecules into O_2, H_2, as well as reactive free radicals like OH and OOH.

1.3.1.5 Electrochemical oxidation

Electrochemical oxidation is a process where electrical energy is used to drive a chemical reaction that involves the loss of electrons from a substance. In this process, an electric current passes through an electrolyte solution, causing oxidation reactions at the anode (the positive electrode). This reaction can degrade or convert organic and inorganic pollutants into less harmful substances, often producing water, carbon dioxide, and other benign byproducts [44]. Electrochemical oxidation is commonly used in water and wastewater treatment, where it helps break down pollutants that are otherwise difficult to remove, such as pharmaceuticals, pesticides, and industrial chemicals. It is also employed in fields like energy storage and conversion, where it plays a role in processes such as the oxidation of fuels in fuel cells. The technique offers high efficiency and controllability, making it a valuable method for sustainable waste treatment and environmental management [44].

1.3.1.6 Persulfate oxidation

Hydroxyl radicals are frequently produced by advanced oxidation processes and can swiftly oxidize a diverse array of organic molecules non-selectively. Nonetheless, the constraints of hydroxyl radicals frequently relate to their stability, as they are swiftly depleted by oxidants, particularly in environments with elevated organic matter [45]. Consequently, the degradation of specific contaminants will not occur. Conversely, sulfate radicals (SO_4) has a comparatively longer half-life than hydroxyl radicals as well as can readily activate persulfate with diverse agents, as SO_4 exhibits a marked predilection for electron transfer reactions [46].Moreover, SO_4 has remarkable reactivity towards specific functional groups, including , aniline, carboxylic and phenolic groups found in tetracycline antibiotics [47].

1.3.2. Adsorption process

It refers to the process in which molecules of the adsorbate adhere to a solid surface (adsorbent), forming a surface film by the conclusion of the process [48]. As a surface phenomenon, the efficiency of adsorption relies on the presence of an adsorbent with an adequately porous structure as well as sufficient surface energy to attract solutes, facilitating effective mass transfer [49]. During this process, the pores, voids, and interstitial spaces of the adsorbent serve as active sites for the adsorption of inorganic, organic, as well as ionic pollutants. The effectiveness of an adsorption process depends on both the solubility of the solute in the bulk fluid phase as well as the characteristics of the adsorbent, which determine the affinity between the solute and the sorbent [50].

1.3.2.1. Carbon-based adsorbents

They are predominantly produced from agricultural residues, by-products of food processing and animal waste as well as municipal solid waste [51]. The utilization of these solid waste derivatives for adsorption applications offers several environmental benefits, including the preservation of landfill space and the reduction of air pollution associated with the open burning of such wastes. Among the primary adsorbents in this category are biochar, hydrochars, and activated carbons. Additionally, carbon nanotubes and graphene-based materials are also classified as carbon-based adsorbents. Hydrochars and biochars are carbonized forms of biomass that undergo no chemical or physicochemical activation, whereas activated carbons are produced through further activation of biochars [51].

1.3.2.2. Plant biomasses

A effective reduction of adsorbent costs is essential for attaining economically viable wastewater treatment [52]. For example, while activated carbon, biochar, and hydrochars effectively store most aqueous pharmaceutical, their synthesis and recycling are costly and time-intensive [53]. The previously mentioned factors further restrict their sustainable implementation in economically challenged settings and need the development of efficient and cost-effective pharmaceutical adsorbents. Plant biomass and various agro-waste materials are appropriate options due to their abundant availability at no expense, biodegradability, and environmental friendliness [54]. Numerous plant biomasses have been employed as adsorbents for pharmaceutical, in both their natural and modified states, according to the examined studies.

1.3.2.3. Clay and clay minerals

Numerous adaptable adsorbents have been synthesized from clay minerals, offering features such as optimal charge density, ion exchange capacity, extensive specific surface area, and accessibility. Moreover, their complex layered architecture facilitates effective surface adsorption and improves their ability to intercalate pollutants [55]. Various clay minerals, including kaolinite and montmorillonite, have been extensively examined in adsorption research; nevertheless, their adsorptive capacity is constrained by a limited affinity for hydrophobic contaminants, attributable to the hydrophilic nature of their interlayer surfaces [50]. Hybrid layered materials (organoclays) are produced through the functionalization with ionic, cationic, as well as non-ionic species [56].

1.3.2.4. Silica-based adsorbents

Silica-based adsorbents are materials derived from silica (silicon dioxide) that are engineered to capture and hold onto specific molecules from gases or liquids [57]. Due to their unique properties, like large surface areas, customizable pore sizes, and high mechanical and thermal stability. These adsorbents are highly effective in separating and purifying substances[50].Silica-based adsorbents can be modified with functional groups (specific chemical attachments) to enhance their ability to adsorb certain molecules. This customization is key to their versatility in various applications, from environmental cleanup to pharmaceutical production. The modification also influences factors like the adsorbent's surface charge, hydrophobicity (water repellence), and overall efficiency in different conditions [58].

1.3.2.5. Zeolite-based adsorbents

They are crystalline aluminosilicates characterized by uniform cavities and significant ion-exchange capacity. This category of materials and geological resources is mostly employed as an ion exchanger and adsorbent for pharmaceuticals. Zeolite is derived from either natural sources or produced; nevertheless, for economic reasons, natural zeolites are favored over synthetic ones [59]. Simultaneously, observations indicate a low affinity of natural zeolite for hydrophobic chemical compounds [60]. Various surface modification techniques have been employed to overcome this constraint. Izzo et al. [61] successfully modified natural zeolite with long-chain cationic surfactants to create a composite material with significant adsorption capacity for Ibuprofen. Simultaneously, meticulous attention should be devoted to utilizing the optimal surfactant concentration. It was reported that the lengthy carbon chain of hexadecyltrimethylammonium, a cationic surfactant, at elevated concentrations, created a comprehensive layer of organic cation that obscured the entire zeolite surface, thereby restricting their ion exchange capacities during adsorptive applications [62].

1.3.2.6. Polymers and resins

Diverse polymeric materials and resins, including polyacrylonitrile, microplastics, chitosan, and macromolecular polysaccharides, have been utilized as adsorbents for the adsorption of pharmaceuticals. These polymeric adsorbents possess a distinctive porous structure that facilitates the adsorption of contaminants from aqueous solutions. Polymeric adsorbents are functionalized to improve their adsorption capacity and selectivity for target organic contaminants [63].

1.3.3. Hybrid adsorbents

This examines the utilization of natural or synthetic adsorbents derived from many precursors with distinct physicochemical properties. Kryuchkova et al. [64] observed that the diversity and complexity of pharmaceuticals micropollutants preclude any single material or adsorbent from possessing all the requisite qualities for effective adsorption. To qualify as a hybrid adsorbent, the unique characteristics of two or more precursors must be skillfully integrated to produce advantageous qualities.

1.4. Agro-industrial Wastes

The sustainable reuse of biomass from agro-industrial waste for the production of food, drugs, biologically active chemicals, biomaterials, and renewable energy generation is unequivocally one of the foremost issues of the 21st century. The agricultural and food sectors produce significant waste that can be used as raw materials to create high-value products, hence fostering sustainable manufacturing opportunities [65]. The Food and Agriculture Organization of the United Nations estimates that over one-third of all food produced for human consumption globally is lost or wasted, totaling around 1.6 billion tons annually [66]. Agro-industrial wastes are categorized into on-farm (agricultural residues) and off-farm (industrial wastes) (Figure 2). In the initial category, we can distinguish between field residues and process residues. Field residues (seeds, leaves, stems, bunches) are the remnants remaining in the field post-harvest, whereas process residues (husks, roots, seeds) are agricultural byproducts produced following the processing of raw materials [16]. The byproducts produced in food processing companies, including peels, oil, pomace, grinds, and molasses, are classified as industrial waste. Agro-industrial waste mostly comprises lignocellulosic material, specifically cellulose and hemicellulose linked by lignin, along with additional components such as proteins, ash, organic acids, and other non-structural substances. Cellulose is a principal structural element of lignocellulosic material, comprising a disaccharide of D-glucopyranose connected by β-(1–4) glycosidic linkages, known as cellobiose. The structure of cellulose forms fibers that can exist in crystalline or amorphous configurations.

Hemicelluloses are short-chain polysaccharides consisting of 500 to 3000 units of two or more monosaccharides. The monosaccharides found in hemicellulose include pentoses such as xylose, rhamnose, and arabinose, as well as hexoses such as glucose, mannose, and galactose, resulting in a disordered, amorphous, and fragile structure. Lignin serves as a binding agent that connects cellulose and hemicellulose, forming the resilient three-dimensional structure of the plant cell wall. Lignin's structure comprises monolignols linked by aromatic rings, usually totaling up to 10,000 units [67], [68].

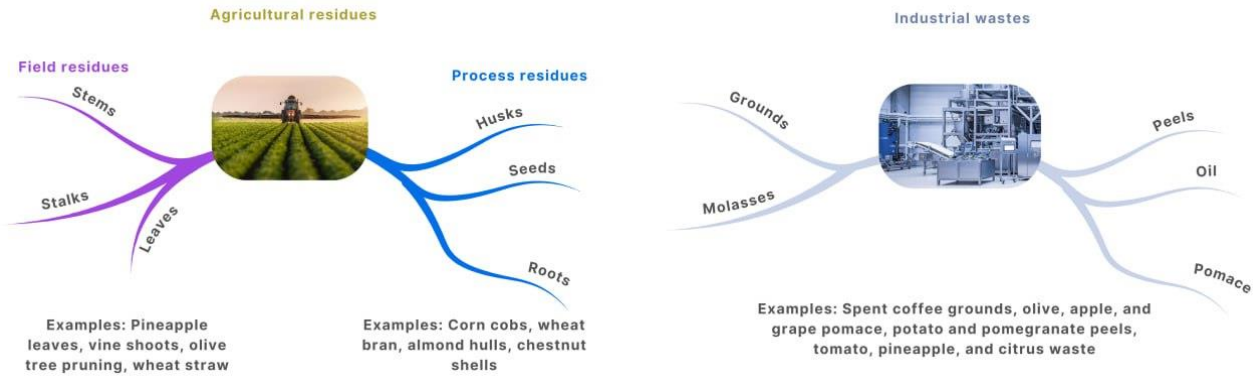

Figure 2 Classification of agro-industrial wastes (redrawn from [67])

The varied form and composition of agro-industrial wastes may necessitate tailored treatment strategies [69]. Materials like stems or leaves necessitate rigorous pre-treatment to improve accessibility to their fundamental structures [70]. Concurrently, specific feedstocks like pomace experience pre-processing in manufacturing, which modifies the structure of the lignocellulosic material. Consequently, it is essential to customize the biorefinery process to the distinct properties of each raw material [71]

1.4.1. Used wastes in this work

1- Banana peel: Banana is a generic name that includes all wild species, cultivars, and landraces that are members of the *Musaceae* family and the Musa genus. *Musa cavendishii*, also known as the cavendish banana, Musa paradisiaca, also known as the plantain, and *Musa sapientum*, are the species that are farmed the most all over the globe [72]. The banana is the second most farmed fruit in the globe, with a total production of 124.97 million tons in 2021 [73]. The cultivation of bananas results in the production of a significant quantity of biomass that is not intended for use, including rachis, leaves, pseudostem, and fruit peels. It has been estimated that the bulk of the fruit accounts for just twelve percent of the overall mass of the banana tree [74]. The peels account for between 35 and 50% of the overall weight of the fruit. Thus, the total waste from banana peels, based on the production of 124.97 million tons, ranges between approximately 43.74 million tons and 62.49 million tons annually. Typically, this waste is discarded, and if not properly managed, it can lead to various health and environmental issues [75]. Researchers examined the possibility of removing various pollutants from banana residues, including metals, organic micropollutants, and dyes [72].

2- **Olive stone:** It is an important byproduct of the olive oil extraction industry. Olive stones are mostly produced in large quantities, and the market focuses on distributing olive products that do not include stones. The residual material, known as a by-product, makes up about 10% of the overall weight of the olive fruit. The Food and Agriculture Organization (FAO) reports that worldwide olive production amounts to 21 million tons per year [76]. However, the olive sector, along with its related byproducts, is now facing significant sustainability issues. Only a meager 20% of the initial olive mass undergoes conversion into olive oil, with around 50% being classified as olive mill wastewater, and the remaining 30% consisting of solid waste such as pulp and pits [77]. In addition, the olive stones produced from harvest olive fruit would weigh around 2.1 million tons. This shows the significant amount of waste generated, if not handled properly, these byproducts could have a substantial impact on the environment. The substantial quantity of agro-industrial waste has the potential to be transformed into valuable materials, such as adsorbents, that could be used in many applications, including water treatment.
3- **Pinewood waste:** it refers to the leftover materials generated during the processing of pine wood, which can include sawdust, wood chips, bark, and off-cuts from lumber production. In 2017, Approximately 761 million m^3 of wood is harvested annually in Europe [78]. This waste can arise from various activities, such as: logging (residual wood materials left after trees are felled and processed), sawmilling (by-products from cutting pine logs into lumber, including sawdust and small pieces of wood) as well as woodworking (scraps and shavings produced during the fabrication of pine products). Europe produces around 60 million tons of waste wood each year, collected from various sectors [79].

1.5. Modification Techniques for Adsorbents

1.5.1. Physical modification

1.5.1.1. Pyrolysis

Pyrolysis is a thermochemical process that generates biochar by the heat degradation of bio-adsorbent in an inert environment. Pyrolysis methods are categorized into three types according to process conditions: fast, flash, and slow pyrolysis. Slow pyrolysis is the predominant method for

biochar production, operating at a reaction temperature of approximately 300 ◦C. The slow pyrolysis procedure produces 25–65% biochar [80]. Rapid pyrolysis at temperatures between 400 and 700 °C leads to a 15–25% modification of the bio-adsorbent. Unlike the other methods, flash pyrolysis operates at temperatures between 700 and 900 °C; nevertheless, it is not employed for biochar modification due to the potential degradation of the adsorption properties of the bio-adsorbent at elevated temperatures. Consequently, slow and fast pyrolysis are the predominant conventional methods employed for the production of biochar from bio-adsorbents [81]. Innovative pyrolysis technology is emerging in the realm of environmental applications. Emerging pyrolysis approaches encompass biomass pyrolysis, hydrothermal pyrolysis, and both fast and slow pyrolysis.

1.5.1.2. Ultrasonication

Ultrasonication employs ultrasonic waves to modify bio-adsorbents. Ultrasound typically denotes sound waves with frequencies beyond the normal human threshold of 20 kHz. Ultrasound can be categorized into two types based on intensity and frequency: high intensity ultrasound and low intensity ultrasound. It produces microbubbles that collapse, creating intense local conditions (high temperature and pressure). These conditions increase the surface area of adsorbents, improve mass transfer, and break down contaminants, leading to a more efficient and faster adsorption process [82].

1.5.1.3. Ball milling and grinding

Grinding is a physical method that alters bio adsorbents by reducing the size of the adsorbent particles to augment their surface area and improve their adsorption capacity. The mechanical process of grinding entails reducing the particle size of the bio adsorbent. This can be achieved through several methods, including ball milling, attrition, or specialized apparatus [81]. The bioadsorbent can be enhanced through grinding, resulting in increased surface area, greater adsorption capacity, enhanced accessibility, reduced adsorption time, uniformity, and regeneration efficiency. Ball milling is a mechanical technique employed to amalgamate and pulverize materials, often leading to a reduction in particle size. Ball milling can modify or enhance the properties of bioadsorbents to augment their efficacy in adsorbing certain compounds, including heavy metals, dyes, or other pollutants from various media. Enhanced surface area, elevated reactivity, uniform distribution, and optimized adsorption kinetics are merely a few benefits of ball

milling for the modification of bioadsorbents. When conducting ball milling to modify bioadsorbents, several critical factors must be considered, including the selection of biosorbent, milling duration and velocity, incorporation of modifiers, characterisation, and adsorption evaluation.

1.5.2 Chemical activating agents

Numerous chemical reagents have been employed as activating agents for carbon. These could be divided into four diverse categories: alkaline, acidic, neutral, and self-activating salts[83]. The alkaline activating agents that are most commonly utilized can be categorized into three distinct types. The first group of alkaline activating elements includes potassium hydroxide (KOH) and sodium hydroxide (NaOH). The second group of medium alkaline activating agents consists of sodium carbonate (Na_2CO_3) and potassium carbonate (K_2CO_3). The third kind of weak alkaline activating agents are potassium silicate (K_2SiO_3), potassium tetraborate ($K_2B_4O_7$), sodium silicate (Na_2SiO_3), potassium acetate (CH_3COOK), potassium oxalate ($K_2C_2O_4$), sodium aluminate ($Na_2Al_2O_4$), potassium hydrogen tartrate ($C_4H_6K_2O_7$), potassium citrate ($C_6H_5K_3O_7$), potassium phosphate (K_3PO_4), and others. These agents are sometimes referred to as salts of strong alkalis as well as weak acids. Acidic activating agents encompass a range of compounds such as phosphoric acid (H_3PO_4), pyrophosphoric acid ($H_4P_2O_7$), phosphorous acid (H_3PO_3), metaphosphoric acid (HPO_3), sulfuric acid (H_2SO_4), nitric acid (HNO_3), tetraphosphoric acid ($H_6P_4O_{13}$), hexamethylphosphoramide ($C_6H_{18}O_{24}P_6$), hydrogen peroxide (H_2O_2), trimethylphosphite ($C_3H_9O_4P$), tributylphosphite ($C_{12}H_{27}O_4P$), triethylphosphite ($C_6H_{15}O_4P$), triphenylphosphine oxide ($C_{18}H_{15}R_3O_4P$), tetraoctylphosphonium bromide ($C_{24}H_{51}O_4P$), and others [83]. Neutral activating agents include zinc chloride ($ZnCl_2$), ferric chloride ($FeCl_3$), ammonium chloride (NH_4Cl), potassium sulfate (K_2SO_4), potassium permanganate ($KMnO_4$), potassium bitartrate ($KHC_4H_4O_6$), calcium chloride ($CaCl_2$), magnesium chloride ($MgCl_2$), potassium chloride (KCl), sodium amide ($NaNH_2$), monosodium phosphate (NaH_2PO_4), potassium dihydrogen phosphate (KH_2PO_4), etc. Finally, self-activating agents consist of organic acid salts, in situ pyrolysis gases, and special natural components in certain carbon precursors [83].

1.6. Scope of the work

The commonly used adsorbents include activated carbon, silica gel, alumina, polyacrylamide, absorbent resin, zeolite etc. [84]. Among them, activated carbon (AC) is increasingly being

acknowledged as a highly effective adsorbent for the elimination of various organic and inorganic contaminants from polluted water. This recognition is primarily attributed to its high specific surface area, porous structure, strong mechanical durability, and acid-resistant properties. The global market valuation of activated carbon in 2022 was estimated to be USD 3.62 billion, with a projected compound annual growth rate of 2.6% from 2023 to 2030 [85]. The main driving force behind this expansion is expected to be the increased demand for water treatment and sewage treatment applications. This underlines the potential environmental and economic significance of AC utilization. However, the high cost of commercial AC, which is around US$135,000 per ton [86], has limited its widespread use in industrial applications owing to the resulting financial pressure. As a result, there has been a shift in the attention of the scientific community towards the discovery of economically viable AC produced from agro-industrial wastes.

Thus, this thesis aims to develop sustainable, cost-effective, and environmentally friendly adsorbents from waste to remove pharmaceutical compounds from water, wastewater and lake water. The effectiveness of all adsorbents in removing diclofenac, ciprofloxacin, amoxicillin, and carbamazepine were further examined through an analysis of their physicochemical properties. The primary factors affecting their capacity to absorb contaminants were examined. Consequently, the primary objectives of this thesis are as follows:

- To develop new activated carbons derived from agro-industrial waste for the removal of pharmaceutical pollutants from different water matrices.
- Testing the recyclability performances in terms of pharmaceuticals removal in different waters (water, wastewater and lake water)
- Characterize both raw and activated carbons to assess whether their removal efficiency exceeds that of currently utilized adsorbents.
- Examine the sorption models to identify the mechanism driving the sorption of pharmaceuticals.
- Find several factors (contact duration, temperature, dose, pH) that affect the efficiency of adsorbents and identify their best values to improve the adsorption rate.

- Investigate Langmuir, Freundlich, intraparticle diffusion isotherms, pseudo-first-order kinetic, and pseudo-second-order kinetic. Furthermore, assess the parameters characterizing the effectiveness of batch processing for adsorption.
- To calculate the cost for all developed ACs and compare it with the commercial AC prices.

2. Experimental

2.1. Materials

The diclofenac ($C_{14}H_{11}C_{l2}NO_2$, CAS No.: 15307-86-5), ciprofloxacin ($C_{17}H_{18}FN_3O_3$, CAS No.: 85721-33-1), amoxicillin ($C_{16}H_{19}N3O_5S$, CAS No.:26787-78-0), carbamazepine ($C_{15}H_{12}N_2O$, CAS No.: 298-46-4), sulfuric acid (H_2SO_4, 99.6 %), nitric acid (HNO_3, 99.8 %), Hydrochloric acid (HCl, 37%), phosphoric acid (H_3PO_4, 85%, CAS No.:7664-38-2), and potassium hydroxide (KOH, 85%) were obtained from Sigma-Aldrich. The McIlvaine citrate–phosphate solution was prepared using citric acid ($C_6H_8O_7$) and disodium phosphate (Na_2HPO_4) provided by AVANTOR (Radnor). Sodium hydroxide (≥ 98%, NaOH), sodium bicarbonate (99.5-100.5%, $NaHCO_3$), sodium carbonate (≥99.5%, Na_2CO_3), sodium ethoxide (≥95%, $NaOC_2H_5$) and ammonium nitrate (NH_4NO_3) (≥99.0%, CAS No.: 6484-52-2) were purchased from Sigma-Aldrich (Burlington, MA, USA). Banana peels (BP), and Olive stone waste (OSW) were obtained from local supermarket in Veszprém, Hungary free of charge. The pinewood (PW) waste was collected from a local source in Veszprém, Hungary, and ground as the biomass feedstock. The other compounds used in this study were obtained from Sigma-Aldrich. The chemicals and reagents of analytical grade were employed without any further purification. During the experimental procedures, Millipore Direct-Q® 5 UV purification system (Merck KGaA, Darmstadt, Germany) was employed to supply ultra-pure water (referred to as MQ hereafter) characterized by a resistivity of at least 18.2 MΩ.cm. This high-quality water was utilized both for cleaning purposes and solutions preparations. Whatman® glass microfiber filters were employed to separate the adsorbents from the treated solution.

2.2. Methods

2.2.1. Method 1: Activated Carbon from Olive Stone Waste (OSAC) by KOH

OSW was used as a biosorbent to remove pharmaceuticals from water. The raw carbonaceous form of OSW underwent a series of preparation processes. Figure 3 illustrates the protocol for OSW activated carbon (OSAC) preparation, highlighting the major steps. Initially, the material was thoroughly cleaned with distilled water to remove dust and other contaminants. Following this, it was sun-dried for a week, then further dried in an oven at 105 °C for 6 h. The desiccated OSW was subsequently pulverized to a particle size range of 0.7–1.0 mm. The OSW particles were then washed again with distilled water for 24 h, followed by additional drying at 105 °C for another 6

h. The carbonization of OSW was conducted following methods from previous studies, with some modifications [87], [88]. A horizontally oriented cylindrical stainless-steel reactor, placed within a furnace, was used for the carbonization process. OSW was heated to 450 °C at a rate of 15 °C/min for 2 h, while maintaining a continuous nitrogen flow at 300 mL/min as a purging gas. This ensured the formation of a solid material with a stable structure. The nitrogen flow continued until the temperature dropped below 200 °C after the furnace was turned off. Next, the impregnation with KOH was carried out using different weight ratios of KOH (1:1, 1:2, and 1:3). Table 1 outlines the OSAC activation temperatures and impregnation ratios, producing different materials coded 1–9. The impregnation process involved stirring the mixture under reflux conditions at 90 °C for 6 h. The samples were then dried at 105 °C for 24 h, followed by activation under a nitrogen flow at temperatures of 550, 650, and 750 °C. The resulting OSAC materials were washed with 1 M HCl to remove any residual KOH, then rinsed with MQ water until a neutral pH was achieved. Finally, the OSACs were dried in an oven at 105 °C overnight and stored in sealed containers until adsorption experiments were conducted.

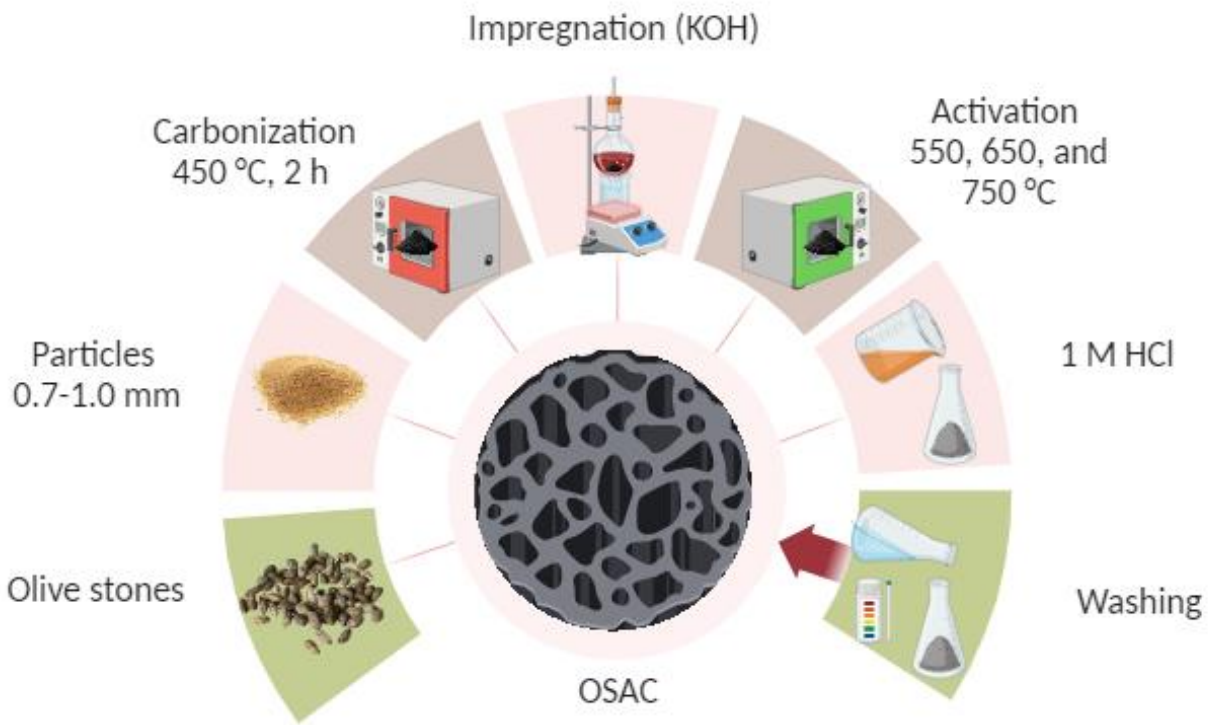

Figure 3 Olive stones activated carbon (OSAC) preparation.

Table 1 OSAC activation temperature and impregnation ratios

Temperature (°C)	1:1 (OSAC g: KOH g)	1:2 (OSAC g: KOH g)	1:3 (OSAC g: KOH g)
550	OSAC1	OSAC4	OSAC7
650	OSAC2	OSAC5	OSAC8
750	OSAC3	OSAC6	OSAC9

2.2.2. Method 2: Activated Carbon from Banana Peel (BPAC) by H_3PO_4

To remove surface dirt and other contaminants, banana peels (BP) were cut into pieces approximately 2 cm in length and thoroughly washed with both tap water and deionized water. The materials were then dried for 24 h in an oven at 100°C, after which they were ground and sieved to obtain particles with diameters less than 0.150 mm. Phosphoric acid (H_3PO_4) is a widely used activating agent that has been investigated for its role in producing activated carbons from agricultural waste [89]. The dried BP (25 g) was soaked in 500 mL of acid solution in a one-liter Erlenmeyer flask, following a previously reported method [90] with slight modifications. The experiment was conducted on an electric hotplate for 4 h at 80°C. Afterward, the impregnation solution was removed, and the impregnated BP was oven-dried at 110°C for 6 h. Subsequently, BP was carbonized at temperatures of 350°C, 450°C, and 550°C for 30 min in a cylindrical stainless-steel reactor positioned within a furnace. After carbonization, the activated carbon derived from banana peel (BPAC) was washed several times with hot distilled water to neutralize the material to a pH of 6–7 and to remove residual chemicals. It was then oven-dried at 105°C to eliminate any remaining moisture and volatile substances that may have adhered to it [91]. Finally, the BPAC was stored in a sealed container for further research.

2.2.3. Method 3: Activated Carbon from Pinewood (FPWAC) by NH_4NO_3 and NaOH

The pinewood (PW) pieces of 2 cm were washed with potable water, followed by drying for 24 h at 105 °C. The first activation step with NH_4NO_3 followed the methodology reported in [92], [93], with slight modifications. Briefly, different NH_4NO_3/PW impregnation ratios of 1-4 wt.% were pyrolyzed at 300-600 °C for activation durations of 1.5 to 3 h. The pyrolysis process was conducted using a vertical stainless-steel reactor equipped with an electric furnace. A continuous stream of nitrogen gas was sustained throughout the process at a volumetric flow rate of 150 cm^3/min. To

identify the best activation parameters, preliminary removal tests for diclofenac and ciprofloxacin were carried out, as detailed in Table 2. After identifying the optimal NH_4NO_3/PW ratio, only one sample was chosen to proceed with the next stage of activation. This sample was mixed with NaOH in a weight-to-weight ratio of 3:1 [94]. The mixture was placed in a beaker and stirred magnetically for 2.5 h. Subsequently, the resulting mixture was desiccated in an oven at 105 °C for 6 h. The sample was then moved to the furnace, where the temperature was increased to 500 °C and maintained at this level for about 2 h while nitrogen gas flowed continuously at a rate of 100 mL /min [94]. Following the cooling phase, the PW was washed multiple times with a 0.1 M solution of HCl, followed by rinsing with hot distilled water to achieve neutral pH and eliminate any residues of the activating agent or other inorganic compounds formed during the process [95]. After washing, the slurry was filtered through 0.45 µm cellulose membranes to collect the Final Pinewood Activated Carbon (FPWAC). Figure 4 shows the activation process of FPWAC. The FPWAC was subsequently desiccated in an oven at 105 °C for 24 h and stored in hermetically sealed containers for subsequent analysis.

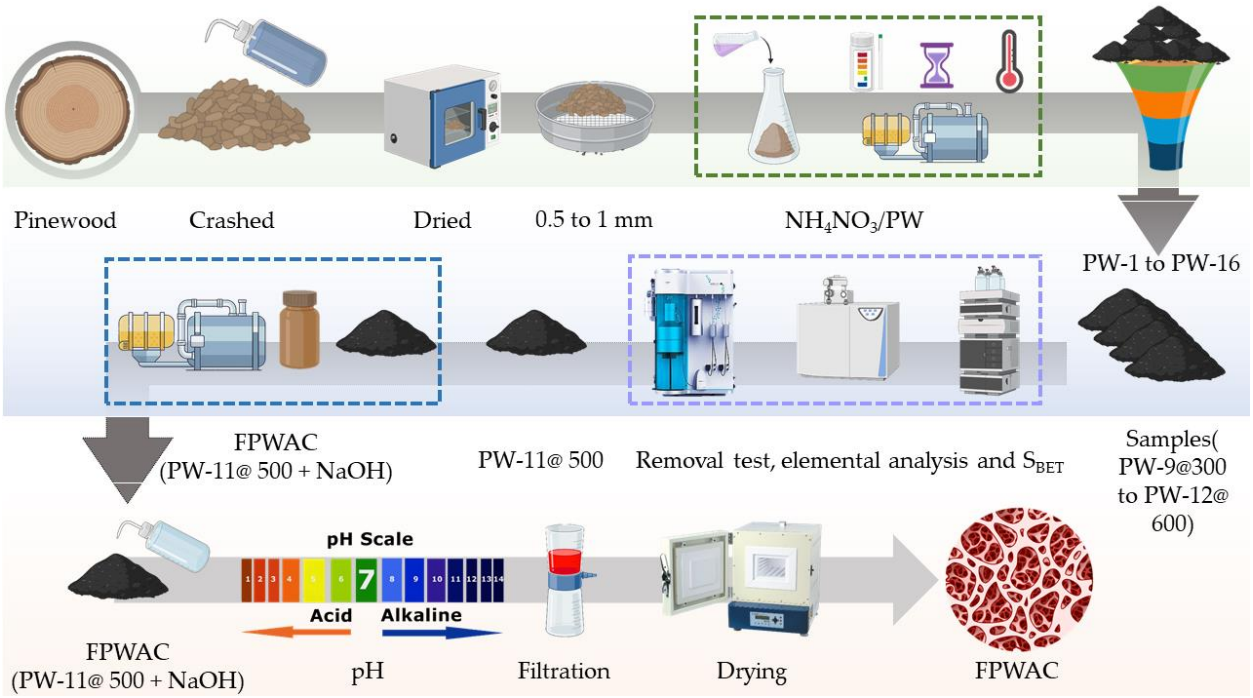

Figure 4 Two stages of FPWAC activation

Table 2 Pinewood (PW) samples for pollutants removal from aqueous solution. The adsorption conditions: pH 6, 25°C, shaking speed of 150 rpm, an adsorbent dosage of 1 g/L, and initial pollutants concentration of 25 mg/L.

Sample Number	Activation time (h)	Temperature (°C)	NH_4NO_3/PW ratio wt. (%)	Diclofenac (Removal %)	Ciprofloxacin (Removal %)
PW-1	1.5	300	1	11.93	19.04
PW-2	2	400	1	15.75	18.46
PW-3	2.5	500	1	25.83	21.06
PW-4	3	600	1	28.02	26.16
PW-5	1.5	300	2	44.92	45.98
PW-6	2	400	2	52.30	47.29
PW-7	2.5	500	2	59.94	58.99
PW-8	3	600	2	55.54	57.27
PW-9	1.5	300	3	57.46	61.80
PW-10	2	400	3	69.81	75.39
PW-11	**2.5**	**500**	**3**	**82.12**	**83.51**
PW-12	3	600	3	79.98	81.33
PW-13	1.5	300	4	56.62	52.47
PW-14	2	400	4	61.84	63.16
PW-15	2.5	500	4	77.02	79.11
PW-16	3	600	4	73.58	69.08

2.3. Characterization Methods

2.3.1. Scanning Electron Microscopy (SEM) and Energy-dispersive X-ray (EDS) Spectroscopy Measurements

The morphology and elemental mapping of the adsorbent surfaces were analyzed using scanning electron microscopy (SEM, model JEOL JIB-4700F and Thermo Scientific Apreo S LoVac), coupled with energy dispersive X-ray spectroscopy (EDS, GENTLEBEAM™ (GB), Tokyo, Japan and EDAX AMETEK Octane Elect Plus), at an accelerating voltage of 3–5 kV and a current of 10

nA. The samples were fixed onto a conductive carbon tape and coated with gold/palladium (Au/Pd) film for 10 min to enhance their conductivity and obtain high-quality images.

2.3.2. Fourier Transform Infrared Spectroscopy Measurements (FTIR)

The Fourier transform infrared spectroscopy (FTIR) spectra of the materials, both before and after the adsorption process, were investigated to evaluate the functional groups present on their surfaces. The analysis was performed using a Nicolet™ iS™ 5 FTIR Spectrometer (Thermo Fisher, Waltham, MA, USA), equipped with an iD7 ATR, within the wavenumber range of 400–4000 cm^{-1} and a resolution of 2 cm^{-1}. Prior to each analysis, a blank background spectrum was acquired to establish a reference scale for absorption intensity and to enable blank subtraction. The materials were dried at 50°C for 2 h to ensure complete removal of water.

2.3.3. Point of Zero Charges (pHpzc)

The evaluation of the point of zero charge (pH_{PZC}) was performed by combining 0.01 g of the biosorbent under investigation with 10 mL of a 0.1 mol/L NaCl solution. The initial pH of the mixture varied within the range of 2 to 11. The dispersions were agitated for 24 h, and the resulting pH values were measured. The pH_{PZC} value was determined as the abscissa point where the curve of ΔpH versus initial pH intersected the line representing zero.

2.3.4. Boehm titration

Boehm titration was used to quantitatively determine the presence of functional groups in the raw and activated carbons[96]. Approximately 1 g of the substance was agitated at room temperature for 72 h in 50 mL of 0.1 M solutions of NaOH, 0.1 M $NaHCO_3$, 0.05 M Na_2CO_3, and 0.1 M $NaOC_2H_5$. After this, the suspensions were decanted and filtered, and the resulting solutions were back titrated with 0.1 M HCl. The basicity of OSAC was evaluated using a similar method: the samples treated with 0.1 M HCl, and the titration was performed using 0.1 M NaOH. The quantification of acidic sites on the adsorbent was carried out by evaluating the neutralization reactions. Specifically, carboxylic groups were neutralized by $NaHCO_3$; carboxylic and lactonic groups were neutralized by Na_2CO_3; and carboxylic, lactonic, phenolic, and carbonyl groups were neutralized by $NaOC_2H_5$.

2.3.5. X-ray Diffraction Measurements (XRD)

An X-ray diffractometer (XRD, D/Max 2500 VB+X, Rigaku, Tokyo, Japan), equipped with Cu Kα radiation at 40 kV and 35 mA, was used to study the crystallinity of the samples over an angular range of 10–80 degrees (2θ).

2.3.6. Thermogravimetric Analysis Measurements (TGA)

The sample was analyzed utilizing thermos-gravimetric analysis (TA Instrument: TGA 550 Model, New Castle, DE, USA). A quantity of 10 mg was used, with 10 mL/min of N_2. The sample was subjected to heating at a rate of 10/min, starting at a temperature of 50 °C and reaching a final temperature of 700 °C.

2.3.7. Proximate and Ultimate Analysis

Proximate analysis of the prepared adsorbents was conducted following the protocols established by the American Society for Testing and Materials (ASTM). The study adhered to the following ASTM standards: ASTM D 3174-04 for determining ash content[97], ASTM D 3173-03 for evaluating moisture content [98], and ASTM D 3175-07 for assessing volatile matter[99]. The fixed carbon content was calculated by subtracting the cumulative values of moisture, ash, and volatile matter from 100%. The elemental composition of the adsorbents was determined using an elemental analyzer (Model EA 1108, Thermo Scientific, USA), in accordance with ASTM D3176 [100]. The elements analyzed included carbon, hydrogen, oxygen, nitrogen, and sulfur.

2.3.8. Specific Surface Area (S_{BET})

Surface area measurements (S_{BET}) were conducted via the Brunauer, Emmett, and Teller (BET) method using the Micromeritics (3Flex) instrument (Unterschleissheim, Germany). Prior to the analysis, samples were outgassed at 150 °C for 24 h. A pressure ratio (P/P0) of 0.95 was employed. The t-plot method was used to determine the surface area and micropore volumes. The measurements were carried out based on the nitrogen (N_2) gas adsorption technique in a liquid nitrogen environment at 77 Kelvin.

2.4. Adsorption/ Desorption, Isotherms and Kinetics and Thermodynamic Experiments

2.4.1. Pharmaceutical Removal by High Performance Liquid Chromatography

1- OSAC: The experiments of OSAC investigated the effects of various factors on the adsorption process in a batch setting, including pH (2–11), OSAC dosage (0.2–1.2 g/L), temperature (5–35°C), and the initial concentration of pollutants (10–60 mg/L). A quantity of 100 mg of OSAC was added to 100 mL of diclofenac and ciprofloxacin solutions. The pH of the solution was carefully controlled throughout the experiment. The mixtures were placed in Erlenmeyer flasks and agitated for 90 min at 150 rpm and 25°C. Preliminary testing indicated that 90 min was sufficient to reach equilibrium. A 2 mL sample was withdrawn every 15 min, filtered, and analyzed using High-Performance Liquid Chromatography (HPLC) [54]. Equations regarding the removal efficiency (R) and adsorption capacity at any time (qt, mg/g) can be found in Table 4.

2- BPAC: To develop the most effective method for BPAC, adsorption tests were conducted in 0.250 L conical flasks at ambient temperature (25 ± 2 °C). The experiments used 0.18 g of biosorbents and 150 mL of a solution containing pollutant mixtures with an initial concentration of 25 mg/L, with the pH adjusted to 5. The contact time was set to 120 min, and the agitation rate was maintained at 150 rpm. To evaluate the effect of initial pH on the adsorption process, the same conditions were applied with pollutant mixtures at various initial pH levels (pH 2–10). These pH values were adjusted using 0.1 mol/L hydrochloric acid (HCl) or 0.1 mol/L sodium hydroxide (NaOH) solutions. The biosorbent was selected for further adsorption studies. The effect of biosorbent dosage was assessed by using different doses of 0.3, 0.6, 0.9, 1.2, and 1.5 g/L in a 150 mL solution containing pollutant mixtures with an initial concentration of 25 mg/L. The contact time was set to 120 min, and the agitation rate was kept at 150 rpm. In the same procedure, additional parameters, such as temperature (5, 15, 25, 30, and 35 °C) and pollutant concentrations (10, 15, 20, 25, 30, and 35 mg/L), were also evaluated. For pollutant quantification, the mixtures were centrifuged, and a 2 mL aliquot of the supernatant was collected and measured using HPLC [11]. The amount of pollutants adsorbed (qe), in mg/g, and the percentage of pollutant removal was determined using Equations in Table 4.

3- FPWAC: A 0.25 g of FPWAC was added to a 250 mL Erlenmeyer flask containing 150 mL of a mixture of diclofenac and ciprofloxacin, each at a concentration of 25 mg/L, at room temperature. The flask was stirred at 150 rpm with the pH set to 6, and the contact time between the FPWAC

and the solution was fixed at 2 h. The removal of diclofenac and ciprofloxacin from the 150 mL solution was studied at different pH values (ranging from 2.0 to 11.0) to evaluate the influence of initial pH on adsorption capacity. The pH of the solution was adjusted using 0.1 M HCl and NaOH. Furthermore, the effect of FPWAC dosage on adsorption efficiency was investigated under the same conditions, at a fixed pH of 6, using different FPWAC dosages (0.2, 0.6, 1, and 1.4 g/L). The impact of temperature (ranging from 5 to 30 °C) and initial pollutant concentrations (ranging from 15 to 45 mg/L) was also examined by varying one parameter while keeping the others constant. All parametric studies were conducted at a stirring speed of 150 rpm. The analytical instrumentation used in this study included an ultra-performance liquid chromatography-mass spectrometry (UPLC-MS) system [101].

2.4.2. Isotherms and Kinetics Studies of Pharmaceuticals

The most common isotherm models, namely Langmuir and Freundlich, were used to study the nature of adsorption [102], [103]. The Langmuir adsorption model (Table 3) is based on the assumption that adsorbents have a uniform surface, allowing for the formation of a continuous monolayer of adsorbate. The separation factor (RL) can be calculated from the Langmuir constant (Table 3) and used to determine the favorability of adsorption. RL ranges between 0 and 1. Adsorption is considered linear (RL = 1), unfavorable (RL > 1), or irreversible (RL = 0). The Freundlich adsorption isotherm (Table 3) is a widely used empirical model that describes non-ideal adsorption of solutes onto surfaces. According to this model, the adsorption capacity of the solid material increases gradually and continuously as the concentration of solute in the solution increases. The adsorption rate characteristics were studied by fitting experimental data to both first- and second-order kinetics models. The pseudo-first-order model (Table 3) suggests that the rate of solute adsorption over time is proportional to the difference between the saturation concentration and the cumulative adsorbent uptake[104]. The pseudo-second-order kinetic model (Table 3) assumes that the rate-limiting step is chemical sorption (also known as chemisorption), where the solute undergoes direct chemical interactions with the sorbent. Chemical sorption restricts the mobility of sorbed contaminants on the sorbent surface. Sorbates typically occupy specific sorption sites, forming a chemisorbed layer of pollutants [105]. This process involves electron exchange between the adsorbent and adsorbate [106].

1- BPAC: The kinetic studies involved incorporating 0.18 g of absorbent with a pollutant solution at a concentration of 25 mg/L and a pH of 5. The mixtures were agitated at 150 rpm and maintained at ambient temperature (25 ± 2 °C) for varying durations (ranging from 10 to 120 min). After each interval, 1 mL of the liquid portion was collected and analyzed using HPLC. The adsorption isotherms, as well as the pseudo-first-order, pseudo-second-order, and thermodynamic models, were evaluated using the equations listed in Table 3 and 4. Additionally, experiments were conducted to determine the biosorption isotherms. A 0.18 g amount of biosorbent was combined with pollutant solutions at initial concentrations ranging from 5.0 to 120 mg/L. The mixtures were shaken for 12 h at a temperature of 25 ± 2 °C and an agitation rate of 150 rpm at pH 5.

2- FPWAC: The kinetic investigations involved adding 0.25 g of FPWAC to a solution containing pollutants at a concentration of 25 mg/L and a pH of 6. The experiments were conducted under controlled conditions at 25 ± 2 °C, with a stirring rate of 150 rpm, over time intervals ranging from 0 to 6 h. At each interval, aliquots of 1 mL were systematically withdrawn from the liquid phase and analyzed using HPLC. To determine the biosorption isotherms, isotherm experiments were performed by mixing 0.25 g of FPWAC with pollutant solutions at initial concentrations ranging from 5 to 80 mg/L. These samples were shaken for 6 h at 25 ± 2 °C, with a stirring speed of 150 rpm and a pH of 6. The isotherms, including pseudo-first-order and pseudo-second-order kinetics, as well as thermodynamic parameters, were evaluated using the equations provided in Table 3 and 4.

3- OSAC: The kinetic studies included the addition of 0.25 g of OSAC to a solution with contaminants at a concentration of 25 mg/L and a pH of 6. The studies were performed under temperature of 25 ± 2 °C 150 rpm, and for 0 to 6 h interval time. At each interval, 1 mL aliquots were systematically extracted from the liquid phase and evaluated using HPLC. Isotherm studies were conducted to determine the biosorption isotherms by combining 0.25 g of OSAC with pollutant solutions at starting concentrations between 5 and 100 mg/L. The samples were agitated for 6 h at 25 °C, 150 rpm and pH 6.

Table 3 Isotherms and kinetics model equations.

	Equations (linear and non-linear)	Parameter	Reference
Langmuir	$\frac{1}{q_e} = \frac{1}{q_m} + \frac{1}{q_m \times K_L} \times (C_e)^{-1}$ $q_e = \frac{C_e K_L q_m}{1+K_L C_e}$ $R_L = \frac{1}{1+K_L \times C_0}$	K_L is the Langmuir constant (L/mg) and qm is maximum adsorption on AC (mg/g) qe is equilibrium adsorption capacity (mg/g) q_m is the maximum adsorption capacity(mg/g)	[102]
Freundlich	$log\ q_e = \frac{1}{n} log\ C_e + log\ K_f$ $q_e = K_f\ Ce^{1/n}$	K_f and n are Freundlich adsorption isotherm. constants and C_e is equilibrium adsorbate concentration (mg/L)	[103]
Pseudo-first-order (PFO)	$ln(q_e - q_t) = ln\ q_e - K_1 t$ $q_t = q_e(\ 1 - e^{-K1t})$	K_1 is PFO constant rate (min^{-1}) and q_t is pharmaceuticals absorbed at time t (mg/g) and qe and qt are the adsorption capacities (mg/g) at equilibrium	[75]
Pseudo-second-order kinetic (PSO)	$\frac{t}{q_t} = \frac{1}{K_2 q_e^2} + \frac{t}{q_e}$ $q_t = \frac{q_e^2 K_2 t}{1+K_2 q_e t}$	K_2 is PSO constant rate (g/mg .min)	[106]

Table 4 Thermodynamics, Dubinin–Radushkevich isotherm, intra-particle diffusion, and adsorption-desorption equations

	Equations	Parameter	Reference
Gibbs free energy (ΔG°), standard entropy (ΔS°) and standard enthalpy (ΔH°)	$\Delta G^{\circ} = -R \times T \times \ln(K_L)$ $K_L = \frac{q_e}{C_e}$ $\ln(K_L) = \frac{-\Delta H^{\circ}}{RT} + \frac{\Delta S^{\circ}}{R}$ $\Delta G^{\circ} = \Delta H^{\circ} - T \times \Delta S^{\circ}$	R is the universal gas constant (8.314 J/mol K), ΔG° is Gibbs free energy, T is temperature (K), ΔS° is standard entropy, ΔH° is standard enthalpy	[107]
Dubinin–Radushkevich (D–R)	$\ln(q_e) = \ln qd - 2Bd \times RT \times \ln(1 + \frac{1}{Ce})$	Bd is the adsorption constant quantifies the average free energy (mol^2/J^2), qd is the maximum adsorption capacity (mg/g) T is the temperature (Kelvin) R is the universal gas constant (8.314 J/K/mol)	[108]
Intra-particle diffusion	$q_t = k_{diff}\, t^{0.5} + I$	K_{diff} is the intra-particle diffusion constant (mg g^{-1} $min^{-0.5}$), I is the IPD model's boundary layer constant (mg/g)	[109]
Removal efficiency (R)	$R\,(\%) = \frac{(C_0 - C_t)}{C_0} \times 100\%$	The variables C_0 and C_t (g/L) represent adsorbate's initial concentration and concentration at time t, respectively, V is the solution volume (L), and m is the mass of activated carbon (g).	
Adsorption capacity	$q_t = \frac{V \times (C_0 - C_t)}{m}$		
Desorption	$\text{Desorption}(\%)_{AC} = \frac{100\,(C_{des})}{C_{sorb}}$	C_{des} and Cs_{orb} are the desorbed and sorbed pollutants concentration (mg/L).	

2.4.3. Thermodynamic Studies of Pharmaceuticals

1- BPAC: The thermodynamic experiment also included conducting biosorption tests at various temperatures (10 ± 1, 20 ± 1, 30 ± 1, and 40 ± 1 °C). Each test was carried out in a 100 mL glass vial containing 0.05 g of adsorbent material and 40 mL of a 25 mg/L solution of pollutants in water. The solutions were agitated in a shaker incubator at a speed of 150 rpm for 24 h at the specified temperature. Subsequently, each combination was subjected to centrifugation, and 1 mL of the solution that formed above the adsorbent was obtained and examined using HPLC. The tests were run in triplicates. The Gibbs free energy change (ΔG°), change in enthalpy (ΔH°), and change in entropy (ΔS°) during biosorption were determined using Equations in Table 4 and determined by plotting ln KL against 1/T

2- FPWAC: Thermodynamic investigations, performed within a temperature range of 10 to 40 °C, aimed to gain a deeper understanding of the temperature-dependent adsorption process. Each experimental run was carried out in a 100 mL glass vial containing 0.25 g of adsorbent material and 50 mL of a solution with a pollutant concentration of 25 mg/L in aqueous medium. The solutions were agitated in a temperature-controlled incubator shaker set to 150 rpm for a duration of 24 h. After the agitation period, each mixture was centrifuged, and a precisely measured 1 mL sample of the supernatant was collected for further analysis using HPLC. The thermodynamic parameters (ΔG°, ΔH°, and ΔS°) were determined according to the equations presented in Table 4 and determined by plotting ln KL against 1/T.

3- OSAC: The experimental determination of the thermodynamic parameters of adsorption was conducted to gain a better understanding of the adsorption energy dynamics and uniformity. It was performed within a temperature range of 10 to 40 °C. The entropy (ΔS, J/K·kg) and enthalpy (ΔH, J/kg) were determined empirically by plotting ln KL against 1/T.

2.4.4. Desorption Experiments

1- BPAC: The desorption procedure was implemented to assess the reusability of polluted banana peel after batch adsorption tests. The batch desorption tests were performed in 100 mL Erlenmeyer flasks that had been cleaned and dried. Water at a pH of 7 and ethanol were used as solvents. A specified quantity of BPAC was placed in 25 mL of solvent and agitated at 150 rpm for 6 h. The samples were dried at 105 °C for one day. During the runs, the flasks were sealed with parafilm to

prevent solvent evaporation. Control experiments, conducted without activated carbon, were carried out to evaluate the potential influence of adsorption on the glass surfaces.

2- FPWAC: Desorption investigations were conducted to evaluate the potential reusability of activated carbon that had been previously contaminated during batch adsorption studies. Various desorbing agents, including 0.5 M hydrochloric acid (HCl), 0.5 M nitric acid (HNO_3), and ethanol, were systematically examined for their efficacy in releasing adsorbed contaminants from the activated carbon matrix. In each desorption experiment, 0.25 g of FPWAC was added to a 500 mL flask containing 250 mL of the selected solvent. The mixture was agitated at 150 rpm for 6 h to ensure complete desorption. After desorption, the samples were dried at 105 °C for 48 h, as detailed in a previous publication [10]. During the experiments, the flasks were tightly sealed with parafilm to prevent solvent evaporation and maintain constant reaction conditions. Control experiments, conducted in parallel without FPWAC, were used to assess any potential adsorption on the glass surfaces of the apparatus. The desorption efficiency was quantitatively determined (Table 4), enabling a thorough evaluation of each desorbing agent's effectiveness in releasing contaminants from the activated carbon matrix. This assessment highlighted the potential for reusing activated carbon in various pollutant removal applications.

3- OSAC: Desorption tests provide valuable insights into the feasibility of the process. The OSAC was regenerated following the procedure described by Ncibi and Sillanpää [110]. After allowing the solution to settle for 90 min, the liquid was carefully removed with a syringe, and the used OSAC was retrieved. The recovered OSAC was washed with MQ water and dried at 50 °C for 24 h. Subsequently, the OSAC was sequentially washed with methanol, ethanol, and MQ water. Finally, the regenerated OSAC was dried at room temperature for 24 h.

2.5. HPLC measurements

This configuration contained an HPLC module coupled with a QExactive Focus mass spectrometer made by Thermo Scientific in America, and ESI interfaced as an ion probe ionization. The Q Exactive Focus mass spectrometer conducted a thorough scan across the mass-to-charge ratio spectrum, ranging from 50 to 1000, exhibiting exceptional precision with a quality error of less than 5 parts per million (ppm). The ESI method was configured in negative polarity, employing an applied voltage of -4.5 kilovolts (kV) to facilitate ionization. Ultrapure nitrogen gas, exceeding 99.99% purity, was utilized for both drying and auxiliary purposes, while ultrapure helium served

as cooling gas. The ion transfer capillary was rigorously maintained at a temperature of 550 °C as well as grounded to a potential of 0V. For sample analysis, one milliliter of the pollutant mixture was carefully collected, subjected to centrifugation to ensure homogeneity, and subsequently evaluated utilizing the HPLC technique, with triplicate measurements performed for enhanced accuracy of the results.

2.6. Quality Control

Before each measurement, glassware was heated to 100 °C and then washed with methanol to remove any potential background contamination. Triplicate measurements were performed for each sample, along with a method blank. Examination of the method blank confirmed the absence of detectable pollutant contamination. The findings are shown as the mean values with standard error bars. The Kolmogorov-Smirnov test was utilized at a significant level of 0.05 to evaluate the normal distribution of all data in this work.

3. Results and discussion

The selected activation methods were tested on all the chosen materials, and only the successful activation methods were continued for further processing. However, the unsuccessful carbon activation methods often result from a combination of factors, typically involving the choice of materials, activation conditions, or process design. The type of carbon precursor used plays a critical role in determining the final properties of the activated carbon. Some carbon sources may not respond well to the activation process, or they may yield products with undesirable surface characteristics, like low surface area or insufficient pore volume. Similarly, the activation agent, which can include chemicals like KOH, H_3PO_4, NH_4NO_3 and NaOH, must be appropriate for the specific carbon source. If the concentration is too low or too high, activation may be ineffective, leading to poor porosity or surface area. The activation temperature is another key factor: too low a temperature may result in incomplete activation, while too high a temperature can cause excessive material loss or degradation of the carbon structure, reducing its overall effectiveness. Activation time must also be carefully optimized; too short a duration may fail to develop sufficient surface area, while too long a time can lead to excessive burn-off and reduced yield. Finally, the quality of raw materials is crucial variations in size, composition, or other physical properties of the precursors can hinder the activation process and result in inconsistent quality of the activated carbon produced.

3.1. OSAC Activation by KOH

3.1.1. Impregnation Ratio and S_{BET}

The activated material at 750 °C with an impregnation ratio of 1:3 (OSAC9) resulted in the highest surface area of 945.61 m^2/g and a total pore volume of 0.479 cm^3/g (Table 5). This material was selected as the adsorbent for the pharmaceutical removal experiments and was the only OSAC characterized in depth. In comparison, OSW had a BET surface area of 265.43 m^2/g and a total pore volume of 0.182 cm^3/g. The OSAC material has a significantly larger surface area with many active sites, enabling efficient transfer of adsorbates [11]. The surface area of OSW is consistent with previous studies on olive waste products. An investigation by Ghouma and colleagues [111], examining the physical activation of olive stones, found a BET surface area of 807 m^2/g. Bohli and co-workers [112], studying the adsorption of heavy metals using olive stone activated carbon,

reported a surface area of 1081 m²/g after thermal activation with phosphoric acid. In another study [113], the activation of OSW with KOH under optimal preparation conditions yielded a BET surface area of 672 m²/g.

Table 5 S_{BET} and pore structures of olive stones samples

Samples	S_{BET} (m^2/g)	V_{tot} (cm^3/g)	V_{mic} (cm^3/g)	V_{mes}(cm^3/g)
OSW	265.43	0.182	0.090	0.092
OSAC1	395.73	0.191	0.081	0.110
OSAC2	473.52	0.195	0.089	0.106
OSAC3	483.92	0.209	0.090	0.119
OSAC4	738.43	0.226	0.061	0.165
OSAC5	682.03	0.382	0.117	0.265
OSAC6	772.24	0.254	0.082	0.172
OSAC7	866.59	0.421	0.134	0.287
OSAC8	935.01	0.404	0.191	0.213
OSAC9	945.61	0.479	0.177	0.302

3.1.2. SEM-EDS Results

Figure 5 shows the SEM images of the activated carbon sample, taken before and after the adsorption tests. The adsorbent exhibited a significant number of intricately formed pores and voids, which are expected to notably enhance its adsorption capacity [114]. After the adsorption of the targeted pollutants (Figure 5 B), both the type and quantity of cavities on the adsorbent's surface were visibly altered, with a marked reduction in their number. This observed change suggests that the outer layer of the OSAC was covered by the adsorbate. Elemental analysis of the OSAC using EDS confirmed the presence of carbon (C), oxygen (O), potassium (K), and chlorine (Cl), consistent with the activation process using KOH and subsequent washing with HCl. After the adsorption phase, the surface of the particles showed the presence of nitrogen (N) and an enrichment of oxygen (O), which could be attributed to the adsorption of pharmaceuticals onto the OSAC.

3.1.3. FTIR Results

Figure 6 shows the FTIR spectra of OSW, OSAC, and OSAC after adsorption. The band at 3331 cm^{-1} in the spectra represents the stretching vibration of –OH groups present in alcohols and phenols [115]. The band at a wavenumber of 2923 cm^{-1} corresponds to the stretching of C–H bonds found in cellulosic materials, indicating the presence of different amino acids [116]. This peak is one of the characteristic peaks of olive stone powder [117]. The same study also showed that olive stones exhibit two distinctive peaks at approximately 1360 cm^{-1} and 1600 cm^{-1}, which is consistent with the findings of this work. The presence of the 1547 cm^{-1} band suggests the elongation of aromatic C–C rings [118]. The band at 1319 cm^{-1} could be attributed to the symmetric bending of CH_2 groups [119]. The peak at 1025 cm^{-1} corresponds to the elongation of C–N bonds in aliphatic amines [120]. The peak at 611 cm^{-1} is linked to the elongation of OH groups [121], which appeared more intense after activation. The increase in carboxylic groups is reflected in the sharper peak observed around the 1300 cm^{-1} region [122]. The peak broadening and increased depth may indicate a rise in acidic groups, such as carboxylic groups [123], which is also supported by the Boehm titration results (section 3.1.5).

3.1.4. X-ray Diffraction Results

Figure 7 shows the XRD patterns of both OSW and OSAC. The notable diffraction peaks at 2θ values of 16.58° and 23.56° correspond to the crystallographic planes (101) and (200), respectively. These peaks indicate the presence of cellulose, aligning with the amorphous type I structure of cellulose in both OSW and OSAC. A study by Akinhanmi and colleagues examined the effectiveness of using agricultural by-products derived from orange peel (OP) to remove cadmium ions from a liquid solution [124]. The XRD analysis of OP revealed two distinct peaks at 2θ = 16.3° and 22.3°, corresponding to the (101) and (200) planes, respectively. These findings suggest the amorphous nature of cellulose type I in the sample [124] .

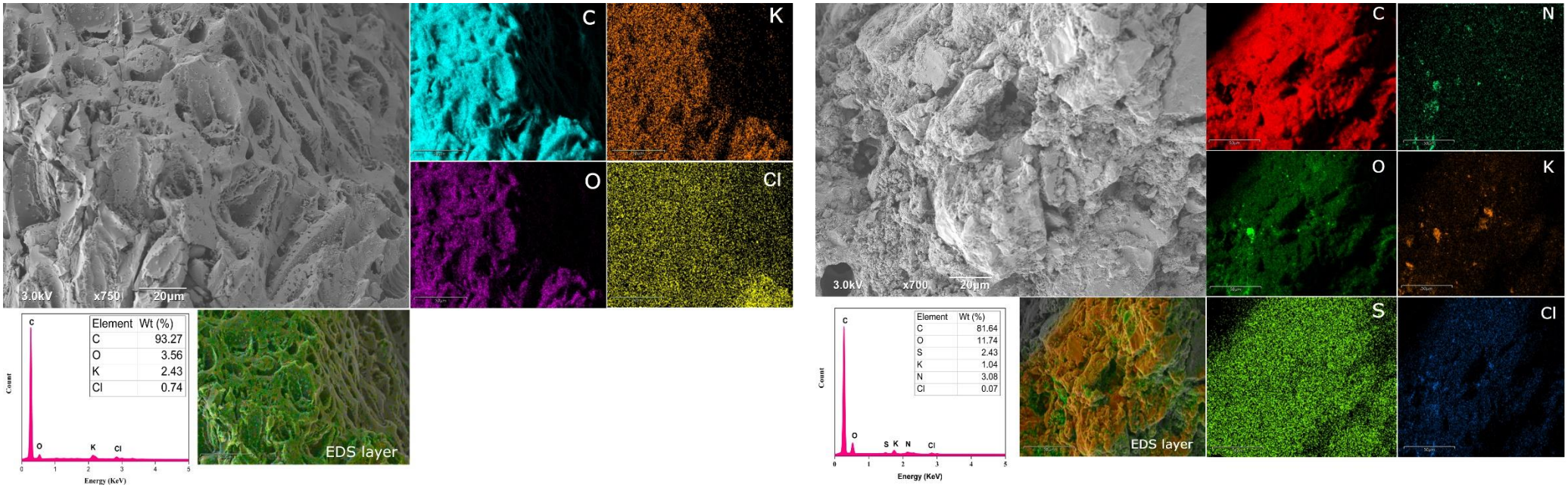

Figure 5 SEM-EDS for OSAC9 (A) and OSAC9 after adsorption (B)

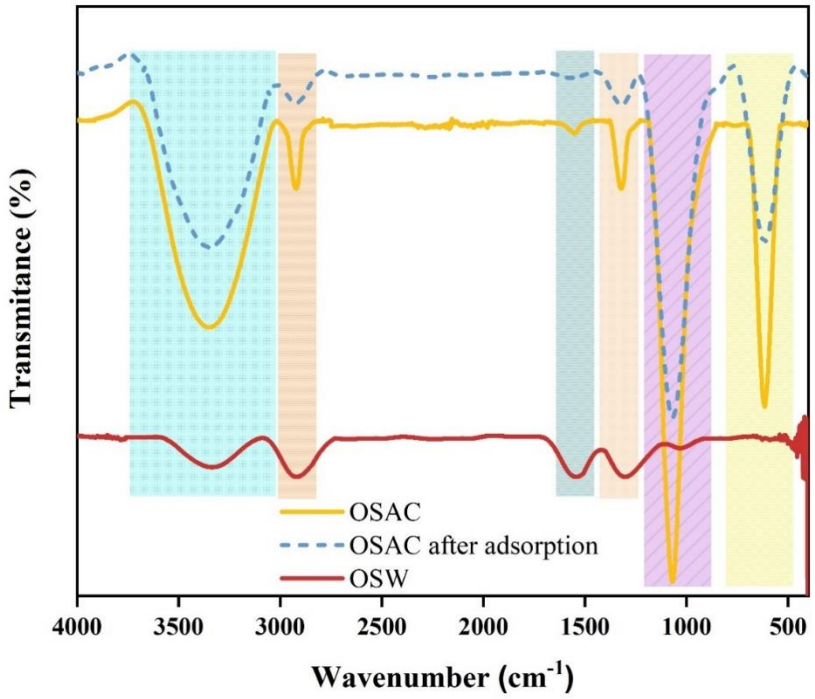

Figure 6 FTIR of OSW, OSAC and OSAC after adsorption

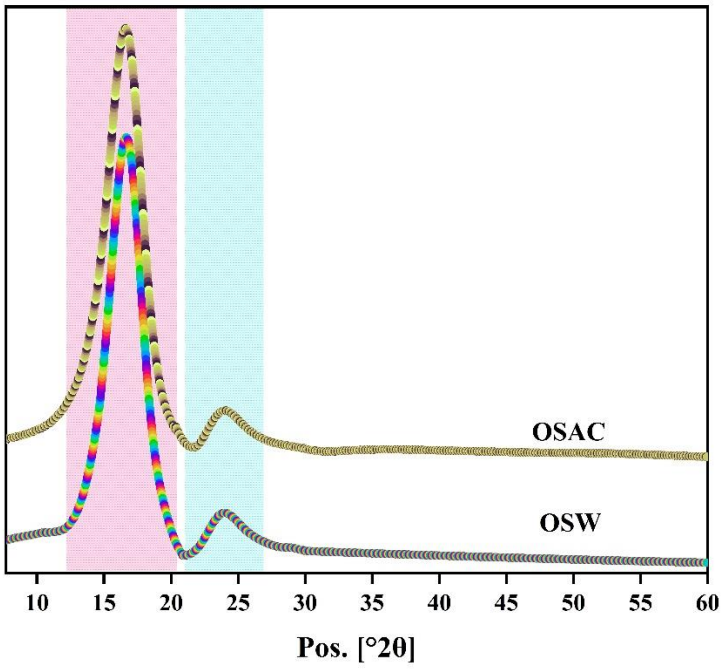

Figure 7 XRD for OSW and OSAC

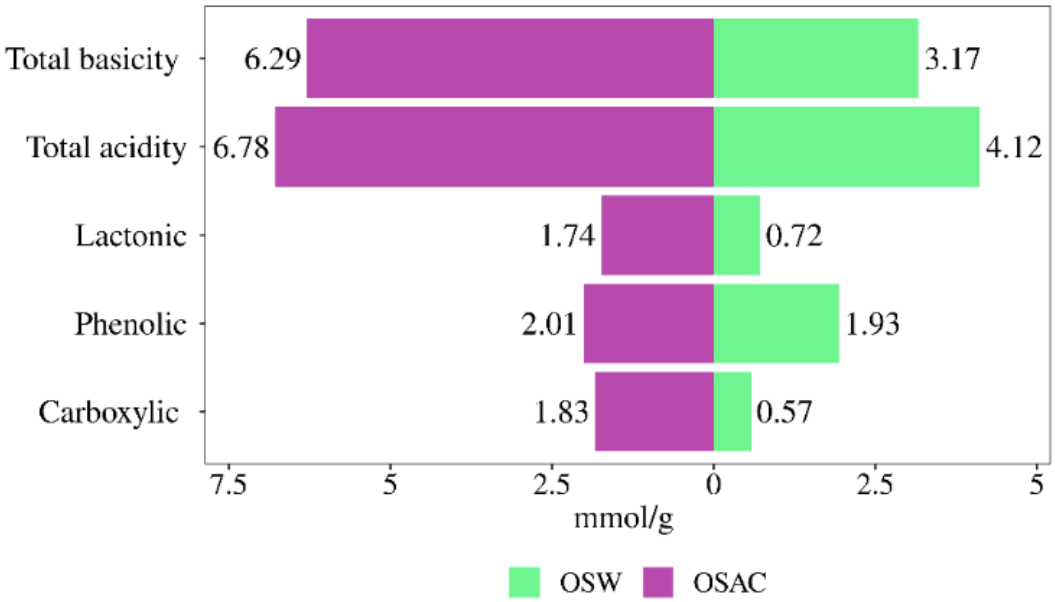

Figure 8 Functional groups for OSW and OSAC

3.1.6. Proximate and Ultimate Analysis

The results of the proximate and ultimate analysis of OSW and OSAC are presented in Table 6. OSW has high volatile matter and moisture content, along with low ash and sulfur content. These findings align well with those reported by Fadhil and Kareem [126] . In their study, the following values were obtained: carbon (47.10%), hydrogen (6.23%), nitrogen (0.21%), oxygen (46.46%), moisture (6.22%), volatile matter (82.22%), fixed carbon (11.11%), and ash (0.45%)[126] , which are similar to our results. After activation, the moisture and volatile content decreased, while the fixed carbon and ash content increased. Additionally, the ratios of hydrogen, oxygen, and nitrogen to carbon decreased, whereas the sulfur-to-carbon ratio increased, which may explain the presence of sulfur in the EDS results.

3.2. Impact of Adsorption Parameters

3.2.1. pH and pH_{pzc}

The pH of the liquid not only affects the ionization of the pharmaceuticals but also the surface properties of the OSAC [95], [127]. Therefore, its effect on the removal of pharmaceuticals was assessed, and the results are presented in Figures 9A and B. Figure 9C illustrates the change in OSAC surface charge with pH. It appears that pH had little impact on the adsorption efficiency of

the contaminants. The adsorption efficiencies remained relatively stable across the pH range of 2 to 8, with a slight decrease observed between pH 9 and 11. At pH 11, the adsorption efficiency was approximately 95.5%. Diclofenac and ciprofloxacin have pKa values of 4.15 and 6.00, respectively. At a pH higher than their pKa, these compounds exist in their ionized forms. OSAC has a pHpzc of 7.85, as shown in Figure 9C.

Table 6 OSW and OSAC physical properties and elemental composition

Parameters (%)	**OSW (Wt%) ±SD**	**OSAC (Wt%) ±SD**
Moisture content	8.21± 0.02	5.93±0.32
Volatile matter	74.52 ±1.08	15.27±1.18
Ash	2.94 ± 0.02	5.32±0.19
Fixed carbon	14.33 ± 1.25	73.48±2.42
C	48.37 ±1.74	72.59±1.93
O	43.38±1.19	18.53±1.08
H	6.33±0.16	2.62±0.16
N	1.81±0.07	4.59±0.10
S	0.11±0.04	1.67±0.06
H/C	0.130	0.036
O/C	0.896	0.255
N/C	0.037	0.063
S/C	0.002	0.023

At a lower pH, the surface of the OSAC carries an overall positive charge, which attracts anions from the solution. At this pH, diclofenac and ciprofloxacin are expected to be ionized, suggesting the possibility of electrostatic interactions playing a role in adsorption [128], particularly within the range of 4.15–7.85 for diclofenac and 6.00–7.85 for ciprofloxacin. The electrostatic attraction

is expected to diminish outside the aforementioned pH ranges for diclofenac and ciprofloxacin. When the pH of the solution is lower than the pHpzc, the adsorbent becomes protonated and develops a net positive charge on its surface [129]. The pKa of pharmaceuticals is also linked to their octanol–water partition coefficient (KOW), a measure of a material's hydrophobicity [130]. It has been reported that hydrophilic interactions between ionizable pharmaceuticals and hydrophilic mesoporous silica dominate at pH values below the pKa [131]. For hydrophobic materials, such as activated carbon, changes in pH can alter the ionization of pharmaceuticals, either enhancing or inhibiting hydrophobic interactions. This suggests that outside the effective range for electrostatic interactions, hydrophobic interactions may contribute to the adsorption process. As the pH increased to 11, the adsorption of both pollutants decreased due to increased electrostatic repulsion between the negatively charged OSAC surface and the anionic pharmaceuticals. This phenomenon becomes more pronounced at higher pH values [132].

3.2.2. Effect of Reaction Time and Pollutant Concentration

The reaction time is a critical parameter that significantly influences the adsorption capacity of OSAC. As shown in Figure 10A, adsorption occurs rapidly during the first hour, primarily due to the large number of unoccupied sites on the OSAC surface that are readily available for the adsorption of contaminant molecules. Once the outer surface of the adsorbent becomes fully saturated, the pharmaceutical molecules are likely to diffuse to internal sites within the adsorbent particles [133]. The removal of both diclofenac and ciprofloxacin remained relatively steady after 75 min. Similar results were reported for diclofenac removal using commercial activated carbon [128] , underscoring the fact that the prepared OSAC has an adsorption capacity comparable to that of commercial products. Wakejo and colleagues studied chemically modified bamboo biochar produced from bamboo sawdust for the efficient removal of ciprofloxacin (CIP) from a liquid solution [134]. The modified bamboo biochar (MBC) demonstrated much higher efficiency in removing CIP (96%) compared to the unmodified bamboo biochar (UBC) (45%). The effect of different initial concentrations of pollutants on the efficacy of OSAC adsorption was evaluated, and the results are shown in Figure 10B. These experiments were conducted for 90 min at a pH of 7, with an optimal adsorbent dose of 1 g/L and a temperature of 25 °C. During the 90-minute reaction time, the removal efficiency decreased from 99.84% to 90.43% as the initial concentration increased from 10 mg/L to 60 mg/L. This reduction in removal efficiency could be attributed to

the decreased availability of active sites for contaminant molecules, as these sites quickly become fully occupied at higher concentrations.

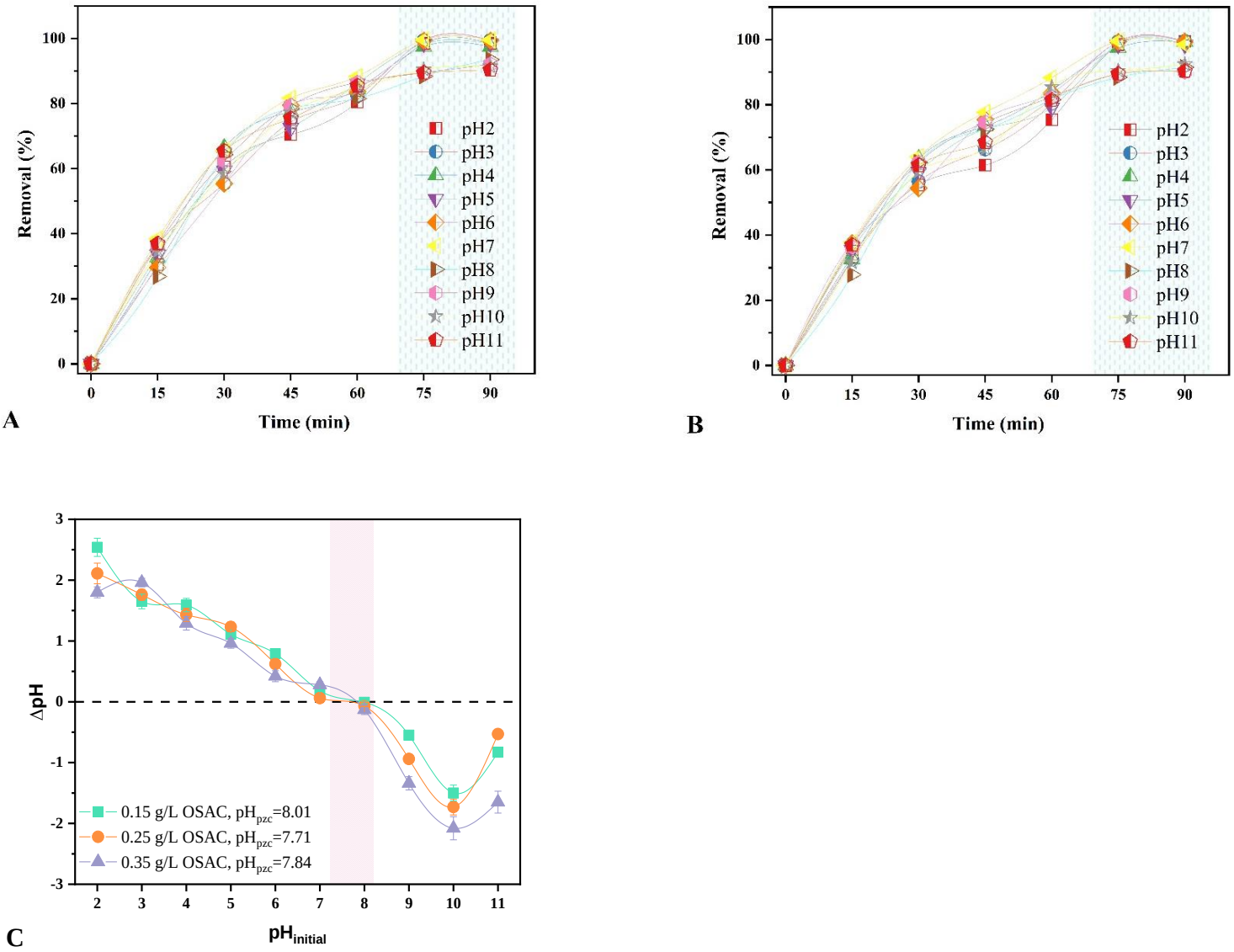

Figure 9 Effect of pH solution on the removal efficiency for diclofenac (A) and ciprofloxacin (B) and pH_{pzc} for OSAC with different concentrations (C)

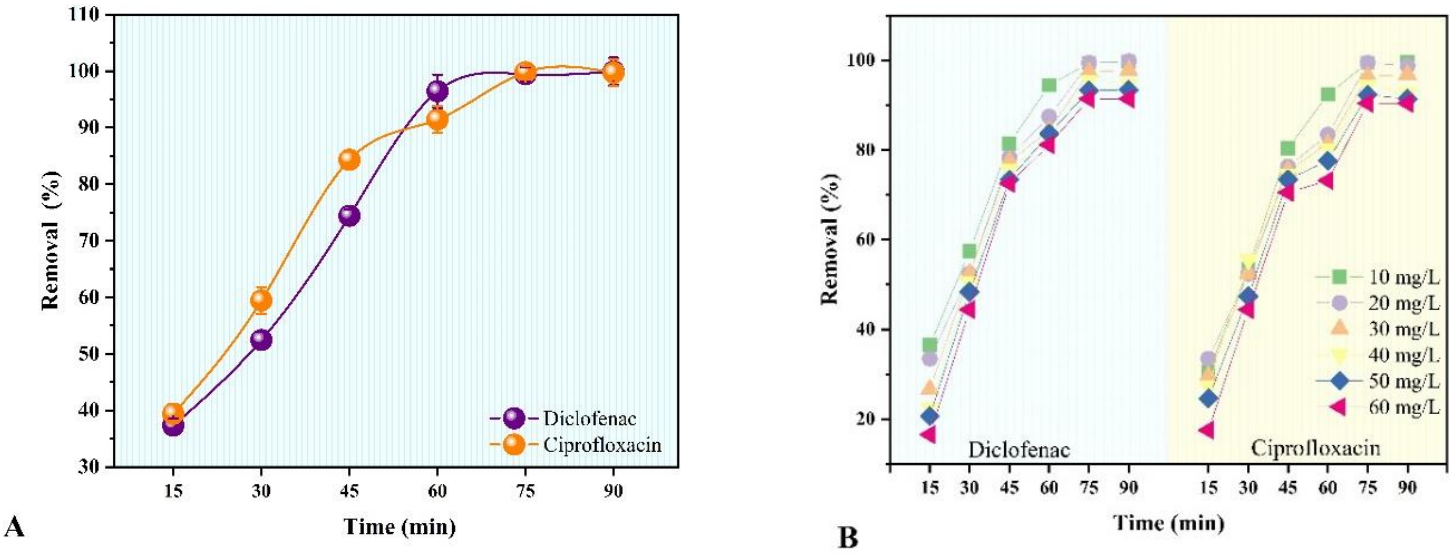

Figure 10 Effect of reaction time on pharmaceuticals removal efficiency (A), Effect of different contaminant's concentrations on removal efficiency (B) (Conditions: pH 7; C_0, 50 mg/L; OSAC dosage, 1 g/L; temperature, 25 °C)

3.2.3. Effect of OSAC Dosage and Temperature

The optimal adsorbent dosage can enhance the efficacy of pollutant elimination while preserving carbon material, which is important for the process's economic feasibility [135]. The impact of OSAC dosage on the adsorption of pollutants was investigated by varying the amount of adsorbent within the range of 0.2 to 1.2 g/L (Figure 11A). As the OSAC dose increased from 0.2 to 1.2 g/L, there was a proportional rise in the adsorption ratio, improving from 63.10% to nearly complete removal (99.93%) after the treatment time elapsed. The increase in adsorbent dosage enhances the surface area available for adsorption, leading to higher removal rates [136]. Conversely, using smaller amounts of adsorbent results in the OSAC surface quickly becoming saturated with contaminants. The capacity of the adsorbent to capture pollutants showed only minimal changes when the dosage exceeded 1 g/L, suggesting that this is the optimal dose for removing diclofenac and ciprofloxacin with OSAC. This trend has also been observed by other researchers who tested different adsorbents for the removal of various contaminants from water [137], [138]. Several possible reasons may explain this behavior. The adsorption process is driven not only by the availability of active sites but also by the concentration gradient between the bulk solution and the adsorbed materials on the adsorbent surfaces. Given the marginal difference between concentrations of 1 g/L and 1.2 g/L, a decision has been made to employ an adsorbent quantity of

1 g/L. This strategic choice aims to mitigate the economic implications associated with the proposed procedural approach.

Temperature is considered a crucial design component that significantly influences adsorption efficacy. Studying the impact of temperature is important to evaluate the adsorbent's performance in various environmental conditions that reflect diurnal and seasonal temperature changes. The removal of diclofenac and ciprofloxacin over a temperature range of 5–35 °C is shown in Figure 11B. Increasing the temperature from 5 °C to 20 °C more than doubled the removal of both pharmaceuticals. Higher temperatures enhance the adsorption processes, as the increase in kinetic energy and the reduction in solution viscosity lead to an improved diffusion rate, thereby boosting the adsorbent's ability to capture pollutants[139]. The removal efficiency increased slightly more at 25 °C; however, further increases in temperature did not result in a significant increase in removal. Desorption was unlikely to occur in our study, as the removal did not decrease but plateaued at temperatures above 30 °C. Changes in removal also depend on whether the adsorption process is endothermic or exothermic [140]. The adsorption of diclofenac and ciprofloxacin onto OSAC was found to be endothermic (see the following section), which explains why a reduction in removal was not observed at 30–35 °C.

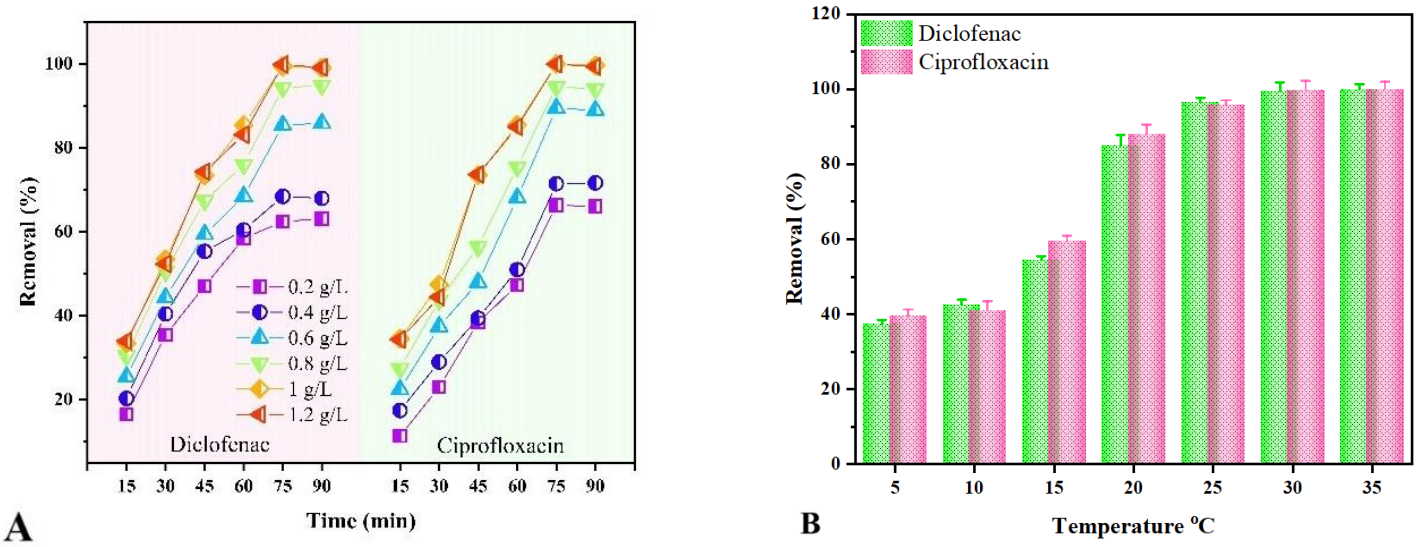

Figure 11 Effect of different OSAC dosages on removal efficiency (A), Effect of virous temperatures on removal efficiency (B). (Conditions: pH 7; C_0, 50 mg/L; OSAC dosage, 1 g/L; temperature, 25 °C)

3.2.4. Kinetic and Isotherm and Desorption Results

The findings from fitting experimental data to the Langmuir and Freundlich isotherm models, as well as the pseudo-first and second-order kinetic models and thermodynamic parameters, are shown in Figures 12 (A-E). The Langmuir isotherm model (Figure 12 A) provided a more accurate representation of the adsorption data for the compounds compared to the Freundlich model (Figure 12 B), resulting in correlation values of 0.971 for diclofenac and 0.943 for ciprofloxacin. The residual sum of squares (SSE), also known as the error sum of squares, was calculated for both the isotherm and kinetic models (Table 3). A low SSE indicates a strong match between the model and the data, which was the case for the Langmuir model as opposed to the Freundlich model. It can be inferred that the pharmaceutical compounds likely formed a monolayer on the surface of OSAC. The maximum theoretical sorption capacities (qm) for diclofenac and ciprofloxacin, based on the Langmuir isotherm, were determined to be 256.41 mg/g and 294.98 mg/g, respectively. The compounds exhibit favorable adsorption, as indicated by the separation factor (RL) values ranging from 0 to 1.

The experimental correlation coefficients showed the strongest alignment with the pseudo-first-order kinetic model (Figure 12 C), suggesting that the adsorption rate of the chemicals onto OSAC is primarily controlled by the concentration difference between the solid and liquid phases. This also indicates that external or internal diffusion may be the rate-limiting step in the process[141]. Table 7 presents the fitting parameters for the isotherm and kinetic models. The adsorption rate constant exhibited an inverse relationship with 1/T, indicating a favorable impact of temperature on the efficiency of adsorption (Figure 12 E). The diclofenac and ciprofloxacin exhibited spontaneous adsorption onto OSAC, as shown by the negative ΔG° values obtained at four different temperatures (Table 8). The calculated enthalpy values (ΔH°) were positive, indicating that the adsorption process is endothermic. Positive entropy values (ΔS°) suggest that the adsorption process is stable and occurs randomly [142]. The calculated values of ΔG°, ΔH°, and ΔS° are presented in Table 7. The desorption efficiency of contaminants from OSAC using different desorbing agents is shown in Figure 12 F. Among the desorbing agents tested, ethanol appeared to be the most efficient, achieving recoveries of 87.83% and 86.41% for diclofenac and ciprofloxacin, respectively.

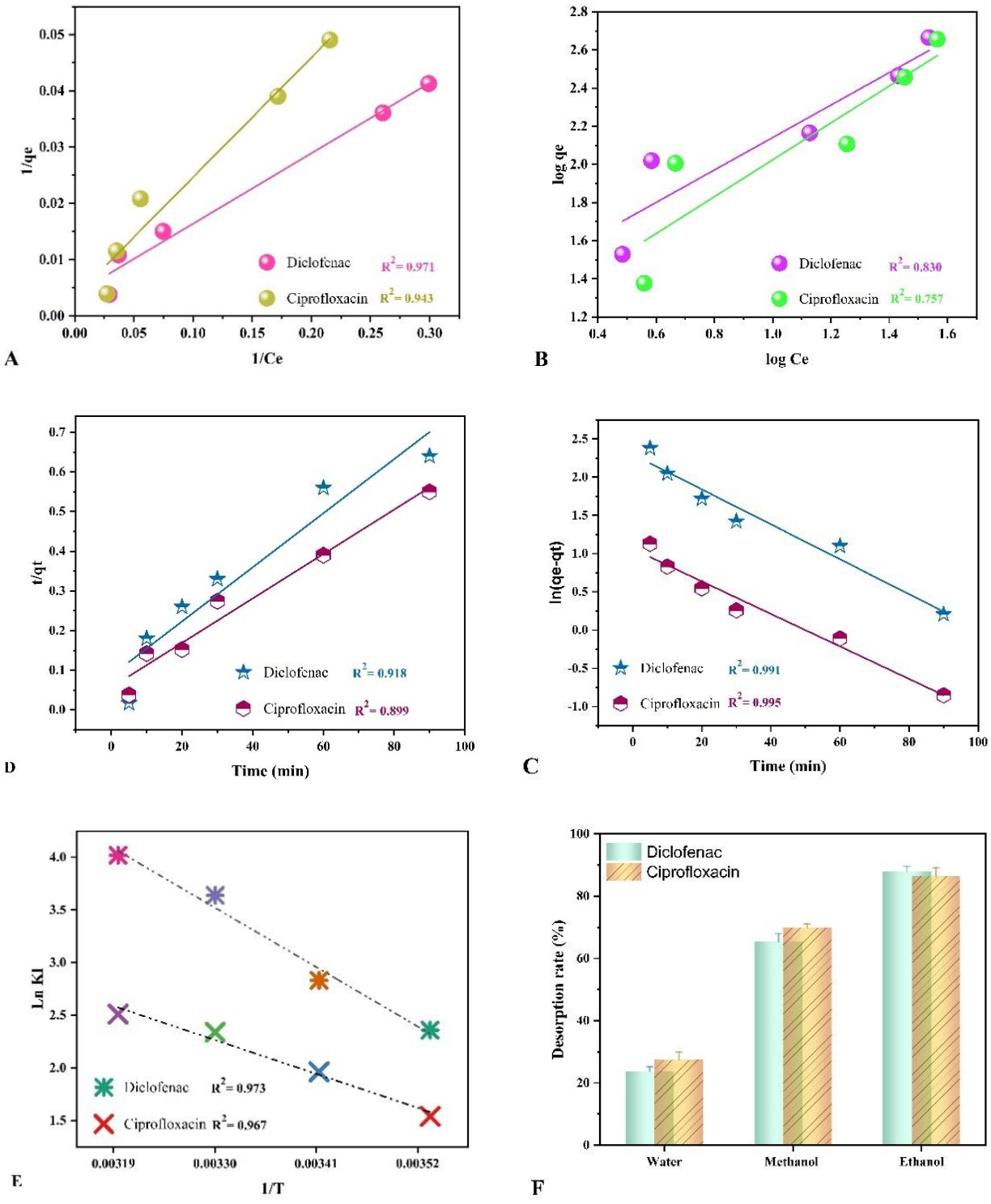

Figure 12 Experimental data fitting against (A) the Langmuir isotherm, (B) the Freundlich isotherm, (C) the Pseudo first-order kinetics model, (D) the Pseudo second-order kinetic model, (E) thermodynamic parameters plot, and (F) desorption with different media.

Table 7 The parameter of Langmuir, Freundlich, Pseudo-1st-Order Model and Pseudo-2nd-Order Model

Langmuir	q_{max} (mg/g)	K_L	R_L	R^2	SSE
Diclofenac	256.410	0.031	0.865	0.971	2.28E-5
Ciprofloxacin	294.985	0.016	0.926	0.943	6.03E-5
Freundlich	1/n	K_f	R^2		
Diclofenac	0.850	19.498	0.83		0.097
Ciprofloxacin	0.966	11.402	0.757		0.175
Pseudo-1st-Order Model	qe (mg g^{-1})	K1	R^2		
Diclofenac	9.944	-1.58E-05	0.948		
Ciprofloxacin	2.906	-1.47E-05	0.961		
Pseudo-2nd-Order Model	qe (mg/g)	qe^2	K2	R^2	
Diclofenac	1.47E+02	2.16E+04	5.34E-04	0.899	
Ciprofloxacin	1.79E+02	3.19E+04	5.50E-04	0.958	

Table 8 Thermodynamic parameters of pollutants adsorption on OSAC

Compound	Temperature (K)	Kl	ΔG°	ΔH°	ΔS°	R^2
Diclofenac	283	10.590	-5.552			
	293	16.281	-6.893	42.650	170.021	0.973
	303	53.624	-9.169			
	313	55.701	-10.461			
Ciprofloxacin	283	4.664	-3.623			
	293	7.120	-4.781	24.351	99.186	0.967
	303	10.381	-5.894			
	313	12.329	-6.536			

3.2.5. Long-term Performance of OSAC in Terms of Pharmaceutical Removal

While using synthetic samples is important for understanding the interaction between adsorbents and adsorbates, we cannot have a firm idea of how effective adsorbents are in removing target contaminants without testing them in a natural sample matrix. The removal of diclofenac and ciprofloxacin was evaluated using spiked lake water and secondary effluent. Table 9 displays the attributes of these water samples. Figure 13 (A-F) shows the removal efficiency of diclofenac and ciprofloxacin from different water matrices over seven cycles using 1 g/L OSAC, pH 7, 25 °C, and a pollutant concentration of 50 mg/L. As seen in Figure 13, the removal efficiency during the first two cycles (R1 and R2) was above 96% across all water matrices, but it began to decrease afterward at different rates. Overall, the developed material consistently performed well over the seven cycles, with a removal efficiency above 50% for both contaminants in R6 for both MQ water and lake water. Wastewater, on the other hand, exhibited a removal efficiency of over 40% for contaminants in R6. OSAC demonstrated better regeneration and overall performance than biochar derived from Melia azedarach fruit, which removed 88% of diclofenac in the first cycle, but the removal dropped to 16% in the sixth cycle [143]. However, graphitic biochar activated with potassium ferrate was reported to maintain a high diclofenac removal rate of over 80% up to the fifth cycle [144]. The modified graphitic biochar, however, was not tested with natural water samples. A biochar prepared from stem extract showed much lower removal of ciprofloxacin compared to OSAC [145]. The removal of ciprofloxacin using Phoenix dactylifera biochar dropped from just above 36% in the first cycle to 7% in the seventh cycle. This highlights the promising potential of OSAC as an effective adsorbent for pharmaceutical removal.

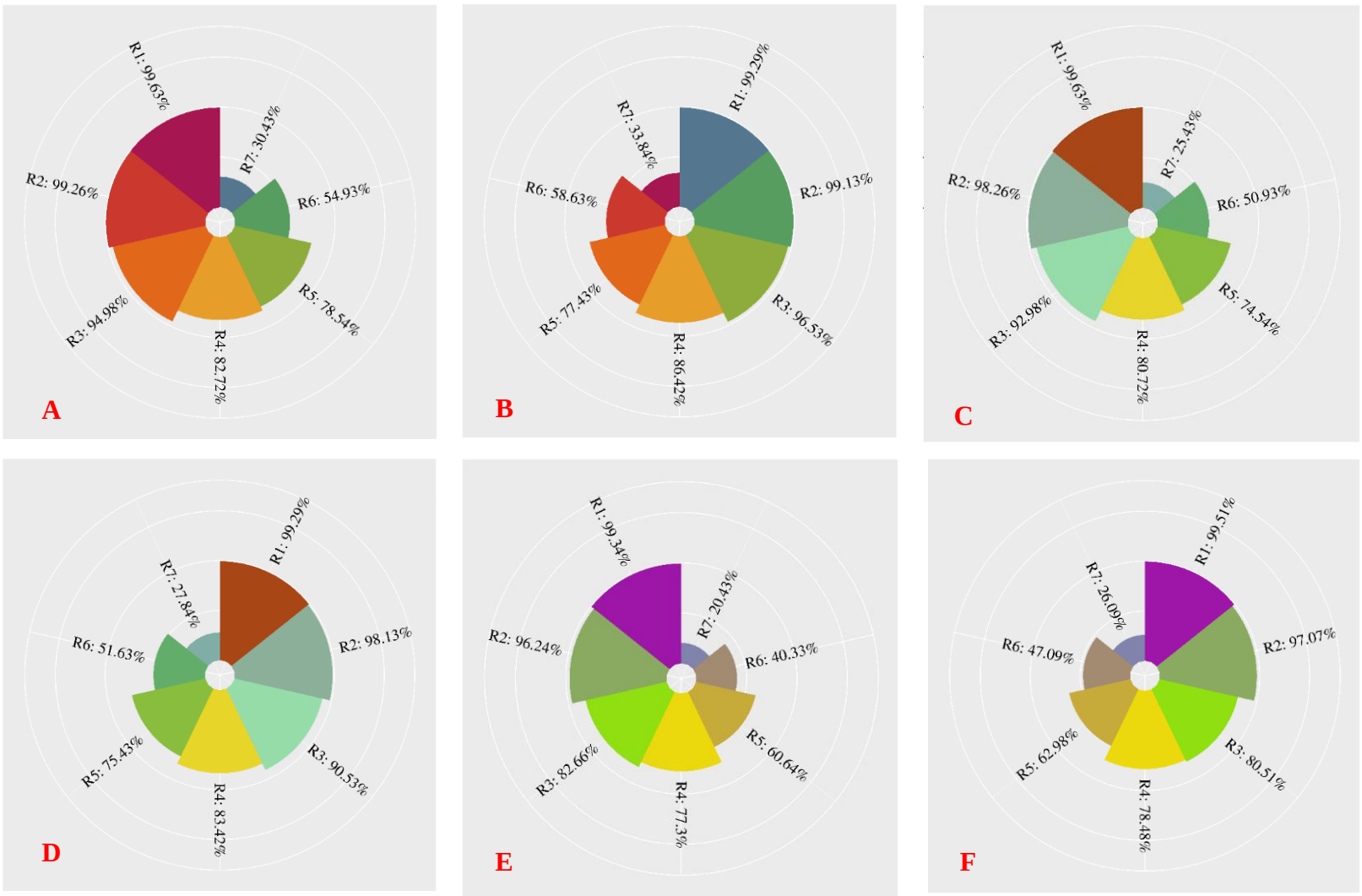

Figure 13 The removal efficiency of diclofenac in MQ water (A), ciprofloxacin in MQ water (B), diclofenac in lake water (Lake Balaton, Hunagry) (C), ciprofloxacin in lake water (Lake Balaton, Hunagry) (D), diclofenac in secondary effluent (E), and ciprofloxacin in secondary effluent (F), over sequential seven cycles. The standard deviations were between 1.53 % for cycles

3.2.6. Comparison of Prepared OSAC with Other Reported Systems

First and foremost, most of the reported applications of olive stone for the removal of pharmaceuticals in different aqueous solutions did not take into consideration a mixture of pollutants but rather tested only one contaminant, which rarely occurs in real polluted solutions. As seen in Table 10, the current activated carbon derived from olive stones shows superior removal of pharmaceutical chemicals, with more than 99% efficiency, whereas other methods showed

lower performance. This makes the current system more suitable for different polluted aqueous media.

Table 9 Secondary effluent and Lake water characteristics

Secondary effluent	Concentration (mg/L)	Lake water	Concentration (mg/L)
Chemical oxygen demand	65.20±3.43	Chemical oxygen demand	25.12±2.48
Biochemical oxygen demand (5 days)	24.19 ±2.42	Biochemical oxygen demand (5 days)	11.41 ±1.02
Suspended solids	26.68±2.10	Total Phosphorus	1.43±0.27
Volatile suspended solids	16.49± 1.24	Ammonium nitrogen (NH_4-N)	0.08±0.02
Total Phosphorus	5.43±0.43	Electrical conductivity	647±2.91µmoss/cm
Ammonia	12.54±0.93 (NH_3-NH_4)	Total nitrogen	2.27± 0.04
Electrical conductivity	849±3.72 µmoss/cm	Turbidity (NTU)	33.09± 1.32
Total Kjeldahl nitrogen	12.43 ± 1.26	pH	8.52
Nitrate-nitrite	3.65 ± 0.39 (NO_2-NO_3)	Temperature (^oC)	23.5
Total solids	562± 3.98		
Total dissolved solids	521± 4.79		
pH	6.9		
Temperature (^oC)	27.4		

Table 10 Reported olive stones applications for pharmaceutical removal from aqueous solution

Compound	Adsorbent	Removal (%)	References
Clofazimine	Olive stone biochar	98.10	[146]
Amoxicillin	Phosphoric acid activation of olive stone	93	[147]
Drin pesticides	Acid treated olive stones	More than 90	[148]
Clofazimine	Magnetic olive stone biochar	98.61	[146]
Paracetamol	Olive stone biochar	98	[149]
diclofenac and ciprofloxacin	KOH activation of olive stone	More than 99%	This work

3.3. BPAC Activation by H_3PO_4

3.3.1. Characterization of BPAC

3.3.1.1. FTIR Results

An FTIR analysis was conducted to examine the surface characteristics of the produced BPAC. Simply put, this analysis highlighted the spectroscopic features of the sample, revealing prominent peaks attributed to functional groups that influence the adsorption process. The FTIR spectra of BPAC displayed distinct bands at 3422 cm^{-1} (bonded O–H group), 1575 cm^{-1} (carbonyl group), and 2919 cm^{-1} (secondary amine group), which are associated with functional groups likely facilitating the effective adsorption of contaminants (Figure 14ii). Previous research has emphasized the importance of these functional groups in adsorption processes [150]. Additional bands detected in the BPAC, potentially contributing to the interactions, included 1301 cm^{-1} (symmetric bending of CH_3), 1080 cm^{-1} (stretching of ethers—C=O=C), 1244 cm^{-1} (stretching of $–SO_3$), and 622 cm^{-1} (stretching of –CN). An observable shift in the adsorption band, particularly at 3422 cm^{-1}, indicated significant modifications in the spectroscopic characteristics of the BPAC

surface due to the successful adsorption of pollutant molecules, as has been noted in other studies [150]. The FTIR spectra of BPAC before and after adsorption clearly shows that the surface interacted with the pollutant molecules, with wider bands observed after adsorption. Similar trends have been reported in previous work [150].

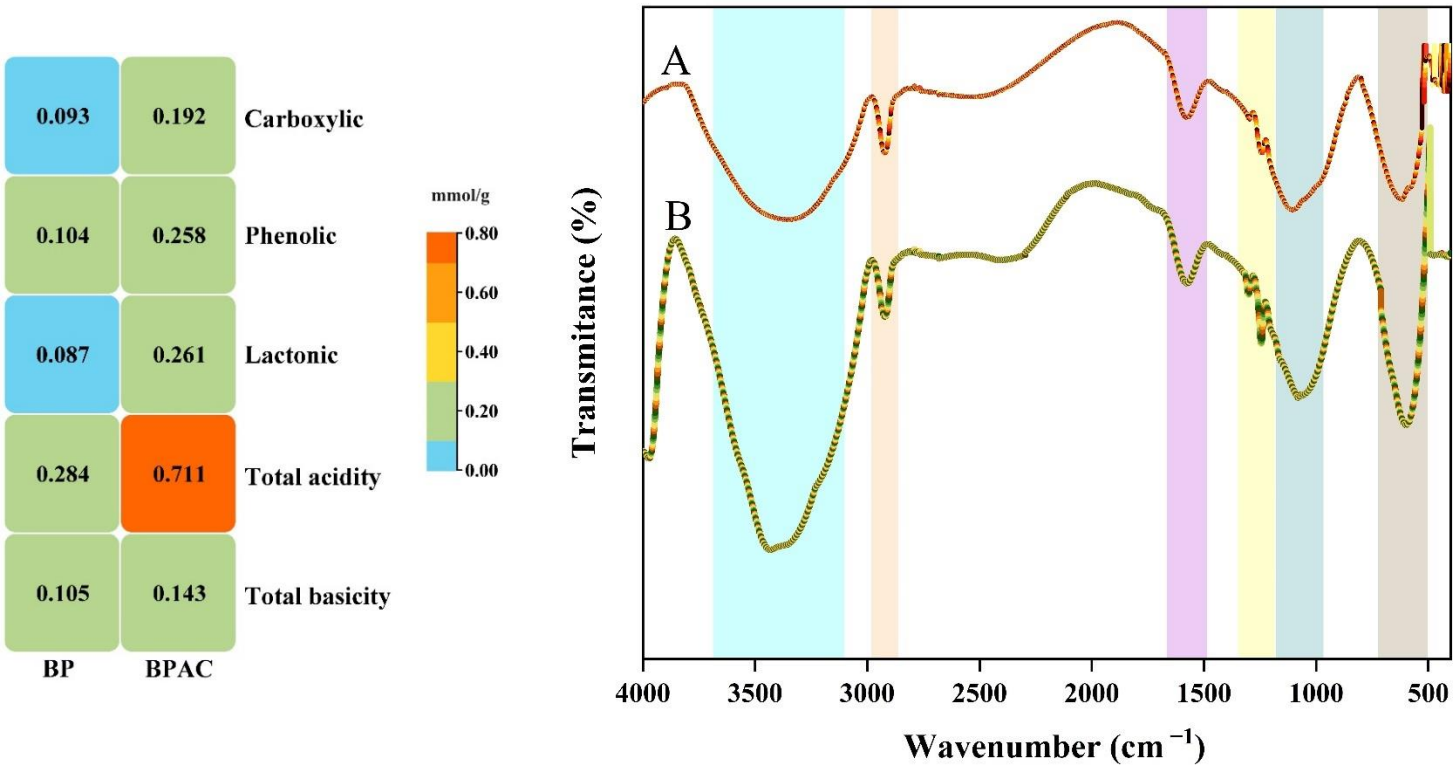

(i) **(ii)**

Figure 14 Boehm titration for BP and BPAC (i) and FTIR for BPAC before the adsorption (A) and BPAC after the adsorption (B) (ii).

3.3.1.2. Boehm Test

Activated carbons are often characterized by the presence of oxygen-containing functional groups, which have a significant impact on the surface characteristics and adsorption capabilities of the carbons. Boehm's titration for BPAC determined that the acid and basic groups present were carboxylic, lactonic, and phenolic at 0.192, 0.261, and 0.258 mmol/g, respectively. The overall concentration of acidic groups of BPAC was 0.711 mmol/g, whereas the concentration of total basicity was 0.143 mmol/g. The data directly demonstrates that the BPAC surface has a greater

abundance of acidic groups compared to basic groups. Furthermore, it has been shown from Figure 14i that the total acidic groups of BPAC have elevated by 2.5 times compared to BP, and by 1.36 times in terms of total basicity. The surface is thus predominantly acidic as suggested by the pH_{pzc} (5) value obtained. Other studies, for example, Agboola and Bello worked on banana stalk activation by phosphoric acid to remove ciprofloxacin from aqueous media [150]. The study revealed the total acidity to be 0.699 mmol/g and the total basicity to be 0.158 mmol/g.

3.3.1.3. SEM-EDS Results

The SEM analysis examined the morphological composition of activated carbon derived from banana peels (Figure 15). The SEM image showed the activated carbon surface with a semi-regular and heterogeneous morphology, characterized by a large number of pores of varying shapes and sizes. After the adsorption process, the SEM image revealed that some pores were filled, while others remained available for further adsorption. This suggests that there are still potential sites available for chemical adsorption. EDS was employed for elemental composition analysis and chemical characterization of the activated carbon. The analysis confirmed the presence of carbon, oxygen, silicon, and potassium in the activated carbon derived from banana peels (Figure 15). The findings were consistent with the results reported by Hussain and colleagues [151], particularly in regard to the silicon content in BPAC, which matched the silicon content of the original fruit peels. Additionally, it was observed that the sulfur content increased after the adsorption process, indicating that a chemical reaction had taken place. The appearance, disappearance, or fluctuation in element concentrations on the EDS spectrum after adsorption is a common observation in both inorganic [152], [153] and organic [154] adsorption studies, highlighting the involvement of these elements in the interaction between adsorbates and adsorbents.

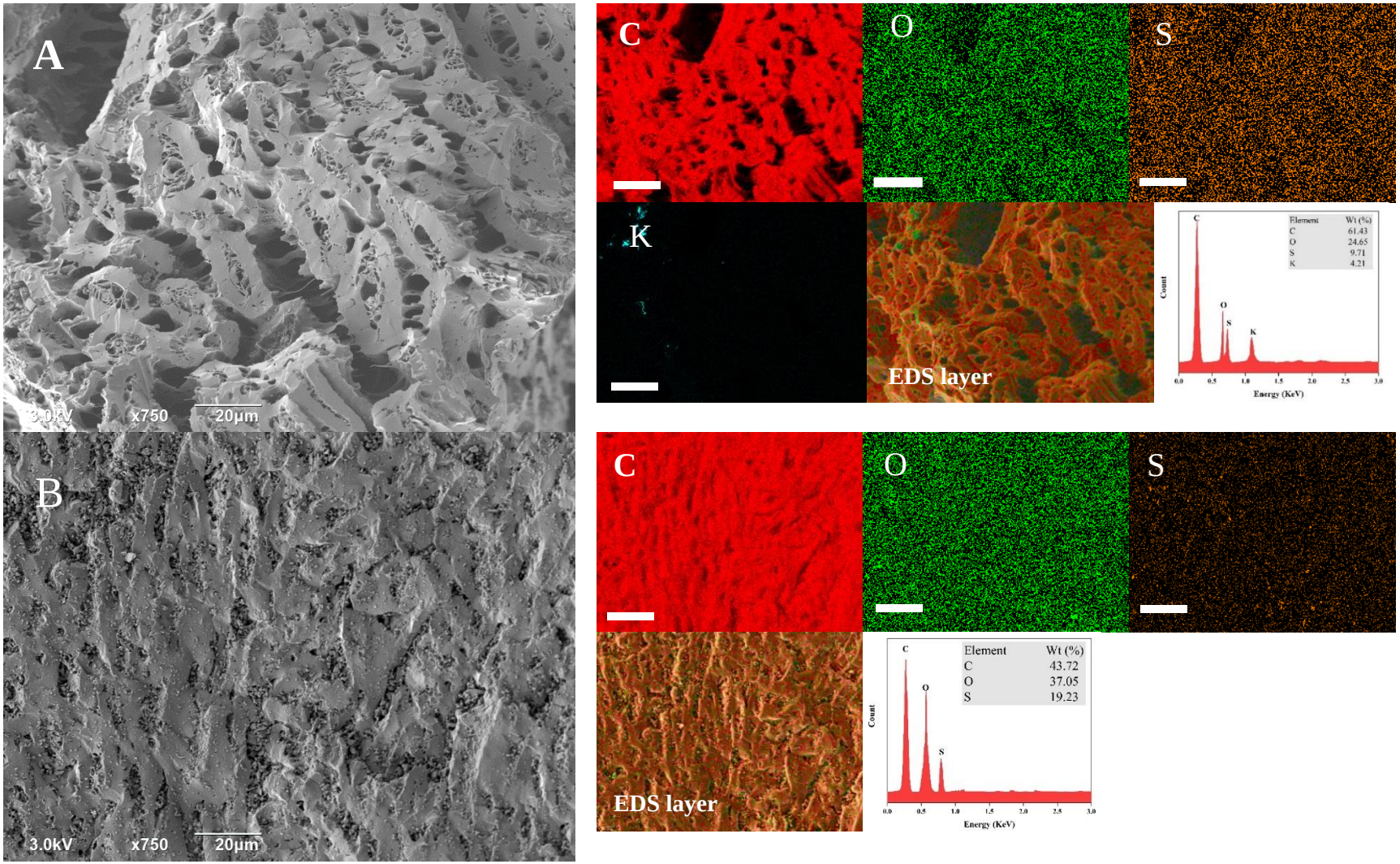

Figure 15 SEM-EDS for BPAC before the adsorption (A) and BPAC after the adsorption. (B) The EDS scale is 20 µm

3.3.1.4. X-ray Diffraction Results

Figure 16A shows the XRD spectrum of BPAC before and after adsorption. It exhibits a prominent peak at a 2θ value of 23.84° (pink), which corresponds to the d-spacing in the aromatic region, indicating the presence of a graphitic structure in BPAC [155]. This peak is associated with the (002) graphitic basal plane, reflecting the presence of graphitic-like microcrystals in BPAC [156]. The broad nature of this peak also results in significant scattering at small angles, suggesting that the highly porous BPAC exhibits amorphous characteristics[157]. Additionally, a smaller peak at 41.86° (green), corresponding to the (100) plane, suggests the presence of small domains with well-organized graphene sheets [156]. The sharp peak at a 2θ value of 29.22° (yellow) indicates the presence of calcite in the material [158]. Pharmaceutical adsorption did not cause any notable changes in the XRD spectrum, which is consistent with previous findings reported by Patel and colleagues, who investigated the use of BPAC for the removal of ciprofloxacin and acetaminophen [158].

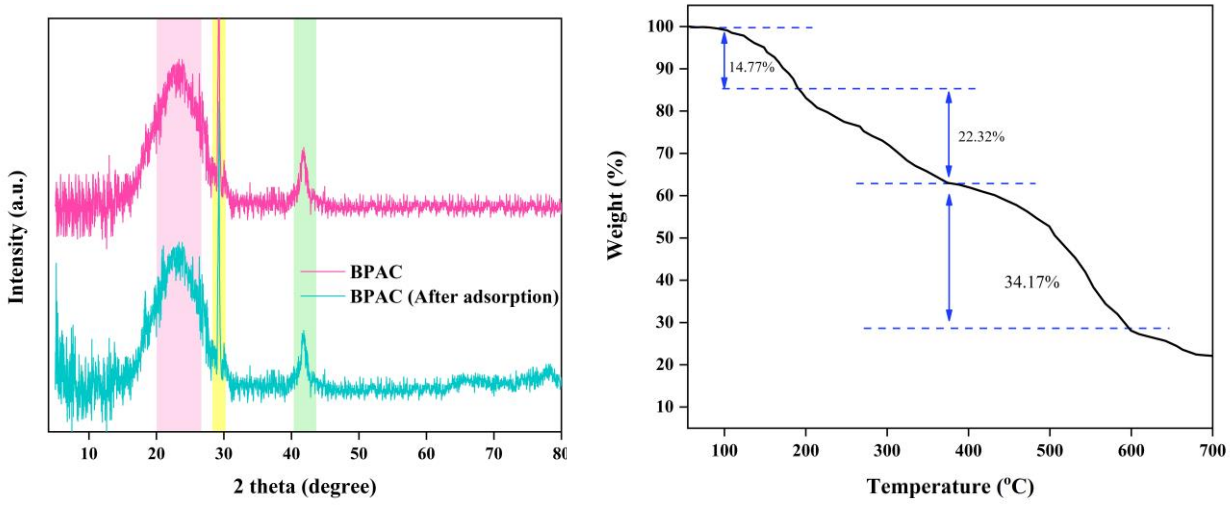

(**A**) (**B**)

Figure 16 X-ray powder diffraction (XRD) for BPAC before and after the adsorption (A) and thermos-gravimetric analysis (TGA) for banana peel (B).

3.3.1.5. Thermogravimetric Analysis Results

The thermogravimetric (TG) analysis of banana peel is shown in Figure 16B. The first phase of the TG curve occurs between 50 and 190 °C, resulting in a weight reduction of about 14.77%. This initial drop is likely due to water loss and the evaporation of volatile organic compounds, including oils, terpenes, and pigments [159]. Additionally, the significant weight reduction may be attributed to the degradation of organic materials such as cellulose and hemicellulose [160]. The second major phase of degradation occurs between 190 and 375 °C. A similar temperature range was reported by Bakar and co-workers [90], who studied the characterization of banana peel activated carbon using phosphoric acid, where the temperature range was between 180 and 350 °C. The final phase of degradation occurs between 375 and 595 °C. Guimaraes and colleagues [161]noted that banana peel, sugarcane bagasse, and sponge gourd fibers experienced significant mass reduction at temperatures above 300 °C, due to the degradation of hemicellulose and cellulose. Moreover, fiber degradation was observed at temperatures above 400 °C, resulting from the breaking of bonds within the fibers' lignin.

3.3.1.6. Point of Zero Charges (pH_{pzc})

The pH at pH_{pzc} of BPAC was calculated to be 5.005, based on the average value shown in Figure 17. These findings indicate that the BPAC surface exhibits a positive charge in the solution up to pH 5, after which it acquires a negative charge. The pH_{pzc} influenced the adsorption of pollutant molecules in the experiment [162]. Pathak and Mandavgane (2015) synthesized raw banana peel to remove citric acid from an aqueous solution [163], and their study found that the pH_{pzc} was 4.98, which aligns with the present results.

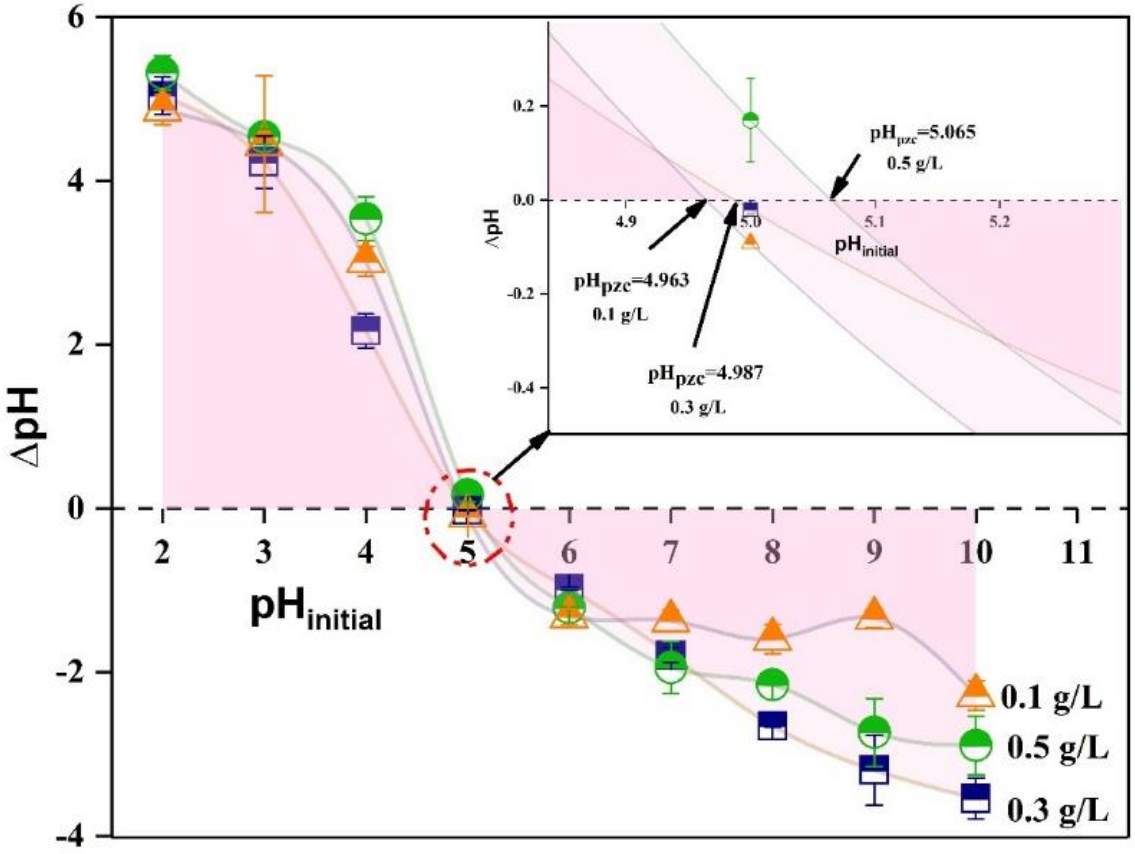

Figure 17 BPAC point of zero charge (pH_{pzc}).

3.3.1.7. Proximate and Ultimate Analysis

The composition and characteristics of the adsorbent are presented in Figure 18, including both the proximate and ultimate analyses. The fixed carbon content increased significantly from 0.67% to 74.07% after the treatment of BP. In contrast, the volatile matter and moisture content dropped substantially from 82.53% and 11.37% to 16.90% and 4.08% for BP and BPAC, respectively. Following treatment, the carbon content rose sharply from 41.83% to 74.03%. However, there was a decrease in hydrogen content (H), from 5.71% to 3.16%, and oxygen content (O), from 51.04% to 19.92%. These changes indicate an elevated level of carbonization in the materials. The molar hydrogen-to-carbon (H/C) ratio reflects the level of carbonization, as hydrogen is mainly associated with plant-derived organic material. The reduction in the H/C ratio after treatment suggests that the sample underwent significant carbonization, as seen in BPAC (H/C = 0.042). The polar groups on the carbon surfaces act as sites for water adsorption and help form water clusters. Therefore, the molar oxygen-to-carbon (O/C) ratio of a char sample can serve as an indicator of

its surface hydrophilicity. The O/C ratio of BP (1.220) suggests that its surface is more hydrophilic compared to BPAC, which has an O/C ratio of 0.269. Adsorbents with a higher O/C ratio typically exhibit a greater concentration of polar groups, likely due to the presence of carbohydrates. The findings from the proximate and ultimate analyses are consistent with other studies by Pathak and Mandavgane [163] and Selvarajoo and colleagues [164].

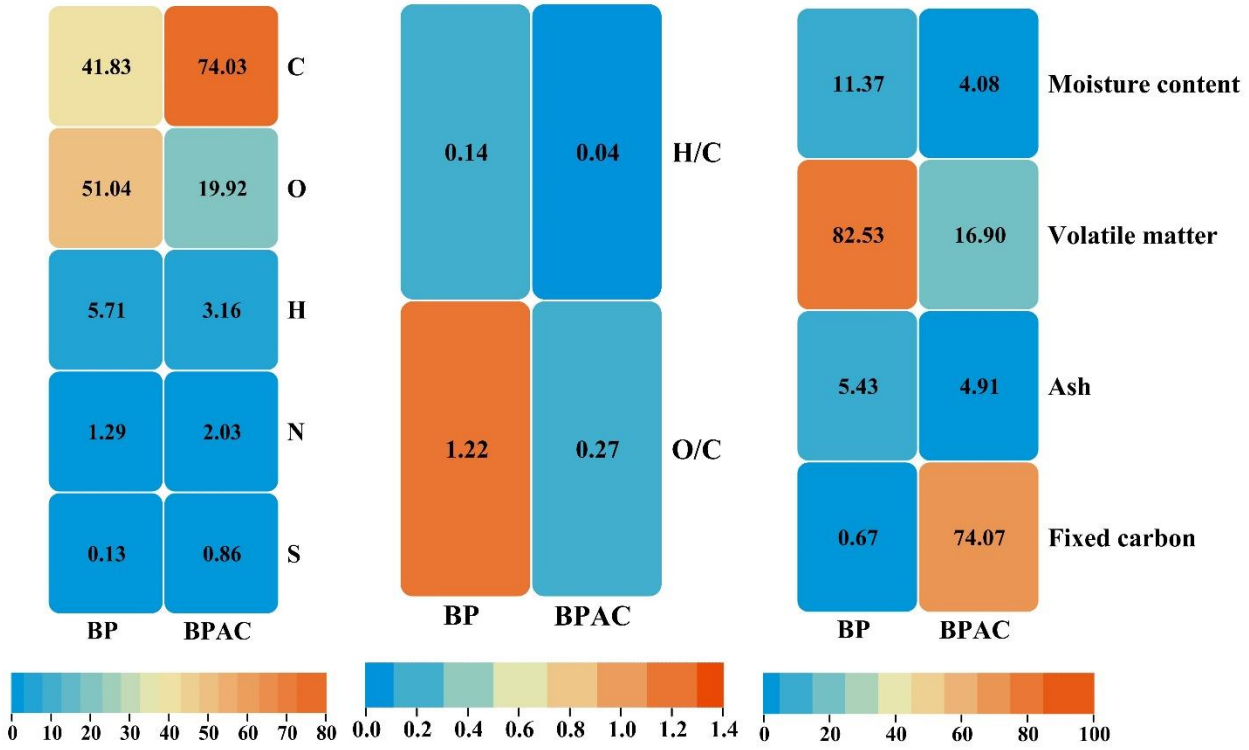

Figure 18 Proximate and ultimate analysis for BP and BPAC.

3.3.1.8. S_{BET} Results

The measured BET surface area of raw BP is 0.650 m²/g. This value is consistent with findings from earlier studies, which reported surface areas of 0.7963 m²/g [165] and 1.73 m²/g [166]. The minimal surface area can be attributed to challenges associated with degassing lignocellulosic materials. Measuring the BET surface area of lignocellulosic waste is difficult due to the premature combustion of the powder before reaching the appropriate degassing temperature. As a result, the degassing temperature is reduced to 100°C, leading to a decrease in surface area due to moisture content [163]. The limited surface area of BP is a characteristic property of carbonaceous materials [167]. Table 11 presents the S_{BET} values for raw BP at different pyrolysis temperatures. After the carbonization process at three different temperatures, it was observed that a carbonization

temperature of 450°C yielded the highest BET surface area of 911.59 m²/g, with better-developed pores. Therefore, the present study was conducted using this material for further investigations. Bakar and co-workers developed activated carbon derived from banana peels at various pyrolysis temperatures [90] . Their study found the highest BET surface area at 470°C (684 m²/g), and 355 m²/g, 587 m²/g, and 503 m²/g at 450°C, 490°C, and 510°C, respectively.

Table 11 S_{BET} and pore structures of BP samples

Samples	**S_{BET} (m^2/g)**	**V_{tot} (cm^3/g)**	**V_{mic} (cm^3/g)**	**V_{mes}(cm^3/g)**
BP raw	0.650	0.062	0.021	0.041
BP @ 350°C	685.75	0.142	0.044	0.098
BP @ 450°C	911.59	0.180	0.070	0.110
BP @ 550°C	508.62	0.136	0.029	0.107

3.3.2. Adsorption Test Results

3.3.2.1. Influence of Adsorption Parameters

The effect of different adsorption parameters on the removal efficiency of amoxicillin and carbamazepine, including BPAC dosages, reaction time, temperature, initial pollutant concentration, and pH ranges, is illustrated in Figures 19 and 20. One of the key components in developing a successful adsorption process is optimizing the BPAC dosage. This optimization can help better predict the equilibrium relationship between the adsorbent and adsorbate, as well as the cost-effectiveness of the treatment process. The influence of BPAC dosage on the adsorption of amoxicillin and carbamazepine was evaluated by introducing different doses, ranging from 0.3 to 1.5 g/L (Figure 19 A and B). When testing concentrations of 0.3 and 0.6 g/L, both pollutants showed only a slight improvement in removal efficiency compared to the higher doses (0.9, 1.2, and 1.5 g/L). This is likely because lower BPAC quantities become saturated with contaminants more rapidly. Increasing the BPAC dosage from 0.9 g/L to 1.5 g/L led to a significant increase in the removal efficiency of amoxicillin, from 84.07% to 96.02%. Carbamazepine followed a similar trend, with its removal efficiency increasing from 87.04% to 90.62% at BPAC concentrations of 0.9 and 1.5 g/L, respectively. According to Shao et al. [168], increasing the BPAC dosage provides

a larger surface area for adsorption, which enhances the removal efficiency of the pollutants. When comparing BPAC dosages of 1.2 and 1.5 g/L for both contaminants, it is clear that only marginal improvements in removal efficiency occurred once the BPAC dose exceeded 1.2 g/L. This suggests that 1.2 g/L is the most effective dosage for removing both amoxicillin and carbamazepine using BPAC. In a related study, Fernandez et al. [169] produced hydrochars from orange peels and used them as bioadsorbents to remove diclofenac sodium, salicylic acid, and flurbiprofen. The highest adsorption capacities for salicylic acid, flurbiprofen, and diclofenac sodium were 0.092, 0.093, and 0.018 mmol/g, respectively, with an optimum adsorbent dose of 0.5 g/L. The adsorption capacity of an adsorbent is enhanced by extending the contact or interaction period. As the duration of contact increases, the adsorption of pollutants rises until it reaches an optimal level [170]. During the adsorption process, there is initially a high rate of sorption due to the large number of available adsorbent sites. However, as time progresses, the rate of adsorption decreases, resulting in a linear relationship between the amount of adsorption and time. This indicates that the adsorbent has reached its saturation point [171]. Selecting the optimal adsorption duration is crucial, as it leads to both time and cost savings. For both amoxicillin and carbamazepine, adsorption reached its saturation point at 120 min, after which no further increase in removal efficiency was observed. Therefore, 120 min was chosen as the optimal time for processing with the other parameters. Hodúr et al. [172] investigated the removal of ammonium nitrogen from milking parlor effluent using pomegranate peel powder, achieving a 71% removal rate in about 5 min. However, after 120 min, the system reached equilibrium, resulting in a maximum removal of 81.8% of ammonium nitrogen. An important factor in determining whether an adsorption process is endothermic or exothermic is temperature [173]. In general, adsorption techniques exhibit endothermic behavior [173]. As the temperature rises (Figure 19), the sorption capacity of the bio-adsorbent increases. This increase in sorption capacity can be attributed to the expansion of active sites on the adsorbent's surface or the enhanced movement of pollutant molecules [173]. Higher temperatures cause the internal structure of the sorbent to expand, allowing pollutant molecules to penetrate more effectively [174]. A similar trend was observed in the study conducted by Sathishkumar and his team (2007), which investigated the removal of dichlorophenol using palm pith carbon [175]. Another important parameter affecting adsorption capacity is the initial concentration of the contaminants. For amoxicillin, increasing its concentration from 10 mg/L to 25 mg/L resulted in a decrease in removal efficiency from 99.43%

to 91.54%, and it continued to decline further at higher concentrations (Figure 20 A and B). This indicates that higher concentrations quickly occupy the vacant sites on BPAC. A similar trend was observed for carbamazepine. Therefore, 25 mg/L was chosen as the optimal pollutant concentration for both contaminants.

3.3.2.2. Effect of pH

Increasing the pH from 2 to 4 resulted in an increase in amoxicillin removal efficiency from 80.43% to 91.42% (Figure 20 C and D). A further increase in pH to 5 led to a slight decrease in removal efficiency by 2%. After that, a dramatic drop in removal efficiency was observed as the pH increased from 6 to 10, reaching 50.65% at pH 10. For carbamazepine, removal efficiency increased from 61.22% to 87.63% when the pH was adjusted from 2 to 4. In contrast to amoxicillin, carbamazepine performed slightly better at pH 5, with a removal efficiency of 90.54%. Comparing the results for both pollutants, a slight improvement in removal efficiency was observed at pH 4 and pH 5. Therefore, pH 5 was selected for further experiments. Ncibi and Sillanpää demonstrated that the adsorption capacity of carbamazepine (CBZ) on mesoporous activated carbon increased within the pH range of 2–8, rising from 113 mg/g to 188 mg/g [176]. However, when the pH was raised from 8 to 10, the adsorption capacity decreased to around 140 mg/g [176]. This decrease can be attributed to a combination of processes, including hydrophobic and π–π interactions between the benzene ring of CBZ and the activated carbon. Naghdi et al. reported an enhancement in CBZ elimination when the pH increased from 3 to 9 [177]. The study suggests that H^+ cations in the medium may be responsible for this increase. Furthermore, at lower pH, the concentration of H^+ ions is higher, facilitating easier interactions between the functional groups of CBZ and H^+ ions. Conversely, at higher pH, when the concentration of H^+ ions is lower, the hydrogen bonding donor groups on CBZ can interact with hydrogen bonding acceptors or donors in the adsorbent material, thereby improving the removal capacity [176], [177].

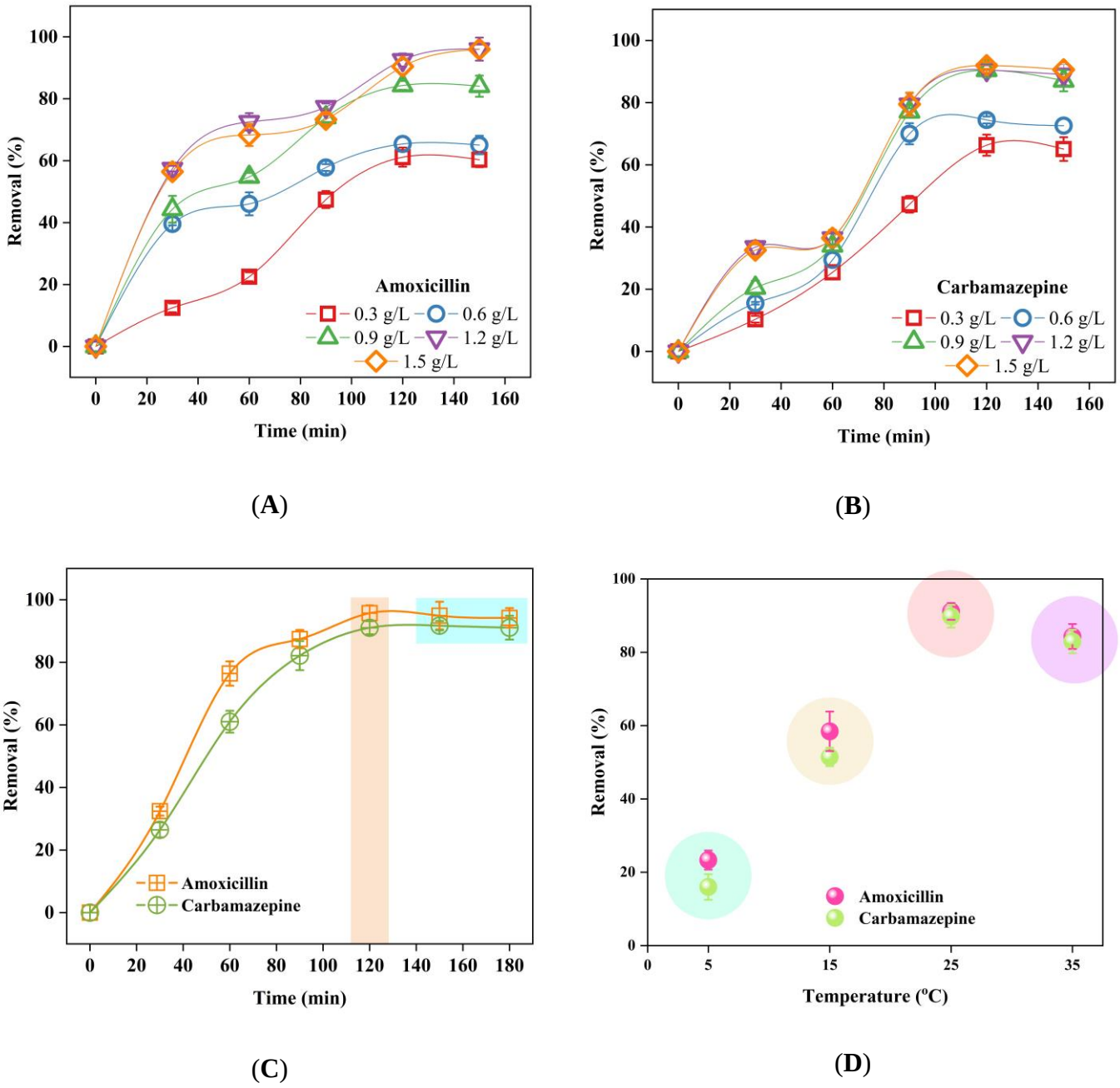

Figure 19 Effect of BPAC dosage on the removal efficiency of amoxicillin (A), and carbamazepine (B), impact of reaction time on the pollutants removal efficiency (C), and effect of the temperature on the pollutants removal efficiency (D).

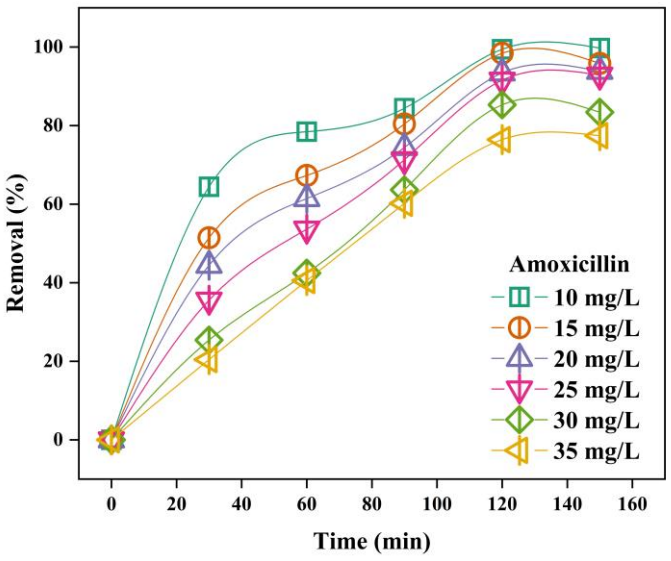

(**A**)

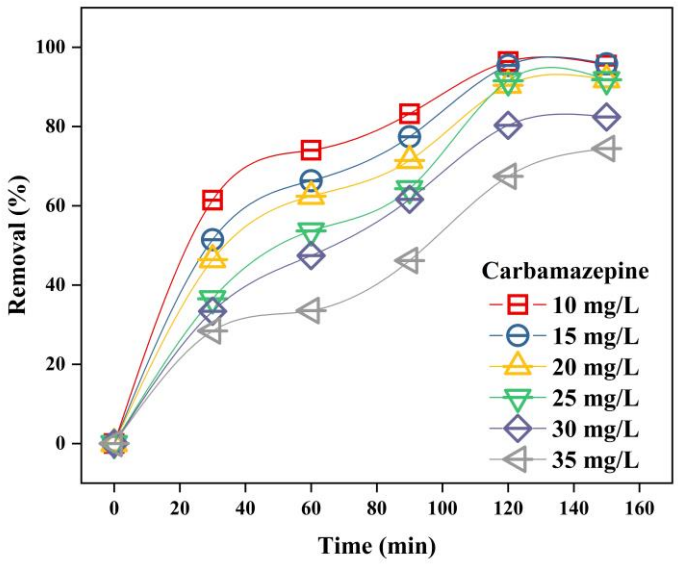

(**B**)

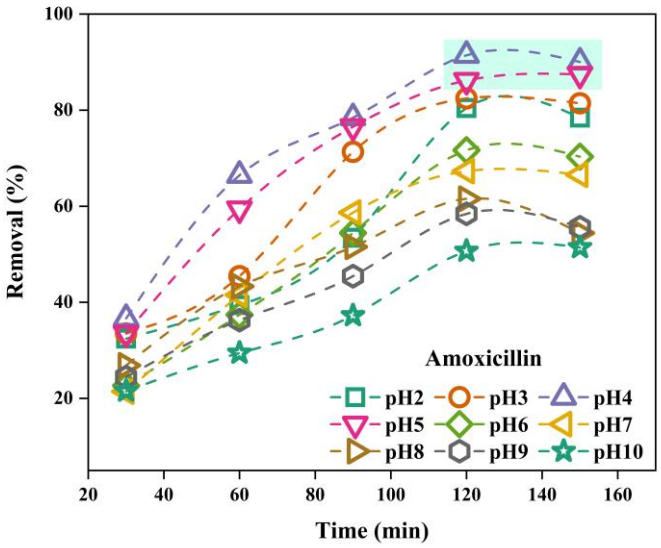

(**C**)

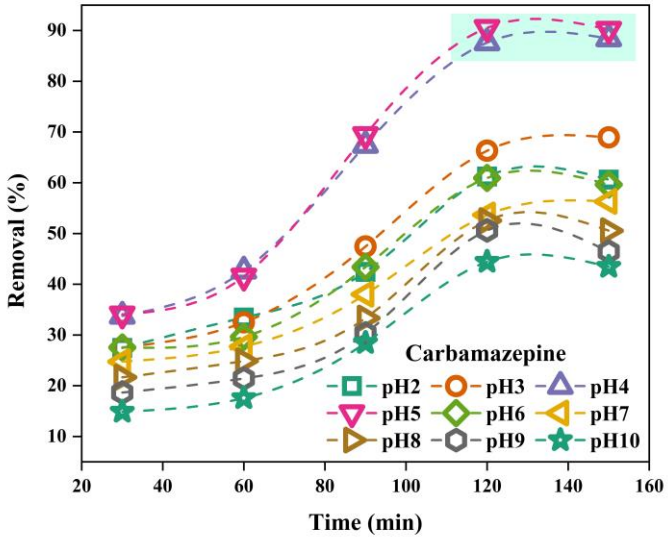

(**D**)

Figure 20 Effect of pollutants initial concentration on the removal efficiency for amoxicillin (A) and carbamazepine (B), effect of different pH ranges on the removal efficiency for amoxicillin (C) and carbamazepine (D).

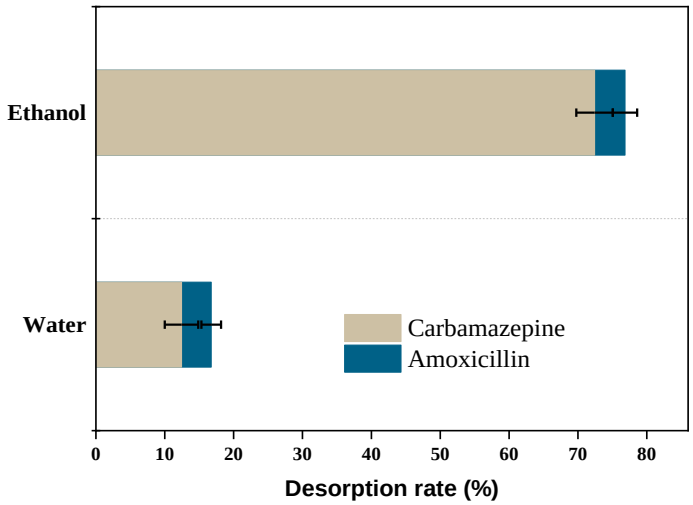

Figure 21 Desorption rate for carbamazepine and amoxicillin.

3.3.2.3. Desorption Results

The desorption rates for both pollutants were 76.83% for amoxicillin and 72.41% for carbamazepine, respectively (Figure 21). However, using water alone resulted in a low desorption rate. Chakraborty et al. [178] confirmed the desorption of ibuprofen from activated biochar derived from sugarcane bagasse. The desorption process involved the use of methanol, with continuous agitation at 130 rpm for 24 h at a temperature of 25°C. This method remained efficient over four cycles, with desorption rates exceeding 65%. An investigation was conducted to assess the effectiveness of various desorbing agents in removing contaminants from olive stone waste activated carbon [107]. The results showed that ethanol was the most efficient agent among those tested, with recovery rates of 87.83% for diclofenac and 86.41% for ciprofloxacin, respectively [107].

3.3.2.4. Adsorbent Reusability with Real Samples Application

When an adsorbent is reused, it not only supports the economic sustainability of the process but also enhances the potential for the adsorbent to be effectively utilized [95]. In particular, the reuse of bio-adsorbents derived from fruit not only improves the cycle process but also reduces the cost of water treatment. To successfully reuse the bio-adsorbent, it is essential to perform multiple re-adsorption and desorption procedures. Amoxicillin and carbamazepine were tested in three

different water matrices: MQ water, lake water, and wastewater. Figure 22 illustrates the removal percentages of amoxicillin and carbamazepine using these three water matrices across different cycles. A total of seven successful cycles were tested to evaluate pollutant removal across the three water matrices. During the first cycle, more than 90% of the pollutants were removed when MQ water was used. However, the removal efficiency was about 6% lower in lake water and 9% lower in wastewater. The average removal efficiency for both pollutants remained above 86.06% in MQ water during the fourth cycle, while it dropped to 74.57% for lake water and 63.89% for wastewater. After these cycles, there was a dramatic decrease in removal efficiency for both pollutants in lake water and wastewater, reaching 53.98% and 43.31%, respectively. In contrast, pollutant removal in MQ water remained relatively constant during the same cycles. In the final two cycles (the sixth and seventh), removal efficiency for both amoxicillin and carbamazepine continued to decline, reaching approximately 41.43% and 37.84% for MQ water, 25.43% and 15.84% for lake water, and 20.43% and 12.09% for wastewater. The decrease in removal efficiency could be attributed to the presence of interfering ions, which may mask the active sites on the adsorbent surface. Achieving these results with unmodified activated carbon derived from biowaste is considered promising. A similar trend in adsorption reduction was observed with biochar made from activated carbon derived from banana peels decorated with nickel sulfide, where the target pollutant was ciprofloxacin [179]. The activated carbon, treated with H3PO4, showed a reduction in efficiency after three cycles, but remained at 77.10% after regeneration. This decline in active sites can be attributed to decreased adsorption efficiency during the regeneration cycles. Nonetheless, BPAC shows promise for the removal of emerging pollutants, indicating its potential for use in environmental remediation.

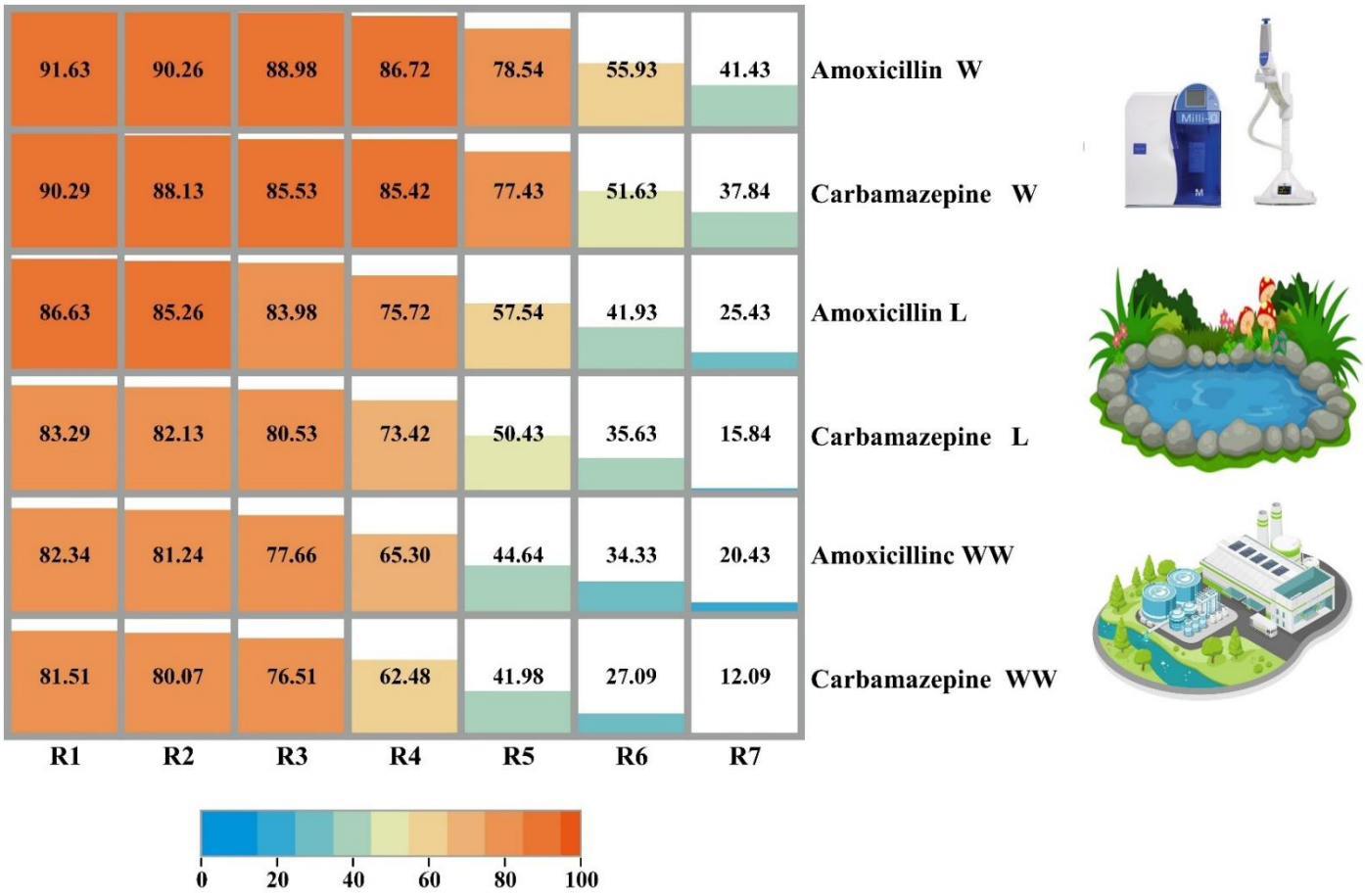

Figure 22 The removal percentage for amoxicillin and carbamazepine using MQ water, lake water (Lake Balaton, Hungary), and wastewater. The SD was less than 3.18% within all cycles. W refers to water, L is lake water, and WW is wastewater

3.3.2.5. Kinetic, Isotherms and Thermodynamics Studies of Pharmaceuticals from Aqueous Solution over BPAC

Figure 23 illustrates the results of fitting the experimental data to the Langmuir and Freundlich isotherm models. While both models reasonably explain the adsorption data, the Langmuir model provides a slightly better fit. The data was evaluated using the residual sum of squares (SSE), which quantifies the variability in the error, or residuals, of a regression model. A smaller SSE value indicates a better fit between the model and the data, while a larger SSE suggests a poorer fit. The Langmuir model exhibited a lower SSE, with values of 2.39×10^{-8} and 1.29×10^{-6} for amoxicillin and carbamazepine, respectively. This indicates that the data fit the Langmuir model better, suggesting the formation of a uniform monolayer of both pollutants on the activated BPAC surface. The maximal sorption capacity (qm) for amoxicillin was 393.70 mg/g, while for

carbamazepine, it was 338.98 mg/g. The dimensionless separation factor (RL) determines the type of isotherm and can be classified as irreversible (RL = 0), linear (RL = 1), favorable (0 < RL < 1), or unfavorable (RL > 1) [180]. According to the results in Table 12 the calculated RL values for both pharmaceutical substances ranged between 0 and 1, indicating that the adsorption process was favorable.

Table 12 Langmuir, Freundlich, Pseudo-1st-Order Model and Pseudo-2nd-Order Model parameter

Langmuir	q_{max} (mg/g)	K_L	R_L	R^2
AMO	393.701	0.037	0.349	0.999
CBZ	338.983	0.058	0.257	0.991
Freundlich	1/n	K_f	R^2	
AMO	0.633	21.877	0.982	
CBZ	0.58	28.840	0.777	
Pseudo-1st-Order Model	qe (mg g^{-1})	K_1	R^2	
AMO	54.81698	1.46E-05	0.909	
CBZ	73.92123	1.18E-05	0.977	
Pseudo-2nd-Order Model	qe (mg/g)	qe^2	K_2	R^2
AMO	1.32E+02	1.73E+04	1.20E-03	0.992
CBZ	1.28E+02	1.64E+04	7.51E-04	0.984

The correlation coefficients for the pseudo-second-order kinetic model were 0.992 for amoxicillin and 0.984 for carbamazepine, compared to 0.909 and 0.977 for the pseudo-first-order model (Figure 24 A and B). These results suggest that chemisorption was the rate-limiting step in the adsorption process. Figure 24 C also displays a plot of $\ln K_1$ versus 1/T, used to estimate the thermodynamic parameters for the adsorption of amoxicillin and carbamazepine. The thermodynamic characteristics responsible for the adsorption are presented in Table 13. These parameters include the change in free energy (ΔG°), the change in enthalpy (ΔH°), and the change in entropy (ΔS°) at different temperatures: 288, 298, 308, and 318 K.

Table 13 Thermodynamic parameters of pollutants adsorption on BPAC

Compound	Temperature (K)	K_l	ΔG°	ΔH°	ΔS°	R^2
AMO	283	5.581	-4.045	18.196	78.841	0.983
	293	7.799	-5.003			
	303	9.737	-5.733			
	313	11.778	-6.418			
CBZ	283	6.243	-4.309	17.116	116.396	0.976
	293	10.848	-5.807			
	303	15.320	-6.875			
	313	20.407	-7.848			

The decrease in ΔG° values with increasing temperature indicates the favorable influence of temperature on the adsorption efficiency. The adsorption of amoxicillin and carbamazepine onto BPAC is shown to occur spontaneously, as evidenced by the negative ΔG° values obtained at all four temperatures.

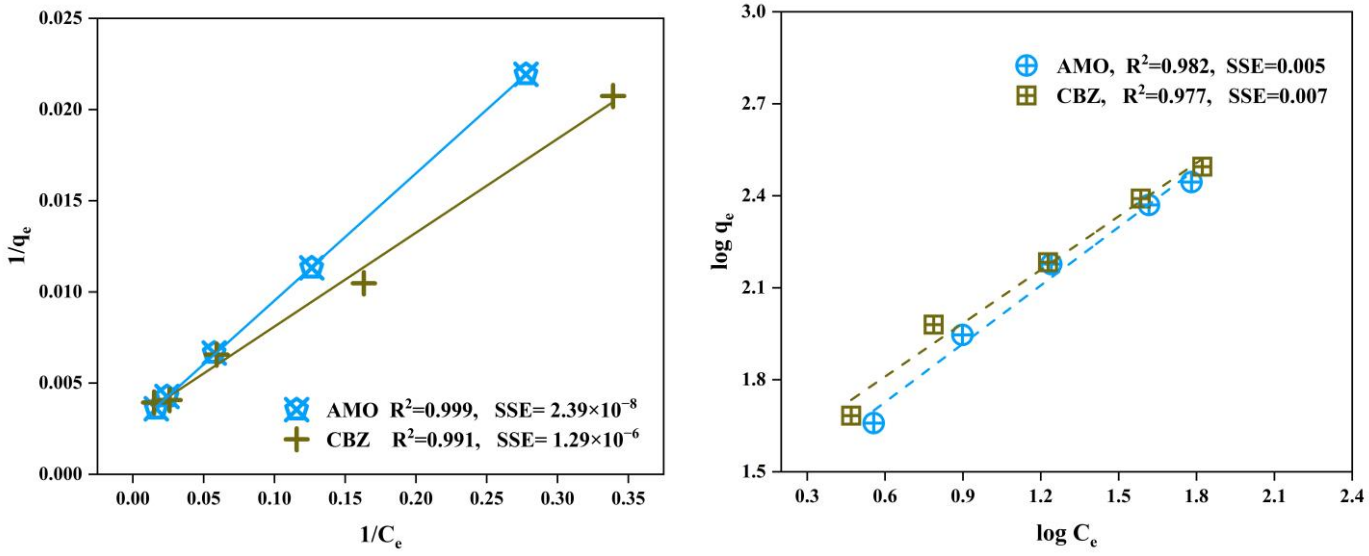

(**A**) (**B**)

Figure 23 Langmuir (A) and Freundlich (B) isotherms

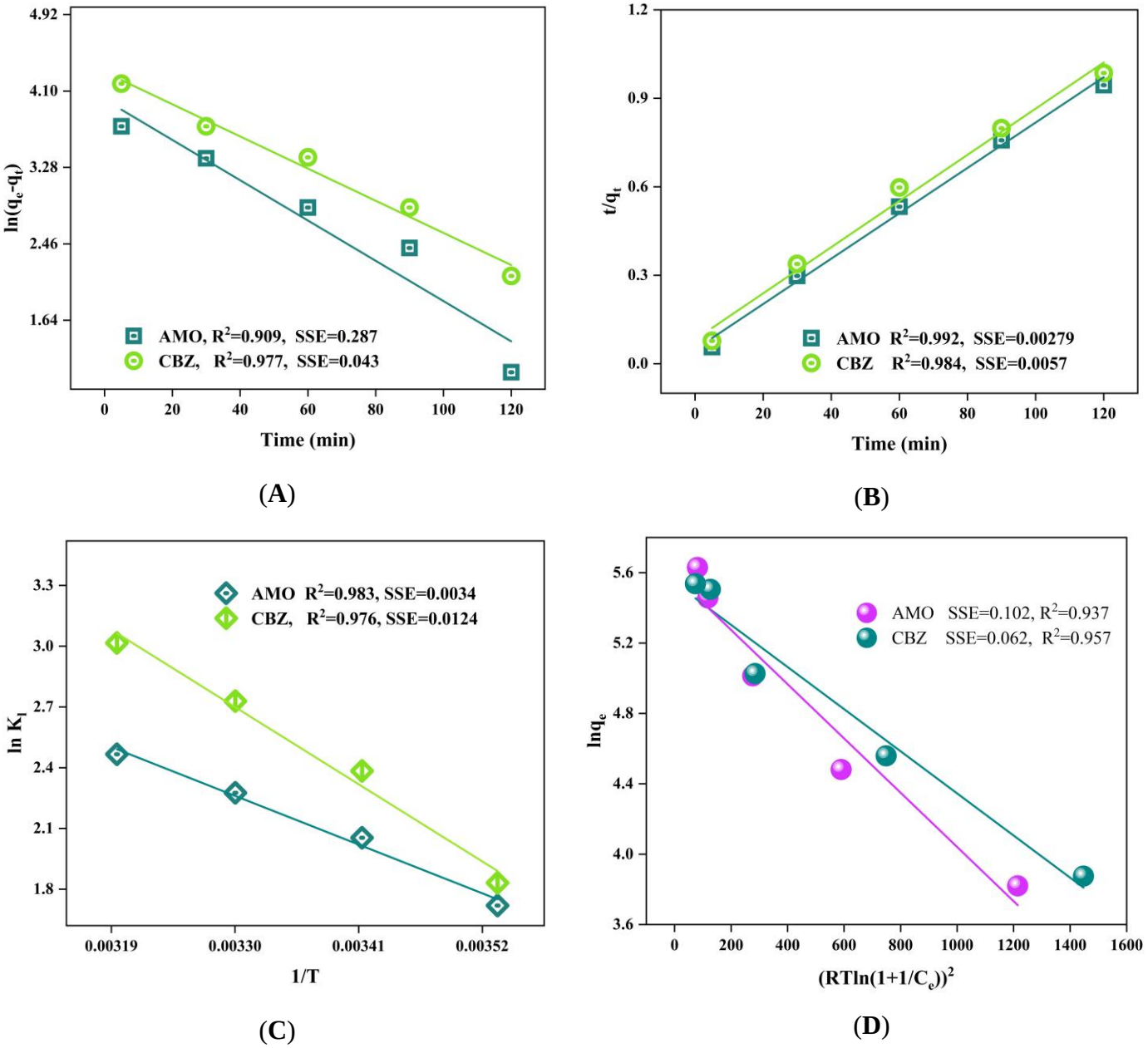

Figure 24 Pseudo-second-order kinetic (A) and pseudo-first-order (B) models, thermodynamic (C), Dubinin–Radushkevich (D–R) (D) for both pollutants

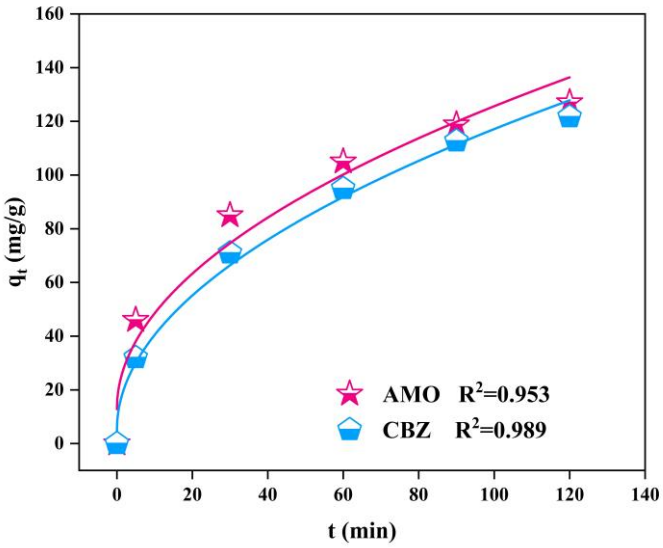

Figure 25 Intra-particle diffusion model for both pollutants

The Dubinin–Radushkevich (D–R) adsorption isotherm model is used to describe the adsorption phenomenon on a heterogeneous surface (Figure 24 D), assuming that the energy distribution follows a Gaussian distribution. This isotherm model is often employed to distinguish between chemical and physical adsorption [108]. The D–R model is an empirical equation that characterizes adsorption by considering the pore-filling mechanism, which differentiates it from the Langmuir and Freundlich models. The model is based on the assumption that multiple layers of adsorption are involved, incorporating van der Waals forces. The apparent energy of adsorption, represented by E (J/mol), is used to indicate changes in the chemical or physical state during adsorption. According to the D–R isotherm model, physical adsorption occurs when the energy (E) is below 8 kJ/mol, whereas chemical adsorption occurs when the energy exceeds 8 kJ/mol. Since both pollutants exhibited E values above 8 kJ/mol, this suggests that chemical adsorption of these pollutants occurred on BPAC. The diffusion mechanisms of the pollutants were investigated by fitting the experimental data to the intra-particle diffusion model. The intra-particle diffusion mechanism is considered the rate-controlling step if the plot of qt vs. t is a straight line passing through the origin ($I \approx 0$) [109]. Figure 25 shows that intra-particle diffusion is the rate-controlling mechanism for the tested pollutants. A combination of processes, including hydrophobic interactions, π–π interactions, and intra-particle diffusion, controls the adsorption of the studied contaminants.

3.3.2.6. Mechanism of Pharmaceuticals Adsorption on BPAC

In this work, the decrease noticed in removal efficiency after pH5 could be attributed to the combination of hydrophobic and π–π interactions between the benzene ring of CBZ and the BPAC. It was stated that the adsorption of amoxicillin onto various adsorbents was enhanced when the pH of the solution rose. This phenomenon is attributed to the change in charge of amoxicillin, transitioning from positive to zwitterionic form [181]. The primary mechanism of adsorption is presumably the electrostatic attraction between the amoxicillin molecules and the surface of the adsorbents. Amoxicillin's carboxylic groups eventually dissociate at high pH levels, resulting in the formation of a negative charge. The adsorption capacity stays relatively constant as the solution pH increases, starting from a pH of 6 or higher [182]. This phenomenon has been ascribed to the presence of two negative charges on amoxicillin at higher pH levels, which leads to repulsion forces and a decrease in amoxicillin adsorption. The elimination of amoxicillin is more effective at pH levels below the pHpzc (5.005), where there is a prevalence of (amoxicillin±) species and the surface charge is negative. When the pH is higher than the pHpzc, the removal of amoxicillin decreases. This could be attributed to the reason that pharmaceuticals and BPAC have negative charges, which results in electrostatic repulsion [183]. Moussavi et al. [184]found that the adsorption of amoxicillin onto NH4Cl activated carbon (pHpzc = 6.6) reduces as the pH increases. Qin and co-workers (2018) investigated the adsorption characteristics of nitric acid (HNO3)-treated coconut shell pellet activated carbon for eliminating Cu(II) and tetracycline [185]. In the acidic pH range of 3 to 6, both Cu(II) (50 mg/L) and tetracycline (250 mg/L) exhibited better adsorption ability near pH6.

3.3.2.7. Comparison of Prepared BPAC with Other Reported Systems

Table 14 presents a comparison of the removal efficiency of contaminants by banana peel residue from several studies, including the present study. The results demonstrate that banana peel is effective adsorbent, with high removal efficiencies for various contaminants. The current study achieved pharmaceutical removal efficiencies (91.63% for amoxicillin and 90.29% for carbamazepine in Milli-Q water) comparable to or higher than the removal rates reported in previous studies. However, the slight decline in pharmaceutical adsorption in real water matrices (lake water and wastewater) in the present study aligns with the trend observed for other contaminants, highlighting the influence of water composition on adsorption efficiency.

Table 14 Pollutant removal efficiencies by banana peels from selected studies

Compound	Matrix	Adsorbent	Removal Efficiency (%)	Reference
Phenol (50 mg/L)	Double-distilled water	Banana peel AC	83	[186]
Phenol (500 mg/L)	Double-distilled water	Banana peel AC	60	[186]
Citric acid	Double-distilled water	Microwave char banana peel	88	[163]
Citric acid	Double-distilled water	Raw banana peel	86	[163]
Rhodamine-B	Double-distilled water	Raw banana peel	81.07	[75]
Atrazine	River and treated waters	Banana peel	>90	[187]
Ametryn	River and treated waters	Banana peel	>90	[187]
Thorium	Wastewater	Banana peel	95.34	[188]
Amoxicillin and carbamazepine	MQ water Lake water Wastewater	Banana peel AC	91.63 and 90.29 86.63 and 83.29 82.34 and 81.51	Current study

3.4. Two-stages FPWAC Activation by NH_4NO_3 and NaOH

3.4.1. First Stage of Chemical Treatment

3.4.1.1. NH_4NO_3/PW Optimum Ratio

Sixteen samples (PW-1 to PW-16) with different NH_4NO_3/PW ratios and other conditions (Table 15) were evaluated for pollutant removal. The findings indicated that PW-9 to PW-12 samples

with an NH_4NO_3/PW ratio of 3% had the highest removal efficiency. Introducing NH_4NO_3 to PW initiates a multifaceted sequence of events. NH_4NO_3 has a melting point of 169°C and can penetrate the lignocellulose matrix of the wood particles. As the temperature gradually rises, the infiltration of NH_4NO_3 into the wood matrix intensifies, leading to the formation of micro-cracks due to heightened internal stresses at elevated temperatures. Concurrently, the cellulose content within the wood undergoes degradation within the temperature range of 210 to 220°C [92] . An increase in temperature causes the decomposition reaction of NH_4NO_3 to proceed, potentially leading to an explosion between 260°C and 300°C [189].

Table 15 Pinewood (PW) samples for pollutants removal from aqueous solution. The adsorption conditions: pH 6, 25°C, shaking speed of 150 rpm, an adsorbent dosage of 1 g/L, and initial pollutants concentration of 25 mg/L.

Sample Number	Activation time (h)	Temperature (°C)	NH_4NO_3/PW ratio wt. (%)	Diclofenac (Removal %)	Ciprofloxacin (Removal %)
PW-1	1.5	300	1	11.93	19.04
PW-2	2	400	1	15.75	18.46
PW-3	2.5	500	1	25.83	21.06
PW-4	3	600	1	28.02	26.16
PW-5	1.5	300	2	44.92	45.98
PW-6	2	400	2	52.30	47.29
PW-7	2.5	500	2	59.94	58.99
PW-8	3	600	2	55.54	57.27
PW-9	1.5	300	3	57.46	61.80
PW-10	2	400	3	69.81	75.39
PW-11	**2.5**	**500**	**3**	**82.12**	**83.51**
PW-12	3	600	3	79.98	81.33
PW-13	1.5	300	4	56.62	52.47
PW-14	2	400	4	61.84	63.16
PW-15	2.5	500	4	77.02	79.11
PW-16	3	600	4	73.58	69.08

These changes contribute significantly to the development of a porous structure with varying pore sizes, which is crucial for enhancing adsorption capacities. The activation process continues and evolves as the temperature reaches 600°C[189] .

3.4.1.2. PW-9 to PW-12

The chosen four samples of PW-9, PW-10, PW-11, and PW-12 (Section 3.4.1.4) were subjected to another round of evaluation, which included yield percentage, elemental composition analysis, O/C and H/C ratios, as well as specific surface area (S_{BET}) measurements. This step was conducted to select only one sample to proceed to the second stage of chemical activation.

3.4.1.3. Yields Percentages of PW-9 to PW-12

The yields reduced progressively with the rise of temperature, producing percentages of 63.74%, 49.02%, 36.84%, and 35.49% for PW-9@300°C, PW-10@400°C, PW-11@500°C, and PW-12@600°C, respectively. This decline in the total yield could be due to the way the material is decomposed into its constituent components, such as cellulose, hemicellulose, and lignin [190]. He et al. (2018) showed that even at lower temperatures, macromolecular compounds might cause a decrease in biochar yield through condensation polymerization [191]. This indicates that the carbonaceous material is preserved at lower temperatures. Pyrolysis of wood residues takes place within temperature ranges where hemicellulose, lignin, and cellulose decompose. The first decomposes from 200°C to 300°C, the second from 200°C to 500°C, and the latter from 300°C to 380°C.

3.4.1.4. Elemental Composition of PW-9 to PW-12

Table 16 shows the comparison of the elemental composition of PW-9@300°C, PW-10 @400°C, PW-11@500°C, and PW-12@600°C samples, as well as raw PW. The carbon (C) profile of the samples changed perceptibly, ranging between 52.03% and 72.01% as the pyrolysis temperature rose from 300°C to 600°C. This marked augmentation underscores the role of elevated temperatures in facilitating the intensified carbonization process of pinewood, leading to a higher concentration of carbonaceous material within the samples. However, the inverse relationship between hydrogen (H) and oxygen (O) contents in the samples decreased with an increase in temperature (Table 16). This observed reduction can be explained by two phenomena related to the pyrolysis process: volatilization of organic compounds and subsequent cleavage of chemical

bonds within the pinewood matrix. These thermal degradation processes lead to the release of volatile components, resulting in a corresponding decline in the concentrations of oxygen and hydrogen within the samples [191]. The decrease in the H/C ratio (Table 16) clearly shows the trend of carbonization, with this ratio decreasing with increased temperature, indicating that PW becomes more carbonized. The degree of oxidation (O/C ratio) represents the number of polar groups which characterize the final biochar product [192]. As the pyrolysis temperature of PW increases, the O/C ratio decreases, suggesting a reduction in the amount of oxygenated binding sites. This specific change is facilitated by the loss of oxygen-functionalized groups on the surface, which leads to a decrease in hydrophilicity. Moreover, an increase in nitrogen (N) content was noted in the samples PW-9 to PW-12 relative to the raw PW, signifying the incorporation of NH_4NO_3 into PW-9 to PW-12. Among other parameters, variation in sulfur (S) content showed no change with temperature fluctuations, as demonstrated in Table 16. Furthermore, the ash content of samples PW-9 to PW-12 surpassed that of the raw PW, denoting heightened production and accumulation of mineral constituents within PW-9 to PW-12 as temperatures escalated [193]. This test provides evidence that temperature plays a crucial role in the compositional transformation of the samples extracted from PW-9 to PW-12, which may shed light on the mechanism of mineral enrichment.

3.4.1.5. Specific Surface Area (S_{BET}) of PW-9 to PW-12

When the pyrolysis temperature rises beyond the critical limit of 260°C, an explosive reaction occurs involving NH_4NO_3, which helps to produce secondary channels and pores of multiple sizes[92], [93], [194]. Among the four samples, PW-11@500°C was found to have S_{BET} of 893.03 m^2/g and a total pore volume (PV) of 0.369 m^3/g, proving to be more efficient in removing contaminants compared to the others, as shown in Table 16. Thus, based on the findings, PW-11@500°C was chosen for the second stage of the activation process.

3.4.2. Second Stage of Chemical Treatment

PW-11@500°C was mixed with NaOH in a 3:1 ratio [94] at 500°C to produce final pinewood-derived activated carbon (FPWAC). After treating the final sample with NaOH, the FPWAC had a better S_{BET} of 913.42 m^2/g and a total pore volume of 0.381 m^3/g. This observation suggests that the activation step involving NaOH has a substantial impact on the formation of new micropores inside the activated carbon structure. A study by Zubrik and colleagues observed that the use of a

strong base in the second pyrolysis process increased the micropore volume. The study employed KOH as an activating agent to enhance the characteristics of biochar that had undergone the first pyrolysis, specifically for adsorbing Cd(II) [195]

Table 16 PW and the PW-9@ 300 to PW-12@ 600 samples physicochemical characteristics at different temperatures

Sample	NH_4NO_3/ PW ratio wt. (%)	C(%)	H(%)	N(%)	S(%)	O(%)	Ash(%)	O/C	H/C	S_{BET} m^2/g	Total pore volume (cm^3/g)	Yield (%)
Raw PW	-	52.03	6.33	0.82	0.14	33.26	7.43	0.63	0.12	14.86	0.021	-
PW-9@ 300	3	57.13	4.05	1.54	0.13	24.20	12.95	0.42	0.07	162.01	0.103	63.74
PW-10@ 400	3	59.21	3.46	0.96	0.11	22.48	13.78	0.37	0.05	471.37	o.208	49.02
PW-11@ 500	3	71.61	1.71	0.84	0.12	8.75	16.97	0.12	0.02	893.03	0.369	36.84
PW-12@ 600	3	72.01	1.67	0.85	0.12	7.84	17.51	0.11	0.02	891.25	0.352	35.49
FPWAC (PW-11@ 500 + NaOH)	3	74.58	1.62	0.89	0.09	4.78	18.04	0.06	0.02	913.42	0.381	32.06

3.4.2. Characterization

3.4.2.1. FTIR Results

Figure 26 (A) displays the FTIR spectra of the FPWAC before and after the adsorption of pharmaceutical compounds. As depicted in Figure 26 (A), a detailed examination of the spectrum of the FPWAC revealed distinctive spectral features. A prominent peak observed at

3431 cm^{-1} signifies the stretching vibration of -OH groups indicative of phenolic groups and carboxylic groups present within the activated carbon [174]. Additionally, an NH_2 group is indicated by the band appearing at 3331 cm^{-1}, observed as a result of vibration stretching of these functional groups.

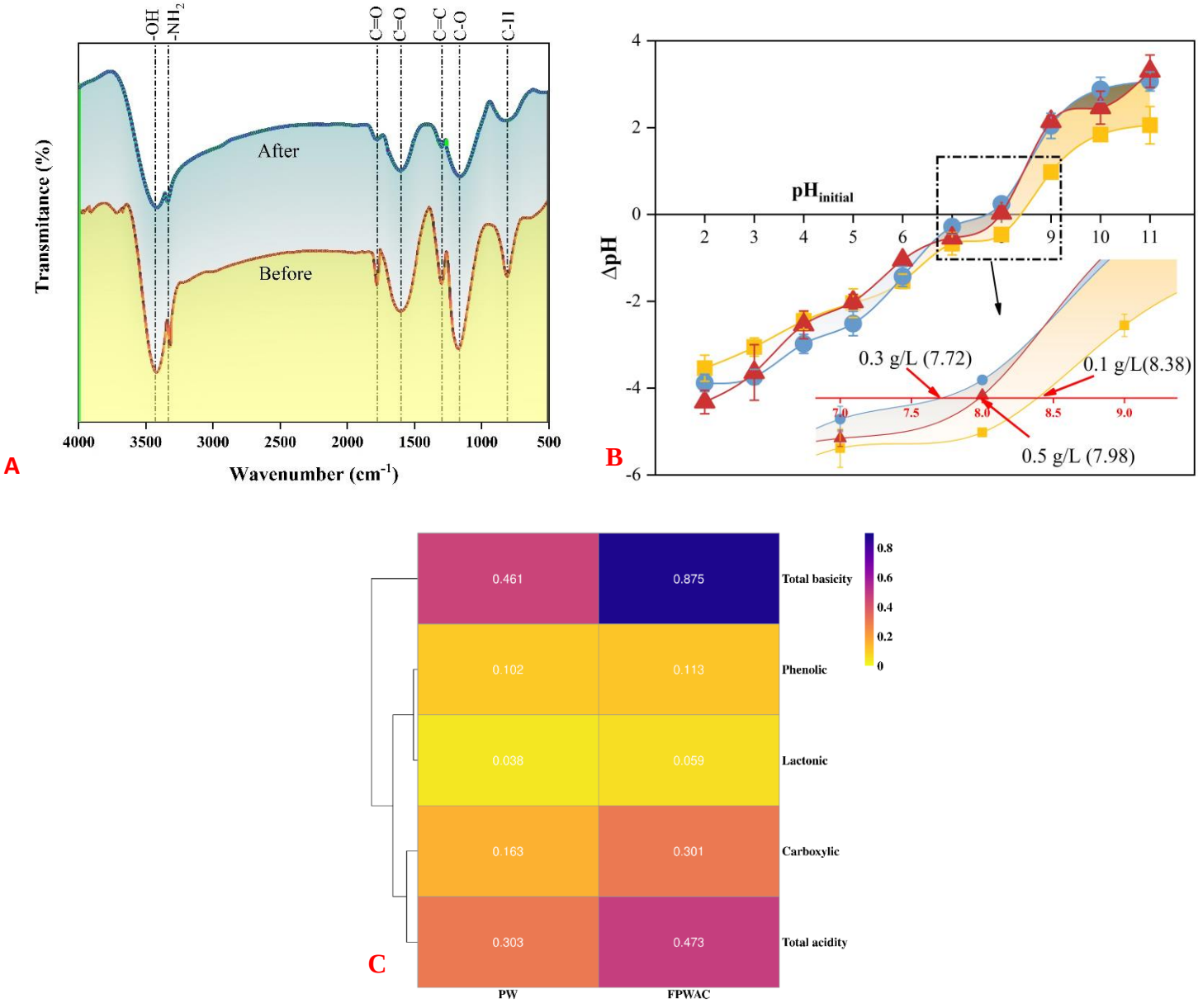

Figure 26 FTIR for FPWAC before and after adsorption (A), pHpzc of FPWAC with different dosages (B), and PW and FPWAC Bohem test (mmol/g) (C).

Furthermore, the spectrum displays two distinct bands at approximately 1596 cm^{-1} and 1779 cm^{-1}, representing the stretching vibrations associated with the C=O bonds linked to lactonic

and carboxylic groups, respectively [92] and the peak at a wavelength of 1168 cm^{-1} indicates the presence of the C-O group. Additionally, a discernible shoulder in the spectrum, observed at 1296 cm^{-1}, indicates the presence of C=C double bonds within aromatic rings. This characteristic feature further underscores the aromatic nature of the carbonaceous material, providing valuable insights into its structural composition [196]. Moreover, the weak peak at around 812 cm^{-1} corresponds to the bending vibration of aromatic C-H bonds out of the plane. Some alterations in the spectral bands for FPWAC after adsorption were observed across all frequencies, suggesting plausible adsorption mechanisms between the compound molecules and the functional groups of FPWAC. The intensity of the band linked to hydroxyl functional groups (at 3412 cm^{-1}) diminishes, implying the presence of hydrogen bonding interactions between the pharmaceutical molecules and the AC (Figure 26 (A)). Similar observations were noticed in the adsorption of paracetamol by granular activated carbon [197].

3.4.2.2. Boehm Test

The surface functional characteristics of both PW and FPWAC are depicted in Figure 26 (C). The overall basicity of PW was 0.461 mmol/g, showing a substantial increase to 0.875 mmol/g in the case of FPWAC. The elevated levels of basicity perceived were anticipated during the activation step using NaOH. In contrast, FPWAC exhibits a combined acidity of 0.473 mmol/g, incorporating carboxylic (0.301 mmol/g), lactonic (0.059 mmol/g), and phenolic (0.113 mmol/g) functional groups. There was a notable increase of approximately 56.10% in the overall surface acidity, indicating a substantial augmentation in the abundance of surface functional groups. The titration of these functional groups in the Boehm test confirms these qualitative observations from the FTIR analysis. Moreover, a study showed similar surface chemistry processes during the development of activated hazelnut bagasse by potassium hydroxide (KOH). In this work, a predominance of basic surface groups was observed, mirroring the findings of the current investigation [125]. The parallels observable in these different carbonaceous materials confirm the universal nature of surface chemistry processes and represent a potential resource for understanding the fundamentals of surface functionalization of porous carbons.

3.4.2.3. Point of Zero Charges (pH_{pzc})

The value of pH_{pzc} is a measure of the change in the electric charge density on FPWAC. The mean pH recorded for FPWAC, illustrated in Figure 26 (B), was 8.02. FPWAC is positively charged at

pH > 8.02 and shows a negative surface charge at pH < 8.02. The determined pH_{pzc} value obtained in the current study is similar to that reported by Sajjadi and co-workers [92], who obtained a pH_{pzc} for pistachio AC of 8.1. Another study that activated pine wood with zinc chloride reported a pH_{pzc} of 7.8 [198]. These differences in the literature values are due to variations in the synthesis and activation conditions, which may induce changes such as the release of water-soluble compounds from the biomass, potentially altering the pH_{pzc} by affecting previously adsorbed molecules on the surface of FPWAC [199]. These subtle aspects emphasize the underlying complexity inherent in determining pH_{pzc} values.

3.4.2.4. SEM-EDS Results

The SEM-EDS surface morphology of FPWAC and FPWAC after adsorption is shown in Figure 27. The FPWAC exhibited well-defined channels with regular honeycomb structures, potentially enhancing the accessibility of organic micropollutants to the inner surface of the activated carbon. Similar SEM images were observed in the activation of pistachio shells by NH_4NO_3 [93]. As the adsorption process takes place, the FPWAC surface becomes filled with a more amorphous structure with irregularly dispersed holes. This change could be attributed to the successful adsorption process of the target pollutants. The EDS analysis reveals the elemental composition of FPWAC. Before the adsorption process, the FPWAC showed a high percentage of carbon (77.62%) and a low percentage of oxygen (9.73%). The successful conversion of pinewood could explain this. However, the carbon content dropped by 14.95%, and the oxygen percentage increased by 5.86% after the adsorption process, which is likely due to the pharmaceuticals' adsorption onto the FPWAC surface. The results of this work are in agreement with other reported studies. For instance, Dilekoglu and colleagues prepared activated carbon derived from sheep manure to remove naproxen micropollutants from an aqueous solution [200]. The study stated a slight decrease in carbon content and a slight increase in oxygen content after the adsorption process. The emergence of the chloride peak is another indication of diclofenac adsorption onto the FPWAC surface.

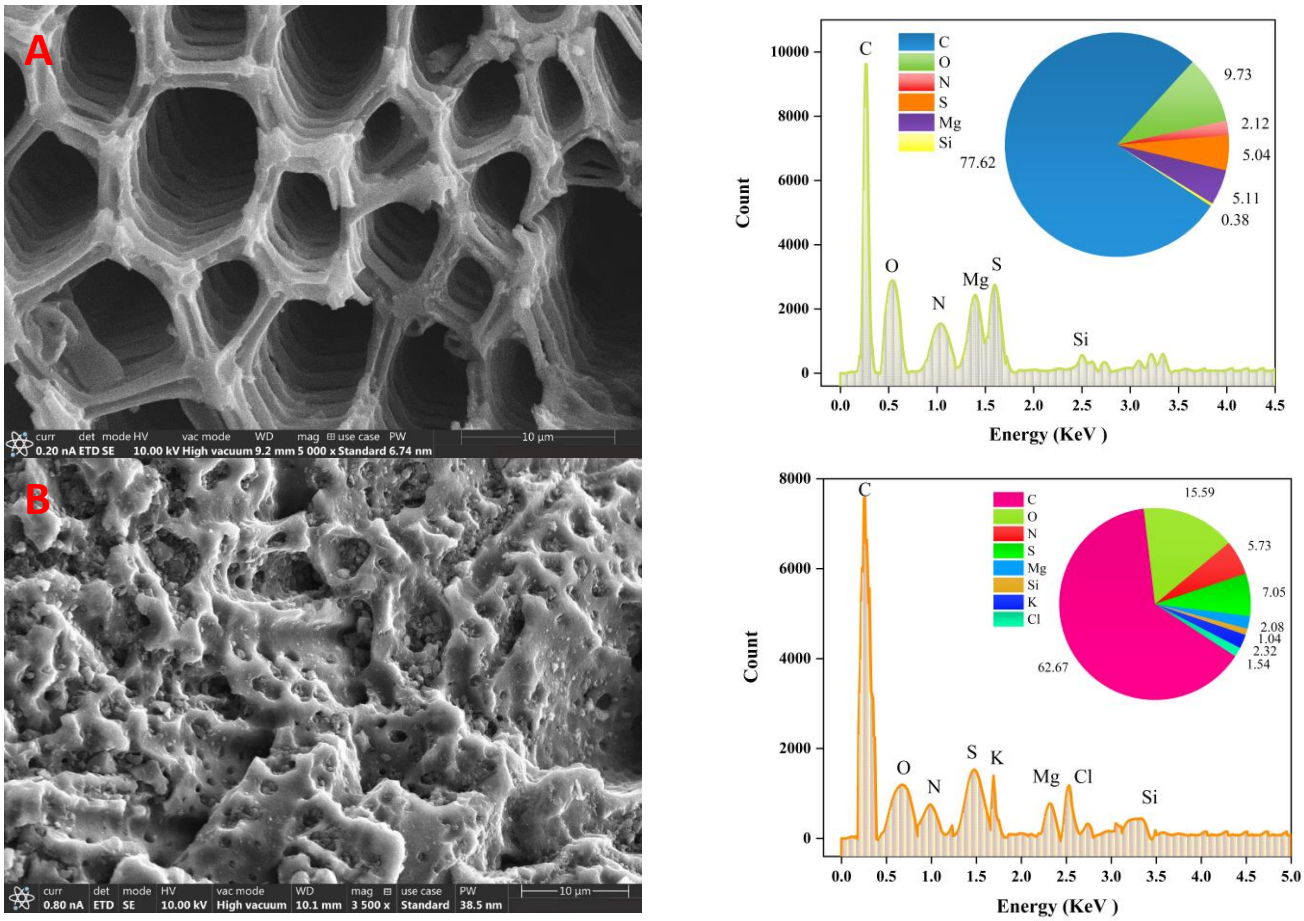

Figure 27 SEM-EDS for FPWAC (A) as well as FPWAC after adsorption (B).

3.4.2.5. X-ray Diffraction Results

The XRD was used to study the structures of the materials consisting of crystalline natures. Figure 28 (A) displays the XRD spectrum of PW and FPWAC both before and after adsorption. The XRD pattern in Figure 28 (A) shows two broad peaks at around ~25° and 43.5° 2θ. The peak at ~25° corresponds to the d-spacings within the aromatic region, indicating the presence of a developed graphitic structure in both FPWAC and PW [201], [202]. This could be attributed to the (002) crystallographic planes of graphitic carbon [101], [156]. The broad peak observed in the XRD spectrum results in pronounced scattering at low angles, indicating the amorphous nature of the highly porous FPWAC and PW [157]. Another noticeable aspect is the presence of a minor peak at approximately 43.5° 2θ, which matches the (100) plane, revealing the existence of small sheets of graphene arranged in an orderly manner [156]. The absence of sharp peaks in the XRD patterns further confirms the amorphous nature of the samples. The adsorption of contaminants in the present investigation

did not result in significant alterations in the XRD spectrum. This indicates that the adsorption of diclofenac and ciprofloxacin onto the FPWAC did not cause a pronounced change in its crystallinity. Similar observations were also reported with activated carbon prepared from spruce sawdust, where phosphate adsorption did not cause a tangible change in the XRD patterns of the activated carbon [203].

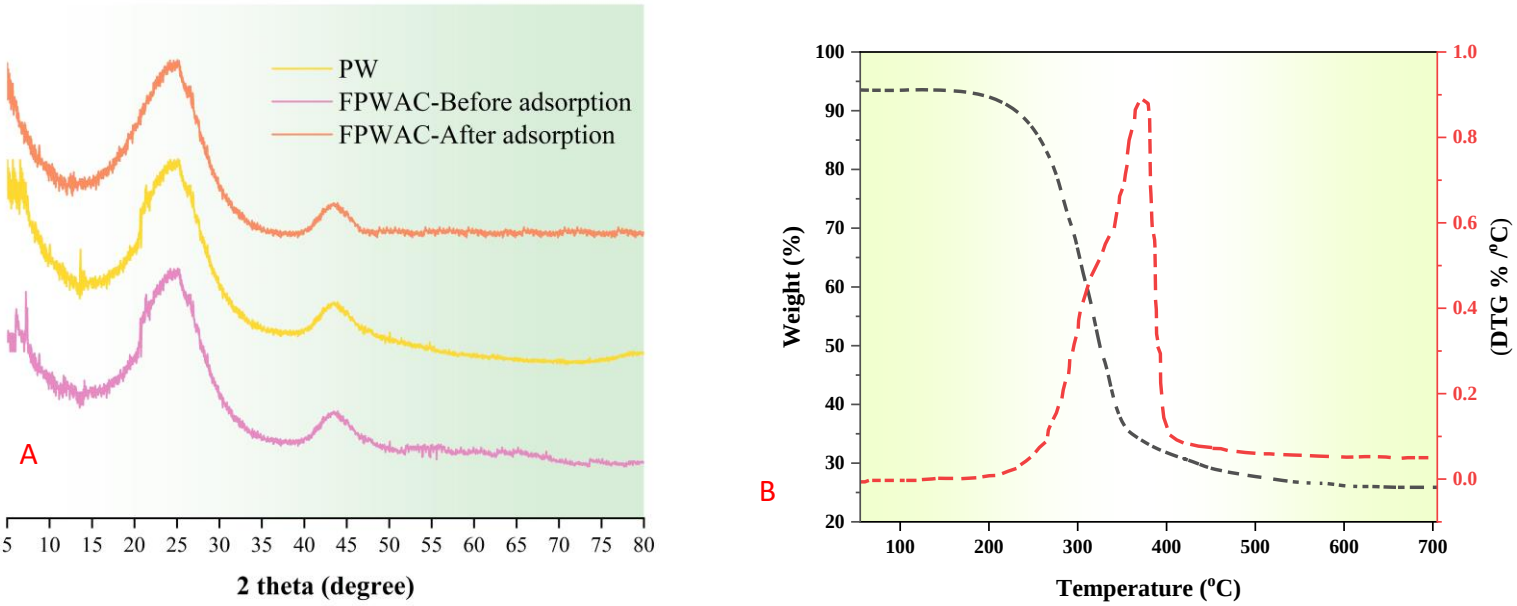

Figure 28 The XRD spectrum for PW, FPWAC before and after adsorption (A) and TGA for pinewood (B).

3.4.2.6. Thermogravimetric Analysis Results

The degradation process of PW can be segmented into three distinct phases (Figure 28 B). Initially, there is a phase commencing from ambient temperature up to approximately 170°C, characterized by moisture loss and volatilization of certain light components. Subsequently, between 170°C and 365°C, there is a phase marked by mass reduction, indicative of the decomposition of the primary constituents of biomass. Finally, the last phase entails the breakdown of lignin, a component possessing a more intricate molecular structure compared to cellulose and hemicellulose constituents, rendering its degradation process notably resistant and slow [204].

3.4.3. Adsorption Test Results

3.4.3.1. Influence of Adsorption Parameters

The impact of various adsorption parameters on the efficacy of removing diclofenac and ciprofloxacin, including FPWAC dosages, reaction duration, temperature, initial concentration of pollutants, and varying pH levels, is depicted in Figure 29 and 30. A crucial aspect of developing an effective adsorption protocol lies in optimizing the quantity of FPWAC dosage. This optimization process plays a pivotal role in identifying the equilibrium stage between adsorbent and adsorbate molecules, alongside discerning the economic implications associated with employing the adsorbent for treatment purposes. The experimental design utilized FPWAC concentrations ranging from 0.2 g/L to 1.4 g/L (Figure 29 A and B). The findings reveal only slight increases in removing diclofenac and ciprofloxacin when treating the water with 0.2 and 0.6 g/L doses compared to 1 and 1.4 g/L. This finding underscores the fact that dose optimization is key in increasing the adsorption capacity of FPWAC, which will, in turn, lead to better pollutant removal. The increase in FPWAC concentration to 1 g/L and 1.4 g/L exhibited a marked increment in removal performance for diclofenac and ciprofloxacin. In particular, the removal efficacy reached 60.87% (at 0.6 g/L) and 94.88% (at 1 g/L) for diclofenac and from 64.98% (at 0.6 g/L) to 90.98% (at 1 g/L) for ciprofloxacin. Additional increases in FPWAC dose did not bring any improvements in diclofenac and ciprofloxacin removal. This points out that a dosage of 1 g/L is most effective for the removal of diclofenac and ciprofloxacin by FPWAC. Fernandez and co-workers conducted research focusing on the production of hydrochars from orange peels for removing diclofenac sodium, salicylic acid, and flurbiprofen [169]. Their investigation demonstrated the highest adsorption capacities of salicylic acid, flurbiprofen, and diclofenac sodium to be 0.092, 0.093, and 0.018 mmol/g, respectively, at the optimal dose of the adsorbent substance, which was 0.5 g/L. The adsorption efficiency of an adsorbate is linked to the duration of adsorbate-adsorbent interaction. The adsorption of pollutants reaches an ideal level when the contact time is extended [170]. Initially, there is a sharp increase in sorbate removal due to the availability of numerous active sites on the adsorbent surface. As time passes, the active sites become occupied, reducing the rate of adsorption until eventually reaching equilibrium [171]. The equilibrium time for diclofenac and ciprofloxacin was observed to be 2 h, after which no additional removal was noted. Consequently, the subsequent experiments were carried out for 2 h.

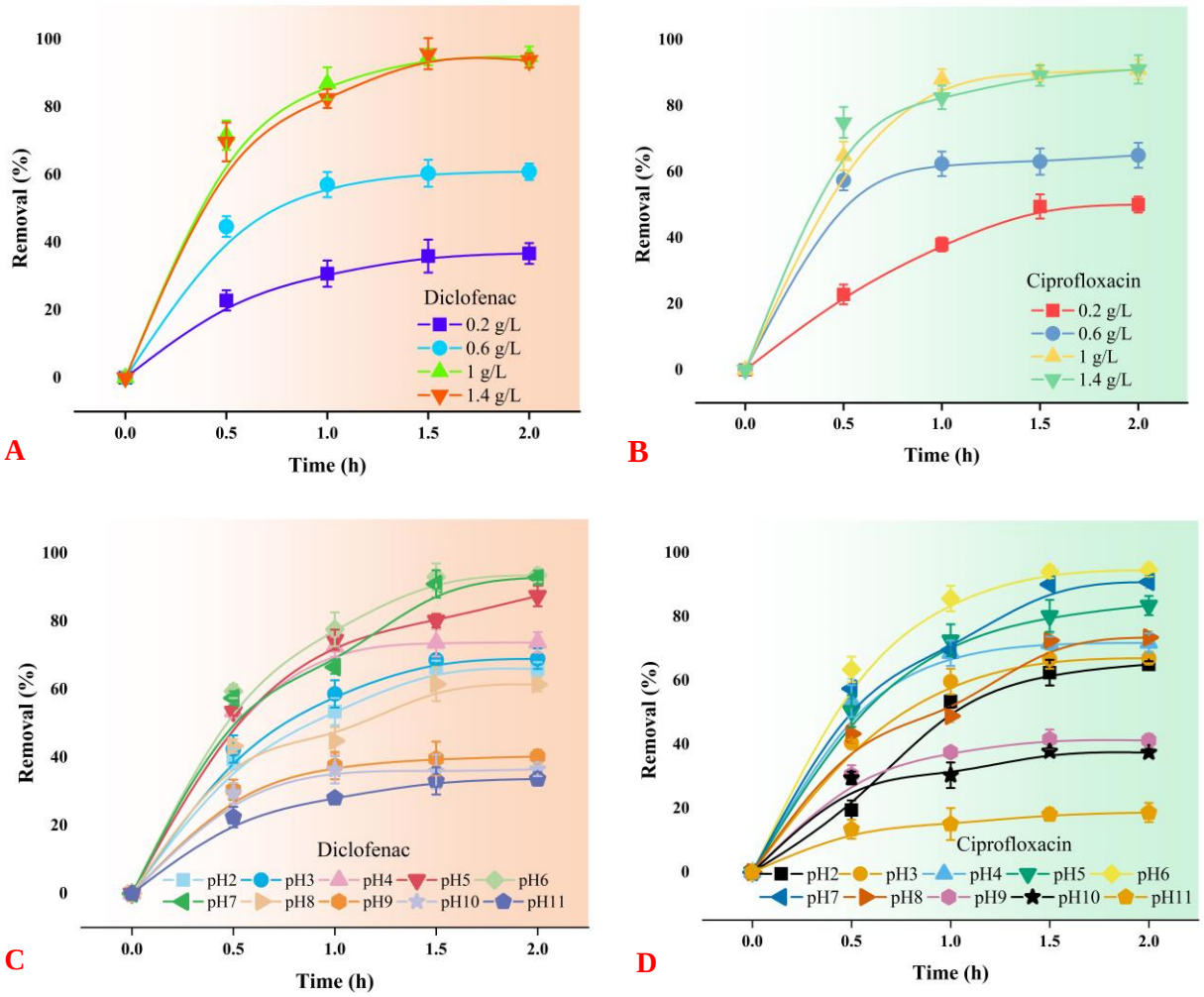

Figure 29 The removal efficiency of diclofenac(A) and ciprofloxacin(B) by using different FPWAC dosages; and the removal efficiency of diclofenac(C) and ciprofloxacin(D) by using different of pH range. The conditions were 1 g/L FPWAC, pH 6, mixture concentration 25 mg/L and 25 °C.

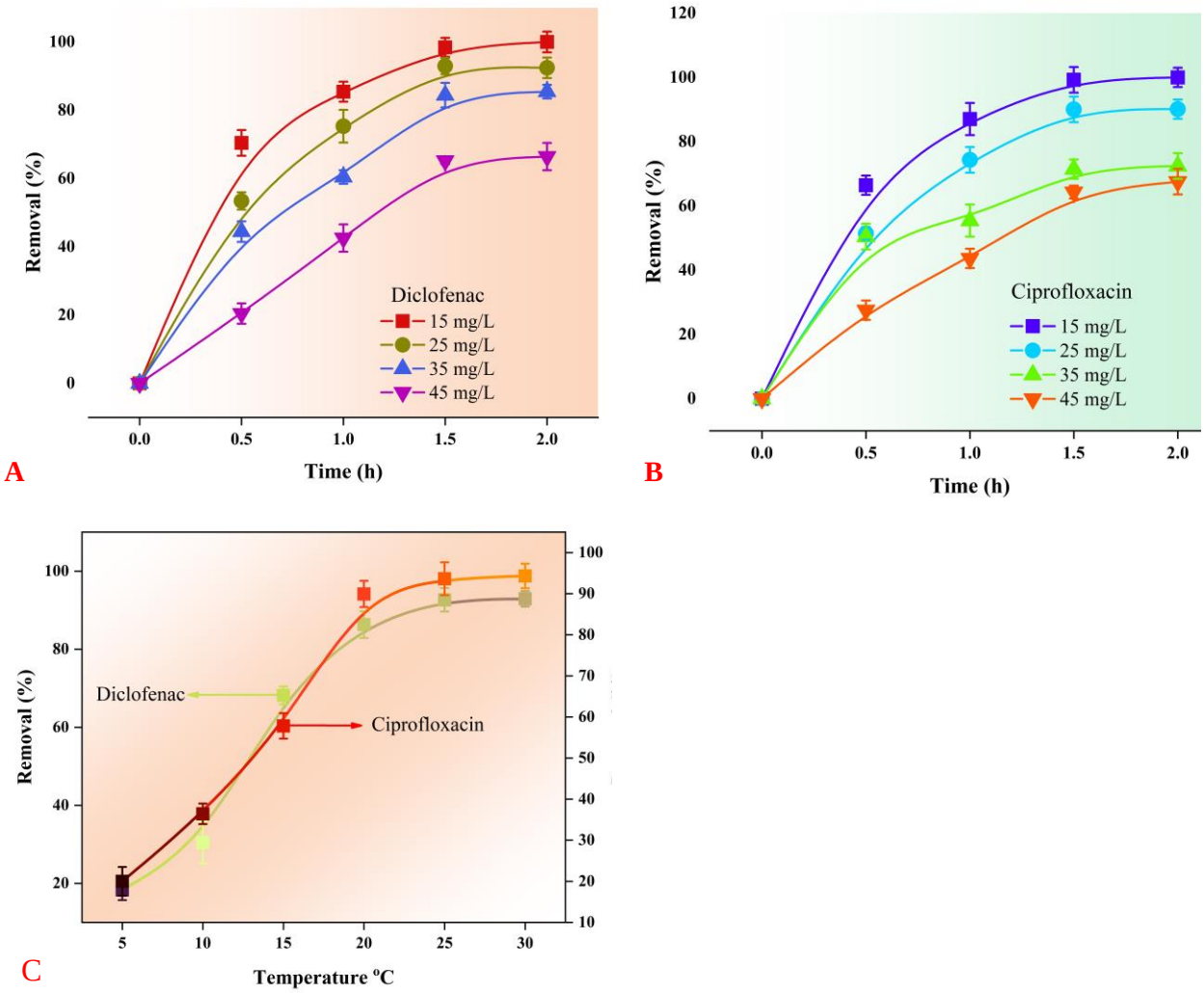

Figure 30 The removal efficiency of diclofenac(A) and ciprofloxacin(B) by using different concentrations; and the removal efficiency diclofenac and ciprofloxacin by using different temperature (C). The conditions were 1 g/L FPWAC, pH 6, mixture concentration 25 mg/L and 25 °C.

Elevating the pH from 2 to 7 (Figure 29 C and D) resulted in a progressive increase in diclofenac removal efficiency from 65.98% to 92.84%, with the highest removal efficiency observed at pH 6 (93.54%). Subsequent pH elevation led to a significant decline in removal efficiency, amounting to 32.10%. This decline persisted, reaching 59.88% at pH 11, where the removal efficiency was 33.66%. Regarding ciprofloxacin, there was a rise in removal efficiency from 64.98% at pH 2 to 94.54% at pH 7, with consistent removal efficacy exceeding 90% at pH 7 (90.84%). Similar to diclofenac, a decline in removal efficiency was observed for ciprofloxacin as pH values exceeded 7. The pH affects both the surface charge of FPWAC and the dissociation (ionization) of

pharmaceuticals. In the pH range of 2-7, FPWAC bears a negative charge that decreases as pH increases. Diclofenac has a dissociation constant of 4.15 [205], while ciprofloxacin has an acidic pKa of 6.1 and a basic pKa of 8.7 [206]. This means that as pH increases above 4.15, the molar fraction of the conjugate base of diclofenac (carrying a negative charge) increases [207]. Based on this information, diclofenac adsorption onto FPWAC cannot be primarily explained by electrostatic interaction, as both the adsorbent and adsorbate carry a negative charge, suggesting that other interactions might be responsible for the processes. Similarly, ciprofloxacin predominantly exists in its cationic form in the pH range of 2-6, while it is in its zwitterionic form at pH 7-8 [208], which also rules out a significant contribution of electrostatic interaction to the adsorption process. Upon comparison of the results for the two pollutants, both exhibited optimal removal at pH 6 and 7, with the highest values recorded at pH 6. Therefore, pH 6 was selected as the optimal pH condition for the experiment. An indispensable factor governing adsorption capacity lies in the initial concentration of contaminants present within the aqueous solution. Notably, in the context of diclofenac, elevating its concentration from 10 to 25 mg/L resulted in a discernible reduction in removal efficiency from 100% to 92.43%, respectively, with subsequent diminishing returns observed beyond this threshold (Figure 30). This observation implies that higher concentrations of diclofenac tend to swiftly saturate the available adsorption sites on the FPWAC, thus limiting its efficacy in pollutant removal. A parallel trend was noted in the case of ciprofloxacin, corroborating the saturation phenomenon observed. Consequently, it was deduced that a concentration of 25 mg/L would serve as the optimal concentration for both pollutants, balancing effective removal while avoiding premature saturation of adsorption sites. Temperature is a significant factor in determining the nature of an adsorption process, whether the process has endothermic attributes or exothermic characteristics [173].

Generally, adsorption processes behave endothermically [173]. It is noticeable that as the temperature rises, the removal efficacy of the bio-adsorbent increases. Such an increase is likely due to the rise in the mobility of pollutants induced by enhanced diffusion and the increase in active sites [174]. The temperature increase may also result in sorbent swelling, thereby increasing its adsorption capacity [174]. Interestingly, both contaminants showed enhanced removal efficiencies as the temperature rose, with optimal performance recorded at 25°C, achieving efficiencies of 92.65% for diclofenac and 93.65% for ciprofloxacin (Figure 30 C).

3.4.3.2. Kinetic, Isotherms and Thermodynamics Studies of Pharmaceuticals from Aqueous Solution over FPWAC

Figure 31 A shows experimental data fitting against the two most common isotherms: Langmuir and Freundlich models. The Freundlich model was found to better fit the experimental data compared to the Langmuir model, suggesting chemisorption with the development of multi-layer adsorbates on the adsorbent surface. The theoretical maximum sorption capacities (qm) attained with the Freundlich isotherm were 295.8 and 254.1 mg/g for diclofenac and ciprofloxacin, respectively, which were close to the experimental values compared to those produced with the Langmuir model of 279 and 228 mg/g. The correlation coefficients for the pseudo-second-order model were 0.987 and 0.991 for diclofenac and ciprofloxacin, respectively, while for the pseudo-first-order model, these coefficients were 0.994 and 0.989 (Figure 31 B). This indicates that the pseudo-second-order kinetic model fits well with the ciprofloxacin data, whereas diclofenac showed better agreement with the pseudo-first-order kinetic model. Although most of the literature suggests that better fitting to the pseudo-second-order model suggests chemisorption, while fitting to the pseudo-first-order model indicates physisorption, this interpretation may solely stem from a mathematical basis [209].

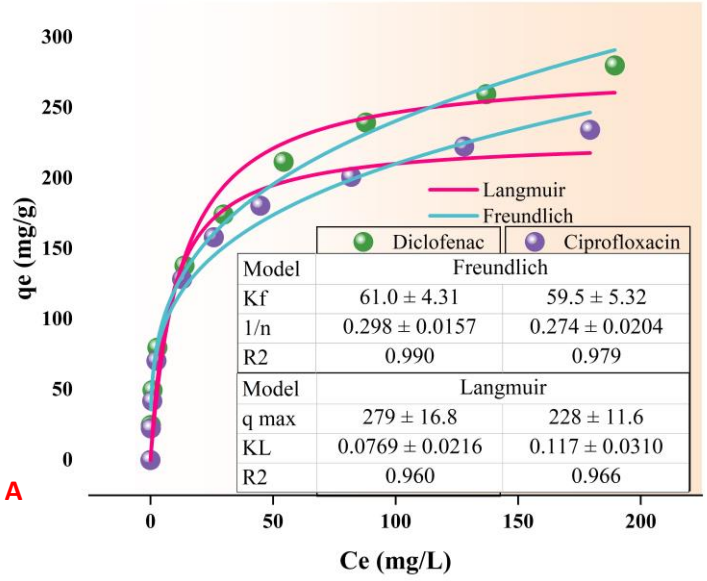

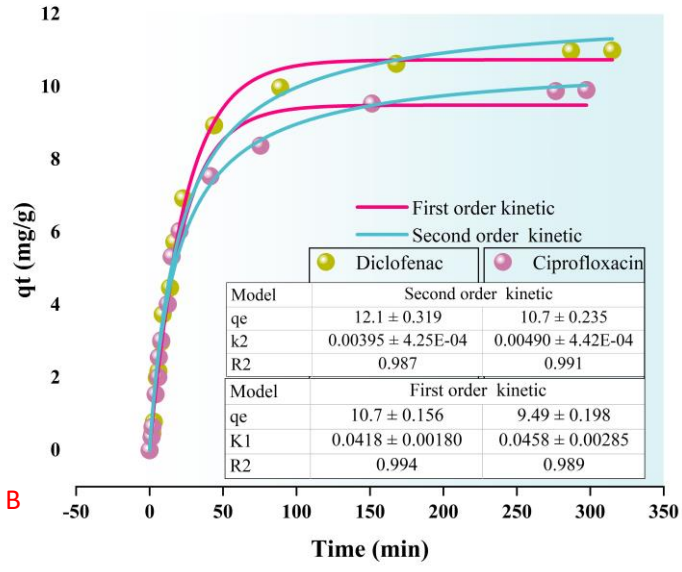

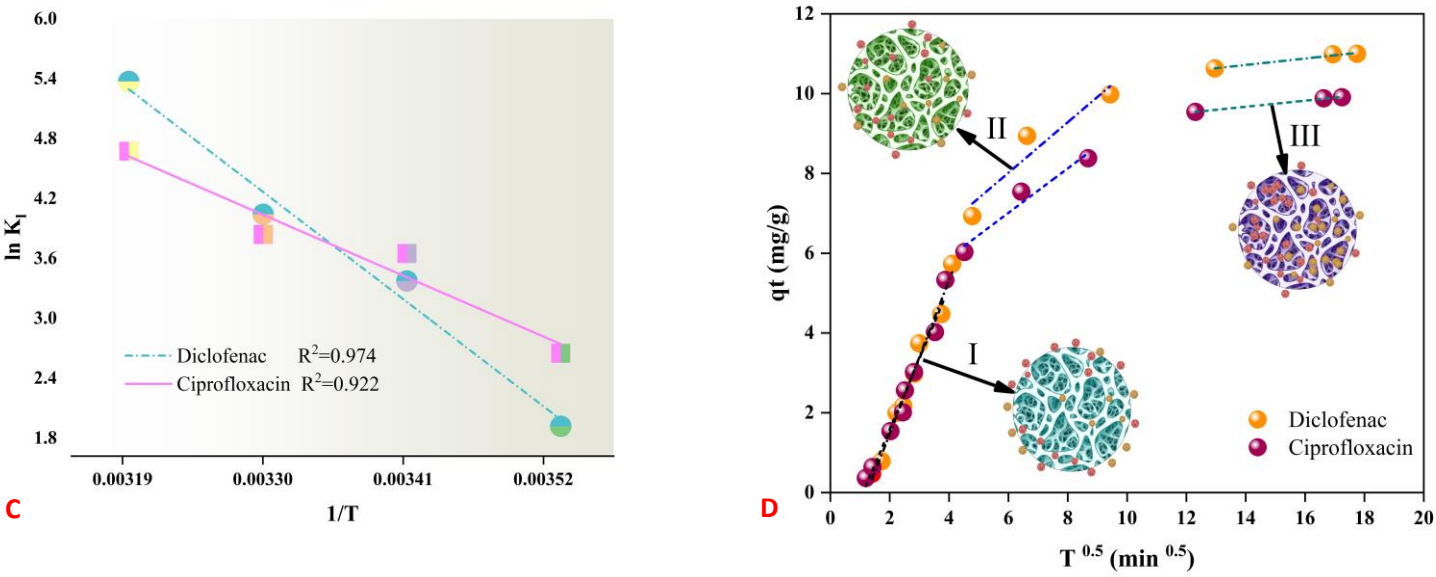

Figure 31 Isotherms (A), kinetic (B), thermodynamic (C), and intraparticle diffusion model (D) for the selected pollutants.

Thermodynamic insights governing the adsorption process of diclofenac and ciprofloxacin onto FPWAC are detailed in Table 17. These parameters encapsulate alterations in free energy (ΔG°), entropy (ΔS°), and enthalpy (ΔH°) at distinct temperatures, specifically 288 K, 298 K, 308 K, and 318 K (Figure 31 C). Notably, the observed reduction in ΔG° values with increasing temperature underscores the favorable impact of temperature on the efficiency of the adsorption process. Furthermore, the attainment of negative ΔG° values across the temperature range signifies the spontaneous nature of the adsorption phenomenon, indicative of its inherent thermodynamic favorability.

Table 17 Thermodynamic and Weber-Morris model parameters of pollutants adsorption on FPWAC

Thermodynamic	Temperature (K)	K_l	ΔG°	ΔH°	ΔS°	R^2
Diclofenac	283	6.8167	-4.516	81.236	303.544	0.974
	293	29.195	-8.219			
	303	56.997	-10.184			
	313	215.508	-13.982			
Ciprofloxacin	283	14.154	-6.235	46.151	184.820	0.922
	293	38.474	-8.891			
	303	46.525	-9.673			
	313	107.018	-12.160			
Weber-Morris model	K(I)	R^2(I)	K(II)	R^2(II)	K(III)	R^2(III)
Diclofenac	1.924	0.980	0.633	0.825	0.080	0.970
Ciprofloxacin	1.774	0.974	0.557	0.913	0.076	0.995

To analyze the steps influencing the rate of pharmaceutical adsorption in water using FPWAC, the data from the adsorption experiment were fitted using the Weber-Morris model [109]. The findings, along with the fitted parameters for each phase, are shown in Figure 31 D and Table 17. Figure 31 D and Table 17 demonstrate that the Weber-Morris model can accurately fit the adsorption data into three distinct phases. The correlation coefficient R^2 for the fit of both pollutants was higher in stage I compared to stages II and III (Table 17), indicating that external mass transfer controls the process. The first phase of adsorption clearly exhibited better alignment with the characteristics of the Weber-Morris model. Regarding the magnitude of the rate constant (k) values in the Weber-Morris model, stage I had the greatest k value for both pollutants,

suggesting that adsorption may occur rapidly during this stage. The declining k values in stages II and III suggest a gradual decrease in the adsorption rate. This indicates that pollutants were starting to move through the internal pores of FPWAC and search for adsorption sites. However, as the external driving force decreases and the internal diffusion resistance increases, the adsorption process gradually approaches saturation [210]. In a study conducted by Lu and colleagues, they observed a comparable three-stage process of adsorption, along with a decline in the rate constants for adsorption, when investigating the adsorption of methylene blue in water using activated carbon [211].

3.4.4. Recyclability of FPWAC and the Desorption Results

While the utilization of synthetic samples is imperative for comprehending the interaction dynamics between adsorbents and adsorbates, a comprehensive assessment of the efficacy of adsorbents in eliminating target contaminants necessitates testing within a natural sample matrix. The removal efficiency of diclofenac and ciprofloxacin was assessed using spiked water and wastewater matrices. Table 18 presents the characteristics of the wastewater matrix. Figure 32 illustrates the removal efficiency of diclofenac and ciprofloxacin from various water matrices across six cycles, employing 1 g/L FPWAC, pH 6, 25°C, and a pollutant concentration of 25 mg/L. The removal of pharmaceutical pollutants was monitored over six cycles in both water and wastewater. Regarding the water medium, it is evident from Figure 32 that the removal of pollutants until the third cycle exceeded 90%, with percentages of 93.06% and 92.10% for diclofenac and ciprofloxacin, respectively. The desorption experiments were carried out using three agents: ethanol, HCl, and HNO_3. These agents were tested throughout the FPWAC recyclability. Figure 32 shows the results of pharmaceutical desorption in each cycle for water (A) and wastewater (B). During the third cycle, ethanol exhibited superior desorption efficacy, achieving percentages of 88.03% and 88.52% for diclofenac and ciprofloxacin, respectively. Conversely, other agents, such as HCl and HNO_3, demonstrated lower efficiency compared to ethanol. In this study, all three agents were evaluated up to the sixth cycle to validate the performance of the optimal desorption agent. Following the third cycle, the removal efficiency of both pollutants gradually declined to 82.57% and 86.73% for diclofenac and ciprofloxacin, respectively. After the initial desorption tests, a significant decline in desorption efficiency was observed, with diclofenac and ciprofloxacin registering reductions to 37.54% and 31.93%, respectively.

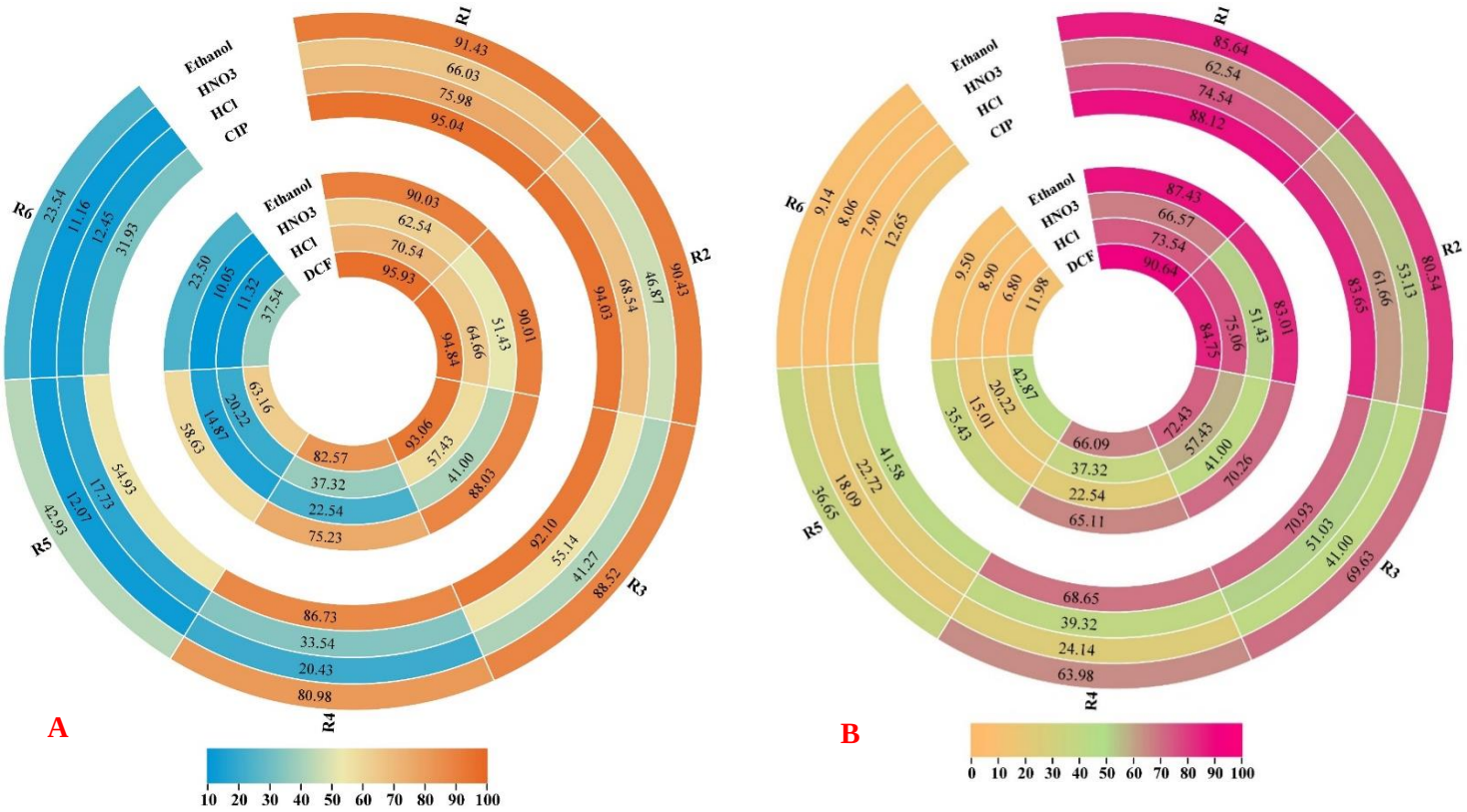

Figure 32 Recyclability of FPWAC (removal percentages %) for diclofenac (DCF) and ciprofloxacin (CIP) along with used desorption agents for water (A) and wastewater(B).

Among the desorbing agents examined, ethanol proved to be particularly effective, allowing for the desorption of 23.50% of diclofenac and 23.54% of ciprofloxacin. A study focused on the desorption characteristics of graphitic biochar activated with potassium ferrate found the removal efficiency to exceed 80%, consistently realized in the first five desorption cycles [144]. The fact that FPWAC is highly effective as a potential adsorbent for pharmaceutical removal illustrates its promising direction in environmental remediation. Testing for the removal of both pollutants from wastewater matrices was carried out using FPWAC. In the first round, the removal efficiencies for diclofenac and ciprofloxacin were 90.64% and 88.12%, respectively. However, the efficiency of pollutant removal declined during the second cycle to 84.75% and 83.65% for diclofenac and ciprofloxacin, respectively. After four cycles, the removal efficiency of pharmaceuticals remained above 65%, followed by a significant drop. Recycling ethanol showed better desorption capability

than both HCl and HNO_3, which is consistent with the data obtained in the water medium previously.

Table 18 Secondary effluent characteristics.

Parameters	Concentration (mg/L)
Biochemical oxygen demand (5 days)	23.86 ±3.05
Chemical oxygen demand	62.04±2.11
Total Phosphorus	6.07±0.51
Suspended solids	15.74±1.89
Volatile suspended solids	17.88± 1.01
Electrical conductivity	886±4.51 μmoss/cm
Ammonia	13.02±1.04 (NH_3-NH_4)
Nitrate-nitrite	4.05 ± 0.44 (NO_2-NO_3)
Total Kjeldahl nitrogen	13.76 ± 2.21
Total dissolved solids	532± 3.09
Total solids	605± 3.17
pH	6.5
Temperature (^oC)	26.2

3.4.5. Comparison of Prepared FPWAC with Other Reported Systems

Table 19 presents selected recent studies[212], [213], [214], [215], [216] that employ different adsorbents for removing pharmaceuticals from an aqueous medium. Compared with other studies using different activated carbon, it can be clearly stated that the currently developed activated carbon [217] has better performance in terms of removing a mixture of pharmaceuticals than other works.

Table 19 Examples of the adsorbents employed in the process of pharmaceutical removal

Compound	Adsorbent	Removal (%)	References
Promazine	Activated carbon modified with metal ferrite $CoFe_2O_4$ nanoparticles	94.08	[212]
Ceftriaxone sodium	Activated carbon based TiO_2 composite	84.50	[213]
Chloroquine	Plantain peels	78.8	[214]
Tetracycline	Composite biochar synthesized from algal biomasses	97.56	[215]
Ciprofloxacin	Jackfruit peels	99.8	[216]
Diclofenac and ciprofloxacin	Pinewood activated carbon	(95.93 and 95.04 respectively in water) (90.64 and 88.12 respectively in wastewater)	Current work

4. Comparison of OSAC, BPAC, and FPWAC

4.1. Kinetic and isotherms

The adsorption behavior of OSAC, BPAC, and FPWAC reflects distinct characteristics in terms of kinetic and isotherm models (Table 20). OSAC exhibited a strong alignment with the Langmuir isotherm model, suggesting monolayer adsorption of diclofenac and ciprofloxacin on a homogeneous surface, with correlation coefficients of 0.971 and 0.943, respectively. The maximum adsorption capacities (qm) for these compounds were 256.41 mg/g and 294.98 mg/g, highlighting OSAC's effectiveness in adsorbing pharmaceutical pollutants. Kinetic studies showed that the pseudo-first-order model provided the best fit, indicating that the adsorption process is primarily influenced by the concentration gradient and that diffusion processes play a significant role, implying a physisorption-driven mechanism. In comparison, BPAC also favored the Langmuir model but demonstrated higher sorption capacities, with 393.70 mg/g for amoxicillin and 338.98 mg/g for carbamazepine, signifying superior adsorption performance. The high correlation coefficients for the pseudo-second-order kinetic model (0.992 for amoxicillin and 0.984 for carbamazepine) suggested chemisorption as the dominant mechanism, governed by the interaction between the adsorbent surface and the adsorbates through chemical bonding. This highlights BPAC’s potential for applications requiring higher binding energies and pollutant removal efficiency. FPWAC, on the other hand, showed better compatibility with the Freundlich isotherm model, indicating multilayer adsorption on a heterogeneous surface. The maximum adsorption capacities calculated from the Freundlich model were 295.8 mg/g for diclofenac and 254.1 mg/g for ciprofloxacin, which closely matched experimental values and were slightly higher than those obtained from the Langmuir model. The kinetic data revealed a mixed mechanism: the pseudo-first-order model was a better fit for diclofenac (R^2 = 0.994), pointing toward physisorption, while the pseudo-second-order model better described ciprofloxacin adsorption (R^2 = 0.991), implying chemisorption.

A unified analysis reveals both similarities and key differences among the activated carbons. OSAC and BPAC shared a preference for the Langmuir model, indicating monolayer adsorption, whereas FPWAC followed the Freundlich model, reflecting surface heterogeneity and multilayer formation. BPAC’s higher sorption capacities suggest it is better suited for adsorbing a wider range of pharmaceutical pollutants compared to OSAC and FPWAC. In terms of kinetics, BPAC and

FPWAC demonstrated a stronger tendency toward chemisorption, whereas OSAC was predominantly governed by physisorption. The differences in adsorption performance and mechanisms can be attributed to the physicochemical properties of the activated carbons, such as pore distribution, surface area, and functional group availability. BPAC's higher adsorption capacities and chemisorption-driven mechanism suggest a greater abundance of active sites compared to OSAC and FPWAC, as supported by SEM-EDS images (Figure 15) and chemical interactions, potentially due to higher surface oxygen-containing groups. FPWAC's preference for Freundlich isotherms and its mixed kinetic mechanisms may indicate a broader pore size distribution compared to BPAC and OSAC, as also evidenced by SEM-EDS images (Figure 27). This broader distribution enables multilayer adsorption but limits specific interactions. OSAC's physisorption-driven behavior and moderate adsorption capacities suggest a more uniform but less chemically active surface.

Table 20 Comparison between the three developed ACs

Adsorbent	**Best Fit Isotherm**	**Best Fit Kinetics**	**Removal Efficiency (%)***	**Recyclability (Cycles)**
OSAC	Langmuir	Pseudo-first-order	MQ water and Lake water (99.63 and 99.29 for diclofenac and ciprofloxacin, respectively) Wastewater (99.34 and 99.51 for diclofenac and ciprofloxacin, respectively)	7
BPAC	Langmuir	Pseudo-second-order kinetic model	MQ water (91.63 and 90.29 for amoxicillin and carbamazepine, respectively) Lake water (86.63 and 83.29 for amoxicillin and carbamazepine, respectively) Wastewater (82.34 and 81.51 for amoxicillin and carbamazepine, respectively)	7
FPWAC	Freundlich	Pseudo-second-order	MQ water (95.93 and 95.04 for diclofenac and ciprofloxacin respectively)	6

	model (ciprofloxacin) pseudo-first-order (diclofenac)	wastewater (90.64 and 88.12 for diclofenac and ciprofloxacin respectively)

* Removal percentages are for the first cycle

4.2. Long-term performances

The long-term performance of OSAC, BPAC, and FPWAC for pharmaceutical removal was evaluated across various water matrices, including MQ water, lake water, and wastewater, with each adsorbent demonstrating unique efficiencies and limitations. OSAC showed high initial removal efficiencies (>96%) for diclofenac and ciprofloxacin in all water matrices during the first two cycles, though performance declined over subsequent cycles. By the sixth cycle, the removal efficiency in MQ and lake water remained above 50%, while wastewater exhibited slightly lower efficiency (>40%). This demonstrates OSAC's resilience in pharmaceutical removal, particularly in cleaner water matrices, though the presence of interfering substances in wastewater impacts its performance. In contrast, BPAC was assessed for the removal of amoxicillin and carbamazepine under similar conditions. The removal efficiency exceeded 90% during the first cycle in MQ water, but lake water and wastewater exhibited reductions of approximately 6% and 9%, respectively. By the fourth cycle, the average removal efficiency in MQ water remained above 86%, whereas it declined to 74.57% in lake water and 63.89% in wastewater. A more pronounced decline occurred in the final two cycles, with MQ water showing approximately 41.43% and 37.84% efficiency for the two pollutants, while lake water and wastewater dropped significantly to as low as 15.84% and 12.09%. The decline in performance is attributed to the saturation of active adsorption sites and the masking effect of ions in wastewater. FPWAC, on the other hand, demonstrated robust performance in removing diclofenac and ciprofloxacin, with removal efficiencies exceeding 90% in water matrices during the first three cycles. However, after the third cycle, a decline in efficiency was observed, particularly in wastewater, due to interfering compounds and the regeneration limitations of FPWAC. Despite operating at a slightly lower pollutant concentration (25 mg/L),

FPWAC exhibited comparable initial efficiency to OSAC but with a steeper decline after multiple cycles.

All three adsorbents displayed high removal efficiencies during the initial cycles, particularly in MQ water, suggesting their strong adsorption capacity in cleaner matrices. However, the presence of interfering substances in lake water and wastewater significantly impacted their long-term performance. This decline is likely due to fouling of the adsorbent surfaces and reduced availability of active adsorption sites, which is a common challenge in environmental applications of activated carbon. Additionally, all materials exhibited removal performance with successive cycles, though the rate of decline varied. The differences in performance are notable in terms of stability and resilience. OSAC outperformed BPAC and FPWAC in maintaining higher removal efficiencies in wastewater during later cycles, indicating its greater resistance to fouling and interference (Table 20). FPWAC, while initially comparable to OSAC, demonstrated a faster decline in efficiency, particularly in wastewater. BPAC, despite its promising early performance, showed the steepest decline overall, particularly in wastewater, likely due to its susceptibility to fouling by ions and other matrix components. While OSAC demonstrates the most consistent long-term performance across various water matrices, BPAC and FPWAC exhibit specific strengths in cleaner matrices but are more vulnerable to interference in complex wastewater environments.

It can be stated that OSAC has better performance in terms of pollutant removal for the following reasons: OSAC was found to be effective across a wide pH range (2–11) and achieved almost complete removal of diclofenac and ciprofloxacin in 75 min. Additionally, the system successfully performed over 7 cycles. On the other hand, BPAC performed well until the seventh cycle, but it had a longer saturation time of 120 min and required a specific pH value (pH 5). Meanwhile, FPWAC had the lowest recyclability performance (six cycles) compared to the others, with the same saturation time as BPAC (120 min).

ACs production cost

To assess the commercial viability of AC production on a large scale, it is essential to estimate production costs at a commercial level. This study evaluated the costs associated with pilot-scale AC production using various activation processes. Based on assumptions outlined in previous studies, the pilot-scale cost analysis was conducted by summing the fixed capital investment and total annual operating costs, using equipment cost reported in the literature [218], [219], [220].

Figure 33 shows the process flow diagram for chemical activation production of OSAC (A), BPAC(B) and FPWAC(C). The capital and operational expenses for large-scale AC production were estimated using vendor quotes and published data to determine manufacturing costs. The cost evaluation for pilot-scale processes was performed in line with methodologies detailed in the literature. For scaled-up production cost estimates, equipment design, sizing, and capital cost assessment methods from prior publications [218], [219], [220] were applied. Cost estimates for consumables, equipment, and capital investments were obtained from vendor quotes (e.g., Sigma-Aldrich, Fisher Scientific and Alibaba) and published literature [220]. The capital cost calculations included the total direct costs such as equipment installation, instrumentation, piping and material transport (augers), electrical installations, building structures, yard improvements, service facilities, and land as well as indirect manufacturing costs, such as engineering and supervision, construction expenses, contractor fees, and contingencies. Key equipment utilized in the cost evaluation included a hammer mill, rotary dryer, rotary kilns, rotary cooler, tanks (for acid/base soaking, washing, recovery, and storage), and sieves. Additional costs, such as equipment installation, instrumentation, material transport systems, electrical installations, structural improvements, land use, maintenance, engineering and management, construction expenses, contractor fees, and contingencies, were also adopted from the literature [218], [219], [220], [221].

The cost estimation for AC production was based on a conservative yield of 30%, ensuring feasibility, and assuming 300 working days per year. With a final chemically activated carbon yield estimated at 3,000 kg/day, the annual output was projected at 900,000 kg per year. The estimated capital costs for AC production from BPAC, OSAC, and FPWAC were $2.1 million, $2.3 million, and $2.6 million, respectively. These low capital costs indicate that setting up production facilities is feasible, especially when compared to the potential revenue generated from a 900,000 kg annual output. Based on annual operating costs and an output of 900,000 kg per year, the estimated production costs for BPAC and FPWAC were approximately $4.27 per kg and $4.53 per kg, respectively. The higher costs for these products are largely attributed to the substantial chemical inputs required during their activation processes. In contrast, the production cost for OSAC was estimated at $3.77 per kg, primarily due to its reduced reliance on chemical inputs during activation. This reduction not only lowers costs but also enhances scalability, minimizes environmental impact, and alleviates challenges associated with chemical procurement. When compared to commercial activated carbon prices, which average around $135,000 per ton (or $135

per kilogram) [86], the synthesized activated carbons (ACs) are significantly more cost-effective. At $135/kg, commercial AC is nearly 10 to 36 times more expensive than the developed ACs, making the latter a highly economical alternative. The cost disparity underscores the substantial economic advantage of the biomass-derived ACs which could disrupt the commercial AC market if production is scaled while maintaining quality and cost advantages. In addition to being cost-effective, the synthesized AC produced in this study exhibited superior quality compared to many commercially available activated carbon products. This makes it highly suitable for scale-up production. Furthermore, the prepared AC demonstrated high efficiency in adsorbing pharmaceutical compounds and was produced at a low estimated capital cost. This suggests that the selected biomass is an excellent precursor for AC production, providing an economical and effective solution for pharmaceutical compound removal. However, to truly challenge the dominance of commercial AC, the synthesized ACs need broader contaminant efficacy, large-scale production trials, and industry acceptance through performance benchmarking. If these hurdles are addressed, the synthesized ACs could redefine the market by delivering affordable, high-quality solutions aligned with sustainability goals.

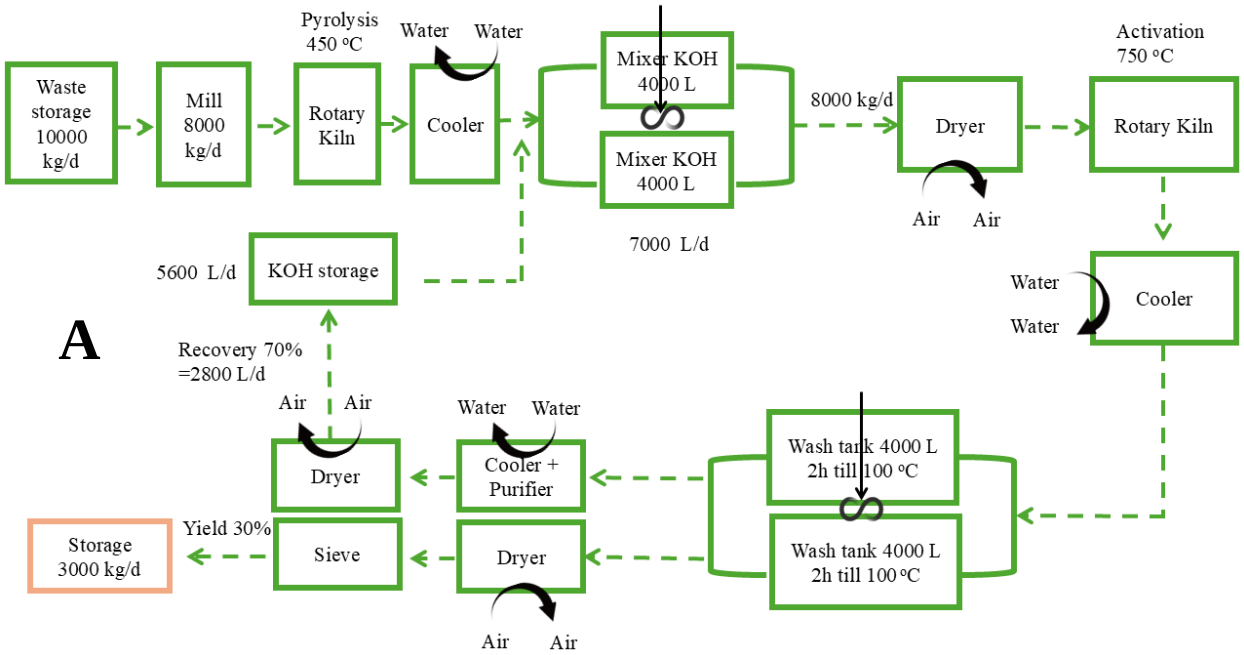

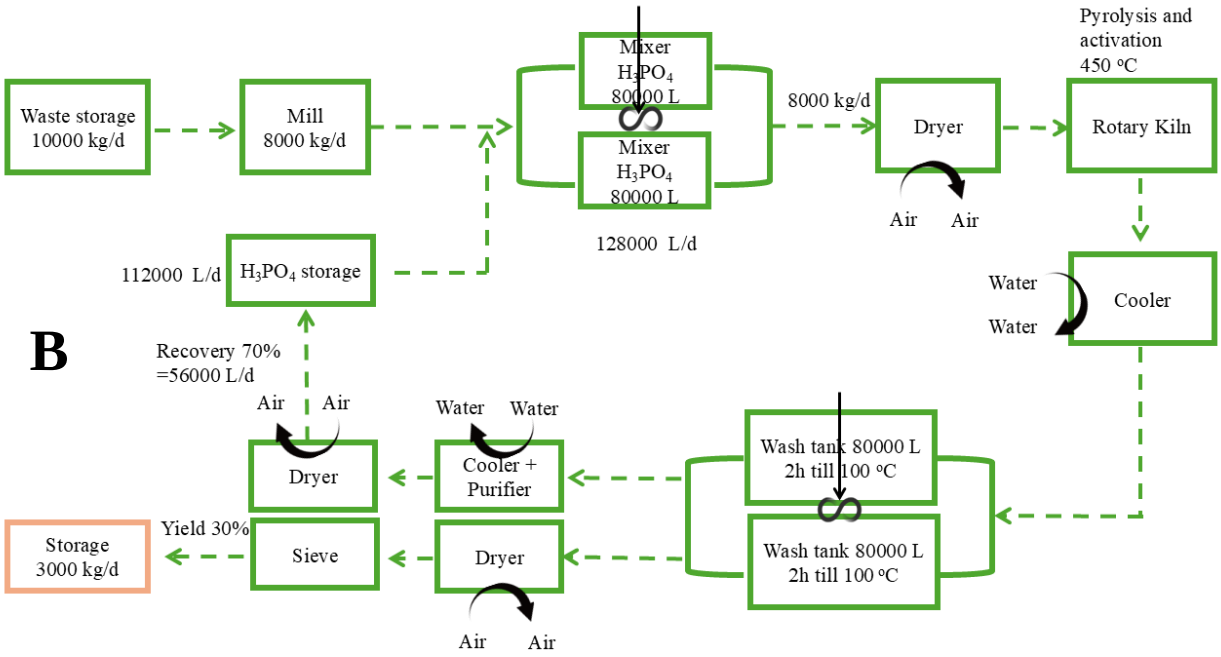
B
Waste storage
10000 kg/d
Mill
8000 kg/d
Mixer
H_3PO_4
80000 L
Mixer
H_3PO_4
80000 L
128000 L/d
8000 kg/d
Dryer
Air
Air
Pyrolysis and
activation
450 °C
Rotary Kiln
Water
Water
Cooler
112000 L/d
H_3PO_4 storage
Recovery 70%
=56000 L/d
Air
Air
Dryer
Water
Water
Cooler +
Purifier
Wash tank 80000 L
2h till 100 °C
Wash tank 80000 L
2h till 100 °C
Storage
3000 kg/d
Yield 30%
Sieve
Dryer
Air
Air

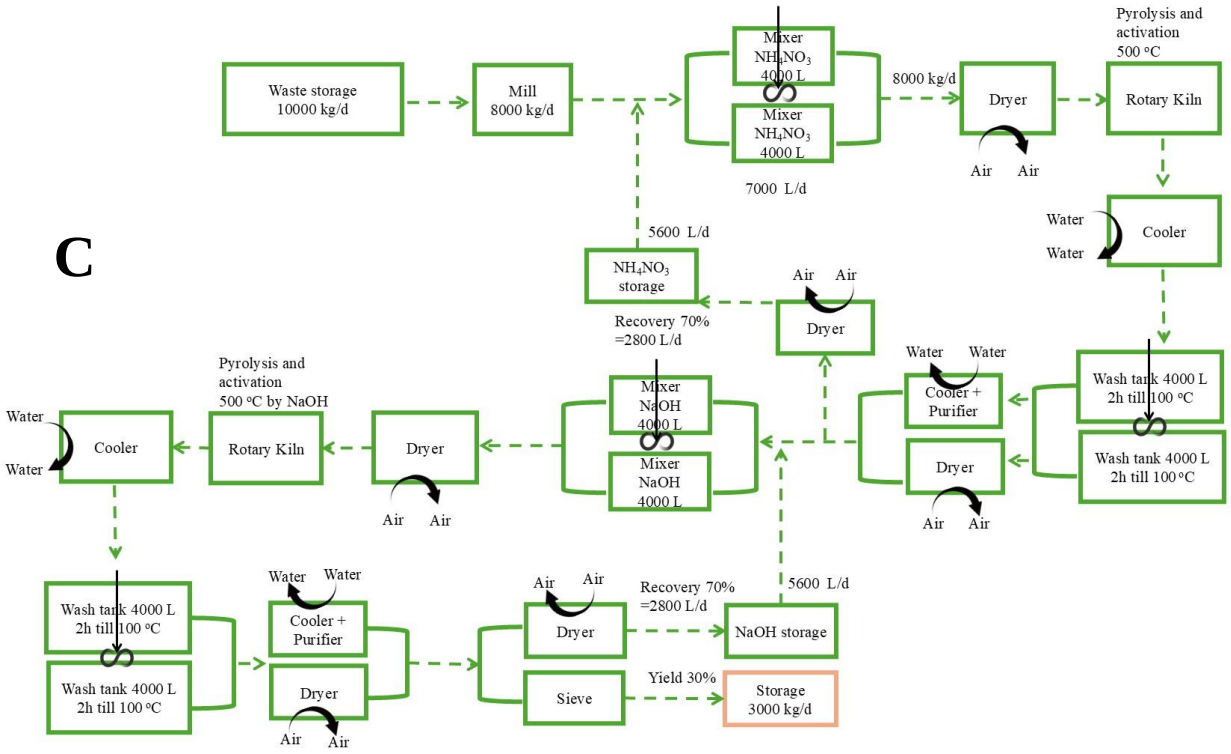

Figure 33 Process flow diagram for chemical activation production of OSAC (A), BPAC(B) and FPWAC(C).

5. Conclusion

The ability to activate carbons obtained from different agro-industrial wastes to remove pharmaceutical compounds from various aqueous solutions was successfully investigated. Below is a summary of each tested activated carbon.

1- BPAC: This work exhibited the use of banana peel, an agricultural waste, in the development of BPAC, which was revealed to be a very efficient adsorbent for amoxicillin and carbamazepine removal from different waters. After a contact period of 120 min, the adsorption of pollutants from aqueous solutions reached a state of equilibrium. The kinetics investigations suggested that the pseudo-second-order model was more suitable for these contaminants. The analysis of the isotherm demonstrated a strong correlation between the adsorption data and the Langmuir isotherm model. The BPAC had maximal monolayer adsorption capabilities of 393.70 mg/g and 338.98 mg/g for the elimination of amoxicillin and carbamazepine pollutants, respectively. BPAC was easily regenerated and effectively used on seven separate occasions across various water matrices. Based on these data, it can be inferred that BPAC is very beneficial, cost-effective, and efficient in eliminating organic microcontaminants from various aquatic environments. This BPAC could be used as a cost-effective substitute for expensive materials like granular, ion-exchange resins, powdered activated carbons, carbon nanotubes, etc., in the treatment of liquid wastes that include organic micro contaminants. To assess the feasibility of using BPAC as a potential adsorbent for pharmaceutical removal in water treatment facilities, it should be tested with a larger number of contaminants that simulate real-life scenarios.

2- FPWAC: A novel activated carbon derived from agro-industrial wastes (FPWAC) was synthesized successfully through dual treatment with NH_4NO_3 followed by NaOH. The adsorption batch experiments for the removal of diclofenac and ciprofloxacin followed a non-linear Freundlich isotherm. The best adsorption parameters for both pharmaceuticals were obtained with an FPWAC dosage of 1 g/L, pH 6, mixture concentration of 25 mg/L, and a temperature of 25 °C. The FPWAC demonstrated superior adsorption performance in treating both diclofenac and ciprofloxacin from water and wastewater for up to six cycles, with more than 95% removal efficiency for water matrices and 90% for wastewater matrices in the first cycle. The main mechanisms involved were the multi-layer behavior of the adsorption in this work, hydrophobic interactions, π–π interactions, and intra-particle diffusion. The developed FPWAC has exceptional potential due to its ease of acquisition and remarkable adsorption capability. Consequently, it is

highly suitable for use as an adsorbent to eliminate other emerging pollutants from water and wastewater.

3- OSAC: This study proposed and tested activated carbon from olive stone waste (OSAC) for pharmaceutical removal from different water matrices. The prepared OSAC at high temperature and a large amount of activation agent had the highest porous surface area. This product was proven to be efficient in removing diclofenac and ciprofloxacin in different water matrices. Most importantly, its efficiency did not drop significantly when changing the medium from pure water to secondary effluent wastewater, which is a strong indication of its feasible application in the water industry. Another important note is the stable performance of OSAC over a wide range of pH. The reusability of OSAC with a high removal percentage over three cycles is another attractive trait of this product. The adsorption of target pharmaceuticals onto OSAC can be categorized as an endothermic process that might be driven mainly by physical means such as electrostatic and hydrophobic interactions. The adsorption was fast reaching equilibrium in 75 min and follows first-order kinetics. While adsorption is a simple and cost-effective process for moving challenging contaminants, they still produce secondary pollution when regenerating them. Hence, the high adsorption efficiency and porous structure of OSWA should be explored in the future as a bed for biological, enzymatic and chemical degradation of the adsorbed contaminants.

6. List of the thesis points

The new scientific findings of this PhD dissertation were the development of sustainable, cost-effective, and environmentally friendly adsorbents from agro-industrial waste to remove a mixture of pharmaceutical compounds from water, wastewater, and lake water. The effectiveness of all activated carbons in removing diclofenac, ciprofloxacin, amoxicillin, and carbamazepine was further examined by testing their recyclability performance. The primary factors affecting their capacity to absorb contaminants were analyzed. Additionally, the production costs for all activated carbons were calculated. The new scientific findings in this thesis can be summarized as follows:

1. I have successfully converted olive stone waste (OSW) **into activated carbon** (OSAC) **using KOH to remove a mixture of diclofenac and ciprofloxacin from** MQ water, **lake water, and wastewater.** I synthesized OSAC at 750 °C using KOH (1:3), which exhibited a high surface area (946 m^2/g) compared to OSW (265 m^2/g). I found that diclofenac and ciprofloxacin were effectively removed from various water matrices within 75 minutes under optimal conditions (25 °C, pH 7, 50 mg/L initial concentration, and 1 g/L dosage). Additionally, I observed that the **adsorption process was endothermic**, maintaining stable efficiency across a pH range of 2–8, with only a slight decline at pH 9–11, while temperature increases beyond 30 °C had no significant impact. Through Boehm titration, I confirmed a 98% increase in basicity, which was supported by EDS mapping that also detected the presence of potassium. OSAC maintained consistent adsorption performance across seven cycles in MQ water, lake water, and wastewater. I concluded that the adsorption followed the Langmuir model (R^2 = 0.971 for diclofenac, 0.943 for ciprofloxacin), indicating monolayer adsorption, while the pseudo-first-order kinetic model demonstrated that the adsorption rate is primarily governed by the concentration gradient between the liquid and solid phases.

> The results of this work were published in *Chemosphere Journal*: Al-Sareji, Osamah J., Ruqayah Ali Grmasha, Mónika Meiczinger, Raed A. Al-Juboori, Viola Somogyi, Csilla Stenger-Kovács, and Khalid S. Hashim. "A sustainable and highly efficient fossil-free carbon from olive stones for emerging contaminant removal from different water matrices." Chemosphere 351 (2024): 141189. (D1, IF = 8.8)

2- I have effectively transformed banana peel waste (BP) **into activated carbon** (BPAC) **using H_3PO_4 to remove a mixture of amoxicillin and carbamazepine from** MQ water**, lake water, and wastewater.** I found that the developed activated carbon showed a significant increase in surface area, from 0.650 m^2/g (BP) to 912 m^2/g (BPAC) after the activation process. I determined that the optimal conditions for adsorption were 25 °C, a dosage of 1.2 g/L, a saturation time of 120 minutes, a pollutant concentration of 25 mg/L, and pH 5, although pH sensitivity could limit its practical application. Additionally, I successfully removed amoxicillin and carbamazepine using BPAC over seven cycles, achieving over 90% removal efficiency in MQ water. However, efficiency declined by 6% in lake water and 9% in wastewater due to matrix effects. Post-adsorption SEM analysis indicated partial pore filling, while Boehm titration revealed a 2.5-fold increase in total acidic groups and a 1.36-fold increase in basicity. Proximate and ultimate analyses showed an increase in fixed carbon content from 0.67% to 74% and in carbon content from 42% to 74%, along with reductions in hydrogen and oxygen content, confirming effective carbonization. Adsorption followed the Langmuir isotherm model, while kinetics were best described by the pseudo-second-order model, with pollutant removal driven by hydrophobic interactions, π–π interactions, and intra-particle diffusion.

The results of this work were published in *Materials Journal*: Al-sareji, Osamah J., Ruqayah Ali Grmasha, Mónika Meiczinger, Raed A. Al-Juboori, Viola Somogyi, and Khalid S. Hashim. "A Sustainable Banana Peel Activated Carbon for Removing Pharmaceutical Pollutants from Different Waters: Production, Characterization, and Application." Materials 17, no. 5 (2024): 1032. (Q2, IF=3.1)

3- I developed a novel activated carbon from pinewood waste (FPWAC) **through a two-stage chemical activation process** using NH_4NO_3 and NaOH **to remove a mixture of diclofenac and ciprofloxacin from MQ water and wastewater.** I found that the FPWAC had a BET surface area of 913 m^2/g. SEM-EDS analysis revealed well-defined honeycomb channels that enhanced pollutant accessibility. The surface morphology after the adsorption process became amorphous with irregular holes, confirming successful adsorption. I determined that the optimal removal conditions were at pH 6, with a 120-minute saturation time, using an FPWAC dosage of 1 g/L, a pollutant concentration of 25 mg/L, and a temperature of 25°C. EDS analysis showed initial carbon and oxygen contents of 78% and 10%, respectively, with post-adsorption changes indicating a

15% decrease in carbon and a 6% increase in oxygen, confirming pharmaceutical molecule attachment. FTIR analysis verified functional group interactions, particularly hydrogen bonding, as evidenced by the diminished hydroxyl band at 3412 cm^{-1}.I successfully tested FPWAC's recyclability, maintaining over 95% removal efficiency for both pollutants in water matrices and 90% in wastewater matrices across six cycles, with ethanol proving to be the most effective regeneration solvent. Adsorption followed multilayer mechanisms, including hydrophobic and π–π interactions and intra-particle diffusion.

The results of this work were published in *Chemosphere Journal*: Al-Sareji, Osamah J., Ruqayah Ali Grmasha, Mónika Meiczinger, Raed A. Al-Juboori, Miklós Jakab, Adrienn Boros, Hasan Sh Majdi, Norbert Miskolczi, and Khalid S. Hashim. "A novel two-stage chemical activation of pinewood waste for removing organic micropollutants from water and wastewater." Chemosphere 363 (2024): 142974. (D1, IF=8.1)

4- I have successfully demonstrated that the produced activated carbons (ACs) are much cheaper than the commercial ones. Therefore, I have proven the economic feasibility of the developed ACs, in addition to their environmental importance. I assessed the commercial viability of large-scale activated carbon production, estimating costs for pilot-scale production using BPAC, OSAC, and FPWAC. The cost evaluation was based on fixed capital investment, total annual operating costs, and vendor quotes for equipment. The estimated capital costs for AC production were $2.1 million for BPAC, $2.3 million for OSAC, and $2.6 million for FPWAC, with annual outputs of 900,000 kg, calculated from a yield of 3,000 kg/day over 300 working days. Production costs were $4.27 per kg for BPAC, $4.53 per kg for FPWAC, and $3.77 per kg for OSAC, with OSAC being the most cost-effective due to its lower chemical input requirements. Commercial AC averages $135 per kg, making the developed ACs significantly more affordable, being 10 to 36 times cheaper. I conclude that the process flow diagram for the chemical activation production of OSAC is the best option among the others (Figure 33, A). This cost advantage, coupled with superior quality and effectiveness in adsorbing pharmaceutical compounds, suggests that biomass-derived ACs could disrupt the commercial AC market if scaled up, provided they meet broader contaminant efficacy and industry standards.

This point was formulated based on the published literature [218], [219], [220], [221].

References

[1] B. S. Rathi, P. S. Kumar, and D.-V. N. Vo, “Critical review on hazardous pollutants in water environment: Occurrence, monitoring, fate, removal technologies and risk assessment,” *Sci. Total Environ.*, vol. 797, p. 149134, Nov. 2021, doi: 10.1016/j.scitotenv.2021.149134.

[2] A. Sudan, A. Ghosh, M. Verma, and P. Tomar, “Impact of Water Pollution & Perspective Techniques to Mitigate It: An Overview,” in *Handbook of Water Pollution*, 1st ed., Inamuddin, T. Altalhi, and A. Alrooqi, Eds., Wiley, 2024, pp. 29–64. doi: 10.1002/9781119904991.ch2.

[3] H. Chawla, S. K. Singh, and A. K. Haritash, “Reversing the damage: ecological restoration of polluted water bodies affected by pollutants due to anthropogenic activities,” *Environ. Sci. Pollut. Res.*, vol. 31, no. 1, pp. 127–143, Dec. 2023, doi: 10.1007/s11356-023-31295-w.

[4] T. Undabeytia, J. M. Jiménez-Barrera, and S. Nir, “Removal of Emerging Contaminants by Degradation during Filtration: A Review of Experimental Procedures and Modeling,” *Water*, vol. 16, no. 1, p. 110, Dec. 2023, doi: 10.3390/w16010110.

[5] J. Kim, L. Dong, H. K. Shon, and K. Park, “Current progress in semi-batch reverse osmosis for brackish water desalination,” *Desalination*, vol. 578, p. 117434, Jun. 2024, doi: 10.1016/j.desal.2024.117434.

[6] J. Osamede Airouyuwa, N. Sivapragasam, A. Ali Redha, and S. Maqsood, “Sustainable green extraction of anthocyanins and carotenoids using deep eutectic solvents (DES): A review of recent developments,” *Food Chem.*, vol. 448, p. 139061, Aug. 2024, doi: 10.1016/j.foodchem.2024.139061.

[7] T. Yu *et al.*, “Recent advances in the applications of encapsulated transition-metal nanoparticles in advanced oxidation processes for degradation of organic pollutants: A critical review,” *Appl. Catal. B Environ.*, vol. 342, p. 123401, Mar. 2024, doi: 10.1016/j.apcatb.2023.123401.

[8] M. Pivokonsky, K. Novotna, R. Petricek, L. Cermakova, M. Prokopova, and J. Naceradska, “Fundamental chemical aspects of coagulation in drinking water treatment – Back to basics,” *J. Water Process Eng.*, vol. 57, p. 104660, Jan. 2024, doi: 10.1016/j.jwpe.2023.104660.

[9] G. Xu *et al.*, “Bibliometric insights into the evolution of uranium contamination reduction research topics: Focus on microbial reduction of uranium,” *Sci. Total Environ.*, vol. 917, p. 170397, Mar. 2024, doi: 10.1016/j.scitotenv.2024.170397.

[10] O. J. Al-sareji, R. A. Grmasha, M. Meiczinger, R. A. Al-Juboori, V. Somogyi, and K. S. Hashim, “A Sustainable Banana Peel Activated Carbon for Removing Pharmaceutical Pollutants from Different Waters: Production, Characterization, and Application,” *Materials*, vol. 17, no. 5, p. 1032, Feb. 2024, doi: 10.3390/ma17051032.

[11] O. J. Al-sareji *et al.*, “Removal of emerging pollutants from water using enzyme-immobilized activated carbon from coconut shell,” *J. Environ. Chem. Eng.*, vol. 11, no. 3, p. 109803, Jun. 2023, doi: 10.1016/j.jece.2023.109803.

[12] J. Tang, M. Feng, and X. Huang, “Metal chalcogenides as ion-exchange materials for the efficient removal of key radionuclides: A review,” *Fundam. Res.*, p. S2667325824000013, Jan. 2024, doi: 10.1016/j.fmre.2023.10.022.

[13] J. Zhang *et al.*, “A review on research progress and prospects of agricultural waste-based activated carbon: preparation, application, and source of raw materials,” *J. Mater. Sci.*, vol. 59, no. 13, pp. 5271–5292, Apr. 2024, doi: 10.1007/s10853-024-09526-3.

[14] R. Kumar Mishra, B. Singh, and B. Acharya, “A comprehensive review on activated carbon from pyrolysis of lignocellulosic biomass: An application for energy and the environment,” *Carbon Resour. Convers.*, vol. 7, no. 4, p. 100228, Dec. 2024, doi: 10.1016/j.crcon.2024.100228.

[15] P. K. Sadh, S. Duhan, and J. S. Duhan, “Agro-industrial wastes and their utilization using solid state fermentation: a review,” *Bioresour. Bioprocess.*, vol. 5, no. 1, p. 1, Dec. 2018, doi: 10.1186/s40643-017-0187-z.

[16] R. Singh *et al.*, “Utilisation of agro-industrial waste for sustainable green production: a review,” *Environ. Sustain.*, vol. 4, no. 4, pp. 619–636, Dec. 2021, doi: 10.1007/s42398-021-00200-x.

[17] R. Toczyłowska-Mamińska, “Limits and perspectives of pulp and paper industry wastewater treatment – A review,” *Renew. Sustain. Energy Rev.*, vol. 78, pp. 764–772, Oct. 2017, doi: 10.1016/j.rser.2017.05.021.

[18] R. Ravindran and A. K. Jaiswal, “Exploitation of Food Industry Waste for High-Value Products,” *Trends Biotechnol.*, vol. 34, no. 1, pp. 58–69, Jan. 2016, doi: 10.1016/j.tibtech.2015.10.008.

[19] J. G. Speight, “Sources of water pollution,” in *Natural Water Remediation*, Elsevier, 2020, pp. 165–198. doi: 10.1016/B978-0-12-803810-9.00005-X.

[20] M. Shahid and M. S. Khan, “Ecotoxicological implications of residual pesticides to beneficial soil bacteria: A review,” *Pestic. Biochem. Physiol.*, vol. 188, p. 105272, Nov. 2022, doi: 10.1016/j.pestbp.2022.105272.

[21] K.-H. Kim, E. Kabir, and S. A. Jahan, “Exposure to pesticides and the associated human health effects,” *Sci. Total Environ.*, vol. 575, pp. 525–535, Jan. 2017, doi: 10.1016/j.scitotenv.2016.09.009.

[22] A. M. Costa, R. G. D. S. M. Alfaia, and J. C. Campos, “Landfill leachate treatment in Brazil – An overview,” *J. Environ. Manage.*, vol. 232, pp. 110–116, Feb. 2019, doi: 10.1016/j.jenvman.2018.11.006.

[23] M. T. Aminzai, E. Yabalak, D. Kalderis, and A. M. Gizir, “Environmental remediation of emerging contaminants using subcritical water: A review,” *J. Environ. Manage.*, vol. 366, p. 121800, Aug. 2024, doi: 10.1016/j.jenvman.2024.121800.

[24] N. Guettai, Y. Kadmi, M. Puri, K. Kerkich, and B. Bouargane, “Occurrence, analysis and removal processes of emerging pharmaceuticals from waters for the protection and preservation of a sustainable environment: A review,” *J. Clean. Prod.*, vol. 466, p. 142654, Aug. 2024, doi: 10.1016/j.jclepro.2024.142654.

[25] G. Singh, A. Singh, and V. Kumar Mishra, “A critical review of occurrence, sources, fate, ecological risk, and health effect of emerging contaminants in water and wastewater,” *Environ. Nanotechnol. Monit. Manag.*, vol. 22, p. 100994, Dec. 2024, doi: 10.1016/j.enmm.2024.100994.

[26] J. Yang *et al.*, “The impact of emerging contaminants exposure on human health effects: A review of organoid assessment models,” *Chem. Eng. J.*, vol. 498, p. 155882, Oct. 2024, doi: 10.1016/j.cej.2024.155882.

[27] European Commision, “Surface water: supporting surface water ecosystems and protecting EU surface waters from chemical pollution.” [Online]. Available: https://environment.ec.europ a.eu/topics/water/surface-water_en#ref-2022-proposal-to-revise-list-of-priority- substances-in-surface-water.

[28] S. Zanni, V. Cammalleri, L. D’Agostino, C. Protano, and M. Vitali, “Occurrence of pharmaceutical residues in drinking water: a systematic review,” *Environ. Sci. Pollut. Res.*, Aug. 2024, doi: 10.1007/s11356-024-34544-8.

[29] I. Vasilachi, D. Asiminicesei, D. Fertu, and M. Gavrilescu, “Occurrence and Fate of Emerging Pollutants in Water Environment and Options for Their Removal,” *Water*, vol. 13, no. 2, p. 181, Jan. 2021, doi: 10.3390/w13020181.

[30] G.-G. Ying, J.-L. Zhao, L.-J. Zhou, and S. Liu, “Fate and Occurrence of Pharmaceuticals in the Aquatic Environment (Surface Water and Sediment),” in *Comprehensive Analytical Chemistry*, vol. 62, Elsevier, 2013, pp. 453–557. doi: 10.1016/B978-0-444-62657-8.00014-8.

[31] U. Anand *et al.*, “Occurrence, transformation, bioaccumulation, risk and analysis of pharmaceutical and personal care products from wastewater: a review,” *Environ. Chem. Lett.*, vol. 20, no. 6, pp. 3883–3904, Dec. 2022, doi: 10.1007/s10311-022-01498-7.

[32] W. Zhou, W. Zhang, and Y. Cai, “Enzyme-enhanced adsorption of laccase immobilized graphene oxide for micro-pollutant removal,” *Sep. Purif. Technol.*, vol. 294, p. 121178, Aug. 2022, doi: 10.1016/j.seppur.2022.121178.

[33] European Commission. Joint Research Centre., *Review of the 1st Watch List under the Water Framework Directive and recommendations for the 2nd Watch List.* LU: Publications Office, 2018. Accessed: Jan. 24, 2025. [Online]. Available: https://data.europa.eu/doi/10.2760/614367

[34] “Directive (EU) 2024/3019 of the European Parliament and of the Council of 27 November 2024 concerning the treatment of urban waste water, (recast) (Text with EEA relevance).” Nov. 27, 2024. [Online]. Available: https://eur-lex.europa.eu/legal-content/IT/ALL/?uri=CELEX:32024L3019

[35] S. T. Alrashood, “Carbamazepine,” in *Profiles of Drug Substances, Excipients and Related Methodology*, vol. 41, Elsevier, 2016, pp. 133–321. doi: 10.1016/bs.podrm.2015.11.001.

[36] B. Bonnefille, E. Gomez, F. Courant, A. Escande, and H. Fenet, “Diclofenac in the marine environment: A review of its occurrence and effects,” *Mar. Pollut. Bull.*, vol. 131, pp. 496–506, Jun. 2018, doi: 10.1016/j.marpolbul.2018.04.053.

[37] National Library of Medicine, “Diclofenac, MedlinePlus, National Institutes of Health (NIH).” [Online]. Available: https://medlineplus.gov/druginfo/meds/a689002.html

[38] A. K. Al-Buriahi, M. M. Al-shaibani, R. M. S. R. Mohamed, A. A. Al-Gheethi, A. Sharma, and N. Ismail, “Ciprofloxacin removal from non-clinical environment: A critical review of

current methods and future trend prospects," *J. Water Process Eng.*, vol. 47, p. 102725, Jun. 2022, doi: 10.1016/j.jwpe.2022.102725.

[39] A. Huttner *et al.*, "Oral amoxicillin and amoxicillin–clavulanic acid: properties, indications and usage," *Clin. Microbiol. Infect.*, vol. 26, no. 7, pp. 871–879, Jul. 2020, doi: 10.1016/j.cmi.2019.11.028.

[40] *Advanced Oxidation Processes for Waste Water Treatment*. Elsevier, 2018. doi: 10.1016/C2016-0-00384-4.

[41] C. Xia and X. Shen, "Analysis of factors influencing on Electro-Fenton and research on combination technology (II): a review," *Environ. Sci. Pollut. Res.*, vol. 31, no. 34, pp. 46910–46948, Jul. 2024, doi: 10.1007/s11356-024-34159-z.

[42] C. Annabi *et al.*, "Degradation of enoxacin antibiotic by the electro-Fenton process: Optimization, biodegradability improvement and degradation mechanism," *J. Environ. Manage.*, vol. 165, pp. 96–105, Jan. 2016, doi: 10.1016/j.jenvman.2015.09.018.

[43] *Clean Energy and Resource Recovery*. Elsevier, 2022. doi: 10.1016/C2020-0-03253-6.

[44] A. L. Camargo-Perea, A. Rubio-Clemente, and G. A. Peñuela, "Use of Ultrasound as an Advanced Oxidation Process for the Degradation of Emerging Pollutants in Water," *Water*, vol. 12, no. 4, p. 1068, Apr. 2020, doi: 10.3390/w12041068.

[45] Z. Wu, S. Gong, J. Liu, J. Shi, and H. Deng, "Progress and problems of water treatment based on UV/persulfate oxidation process for degradation of emerging contaminants: A review," *J. Water Process Eng.*, vol. 58, p. 104870, Feb. 2024, doi: 10.1016/j.jwpe.2024.104870.

[46] Y. Huang, S. Zhao, K. Chen, B. Huang, and R. Jin, "A review of persulfate-based advanced oxidation system for decontaminating organic wastewater via non-radical regime," *Front. Environ. Sci. Eng.*, vol. 18, no. 11, p. 134, Nov. 2024, doi: 10.1007/s11783-024-1894-2.

[47] C. Liang *et al.*, "The critical role of minerals in persulfate-based advanced oxidation process: Catalytic properties, mechanism, and prospects," *Chem. Eng. J.*, vol. 482, p. 148969, Feb. 2024, doi: 10.1016/j.cej.2024.148969.

[48] P. Pourhakkak, A. Taghizadeh, M. Taghizadeh, M. Ghaedi, and S. Haghdoust, "Fundamentals of adsorption technology," in *Interface Science and Technology*, vol. 33, Elsevier, 2021, pp. 1–70. doi: 10.1016/B978-0-12-818805-7.00001-1.

[49] J. O. Ighalo *et al.*, "A review of treatment technologies for the mitigation of the toxic environmental effects of acid mine drainage (AMD)," *Process Saf. Environ. Prot.*, vol. 157, pp. 37–58, Jan. 2022, doi: 10.1016/j.psep.2021.11.008.

[50] T. Liu *et al.*, "Technologies for removing pharmaceuticals and personal care products (PPCPs) from aqueous solutions: Recent advances, performances, challenges and recommendations for improvements," *J. Mol. Liq.*, vol. 374, p. 121144, Mar. 2023, doi: 10.1016/j.molliq.2022.121144.

[51] J. Bedia, M. Peñas-Garzón, A. Gómez-Avilés, J. J. Rodriguez, and C. Belver, "A Review on the Synthesis and Characterization of Biomass-Derived Carbons for Adsorption of Emerging Contaminants from Water," *C*, vol. 4, no. 4, p. 63, Nov. 2018, doi: 10.3390/c4040063.

[52] J. O. Ighalo, F. O. Omoarukhe, V. E. Ojukwu, K. O. Iwuozor, and C. A. Igwegbe, "Cost of adsorbent preparation and usage in wastewater treatment: A review," *Clean. Chem. Eng.*, vol. 3, p. 100042, Sep. 2022, doi: 10.1016/j.clce.2022.100042.

[53] V. Choudhary and L. Philip, "Sustainability assessment of acid-modified biochar as adsorbent for the removal of pharmaceuticals and personal care products from secondary treated wastewater," *J. Environ. Chem. Eng.*, vol. 10, no. 3, p. 107592, Jun. 2022, doi: 10.1016/j.jece.2022.107592.

[54] O. J. Al-sareji *et al.*, "Ketoprofen and aspirin removal by laccase immobilized on date stones," *Chemosphere*, vol. 311, p. 137133, Jan. 2023, doi: 10.1016/j.chemosphere.2022.137133.

[55] Y. Park, Z. Sun, G. A. Ayoko, and R. L. Frost, "Bisphenol A sorption by organo-montmorillonite: Implications for the removal of organic contaminants from water," *Chemosphere*, vol. 107, pp. 249–256, Jul. 2014, doi: 10.1016/j.chemosphere.2013.12.050.

[56] M. Slaný, Ľ. Jankovič, and J. Madejová, "Structural characterization of organo-montmorillonites prepared from a series of primary alkylamines salts: Mid-IR and near-IR study," *Appl. Clay Sci.*, vol. 176, pp. 11–20, Aug. 2019, doi: 10.1016/j.clay.2019.04.016.

[57] M. Barczak, R. Dobrowolski, P. Borowski, and D. A. Giannakoudakis, "Pyridine-, thiol- and amine-functionalized mesoporous silicas for adsorptive removal of pharmaceuticals," *Microporous Mesoporous Mater.*, vol. 299, p. 110132, Jun. 2020, doi: 10.1016/j.micromeso.2020.110132.

[58] R. Dobrowolski, M. Oszust-Cieniuch, J. Dobrzyńska, and M. Barczak, “Amino-functionalized SBA-15 mesoporous silicas as sorbents of platinum (IV) ions,” *Colloids Surf. Physicochem. Eng. Asp.*, vol. 435, pp. 63–70, Oct. 2013, doi: 10.1016/j.colsurfa.2012.12.001.

[59] G. Cerri *et al.*, “Natural zeolites for pharmaceutical formulations: Preparation and evaluation of a clinoptilolite-based material,” *Microporous Mesoporous Mater.*, vol. 223, pp. 58–67, Mar. 2016, doi: 10.1016/j.micromeso.2015.10.034.

[60] C. Lei, Y. Hu, and M. He, “Adsorption characteristics of triclosan from aqueous solution onto cetylpyridinium bromide (CPB) modified zeolites,” *Chem. Eng. J.*, vol. 219, pp. 361–370, Mar. 2013, doi: 10.1016/j.cej.2012.12.099.

[61] F. Izzo *et al.*, “Surface modified natural zeolites (SMNZs) as nanocomposite versatile materials for health and environment,” *Colloids Surf. B Biointerfaces*, vol. 182, p. 110380, Oct. 2019, doi: 10.1016/j.colsurfb.2019.110380.

[62] Q. Xie, J. Xie, Z. Wang, D. Wu, Z. Zhang, and H. Kong, “Adsorption of organic pollutants by surfactant modified zeolite as controlled by surfactant chain length,” *Microporous Mesoporous Mater.*, vol. 179, pp. 144–150, Sep. 2013, doi: 10.1016/j.micromeso.2013.05.027.

[63] N. Zhuo *et al.*, “Adsorption of three selected pharmaceuticals and personal care products (PPCPs) onto MIL-101(Cr)/natural polymer composite beads,” *Sep. Purif. Technol.*, vol. 177, pp. 272–280, Apr. 2017, doi: 10.1016/j.seppur.2016.12.041.

[64] M. Kryuchkova *et al.*, “Pharmaceuticals Removal by Adsorption with Montmorillonite Nanoclay,” *Int. J. Mol. Sci.*, vol. 22, no. 18, p. 9670, Sep. 2021, doi: 10.3390/ijms22189670.

[65] H. S. Ng, P. E. Kee, H. S. Yim, P.-T. Chen, Y.-H. Wei, and J. Chi-Wei Lan, “Recent advances on the sustainable approaches for conversion and reutilization of food wastes to valuable bioproducts,” *Bioresour. Technol.*, vol. 302, p. 122889, Apr. 2020, doi: 10.1016/j.biortech.2020.122889.

[66] L. C. Freitas, J. R. Barbosa, A. L. C. Da Costa, F. W. F. Bezerra, R. H. H. Pinto, and R. N. D. Carvalho Junior, “From waste to sustainable industry: How can agro-industrial wastes help in the development of new products?,” *Resour. Conserv. Recycl.*, vol. 169, p. 105466, Jun. 2021, doi: 10.1016/j.resconrec.2021.105466.

[67] I. Prado-Acebo, J. Cubero-Cardoso, T. A. Lu-Chau, and G. Eibes, “Integral multi-valorization of agro-industrial wastes: A review,” *Waste Manag.*, vol. 183, pp. 42–52, Jun. 2024, doi: 10.1016/j.wasman.2024.05.001.

[68] T. Arpit Singh, M. Sharma, M. Sharma, G. Dutt Sharma, A. Kumar Passari, and S. Bhasin, “Valorization of agro-industrial residues for production of commercial biorefinery products,” *Fuel*, vol. 322, p. 124284, Aug. 2022, doi: 10.1016/j.fuel.2022.124284.

[69] O. Awogbemi and D. V. V. Kallon, “Pretreatment techniques for agricultural waste,” *Case Stud. Chem. Environ. Eng.*, vol. 6, p. 100229, Dec. 2022, doi: 10.1016/j.cscee.2022.100229.

[70] G. Velvizhi, P. J. Jacqueline, N. P. Shetti, L. K, G. Mohanakrishna, and T. M. Aminabhavi, “Emerging trends and advances in valorization of lignocellulosic biomass to biofuels,” *J. Environ. Manage.*, vol. 345, p. 118527, Nov. 2023, doi: 10.1016/j.jenvman.2023.118527.

[71] A. Langsdorf, M. Volkmar, D. Holtmann, and R. Ulber, “Material utilization of green waste: a review on potential valorization methods,” *Bioresour. Bioprocess.*, vol. 8, no. 1, p. 19, Dec. 2021, doi: 10.1186/s40643-021-00367-5.

[72] T. Ahmad and M. Danish, “Prospects of banana waste utilization in wastewater treatment: A review,” *J. Environ. Manage.*, vol. 206, pp. 330–348, Jan. 2018, doi: 10.1016/j.jenvman.2017.10.061.

[73] FAO, *Food and Agriculture Organization of the United Nations Crops and Livestock Products. 2021*. [Online]. Available: https://www.fao.org/faostat/en/#data/QCL/visualize

[74] M. S. Ahmed, T. Attia, A. A. Abd El-Wahab, R. Elgamsy, and M. H. Abd El-latif, “Assessment of the physical properties of banana pseudo stem/ABS composites,” *IOP Conf. Ser. Mater. Sci. Eng.*, vol. 634, no. 1, p. 012023, Oct. 2019, doi: 10.1088/1757-899X/634/1/012023.

[75] S. Singh, N. Parveen, and H. Gupta, “Adsorptive decontamination of rhodamine-B from water using banana peel powder: A biosorbent,” *Environ. Technol. Innov.*, vol. 12, pp. 189–195, Nov. 2018, doi: 10.1016/j.eti.2018.09.001.

[76] M. Corral-Bobadilla, R. Lostado-Lorza, F. Somovilla-Gómez, and R. Escribano-García, “Effective use of activated carbon from olive stone waste in the biosorption removal of Fe(III) ions from aqueous solutions,” *J. Clean. Prod.*, vol. 294, p. 126332, Apr. 2021, doi: 10.1016/j.jclepro.2021.126332.

[77] S. Eder, K. Müller, P. Azzari, A. Arcifa, M. Peydayesh, and L. Nyström, “Mass Transfer Mechanism and Equilibrium Modelling of Hydroxytyrosol Adsorption on Olive Pit–Derived Activated Carbon,” *Chem. Eng. J.*, vol. 404, p. 126519, Jan. 2021, doi: 10.1016/j.cej.2020.126519.

[78] M. Zbieć, J. Franc-Dąbrowska, and N. Drejerska, “Wood Waste Management in Europe through the Lens of the Circular Bioeconomy,” *Energies*, vol. 15, no. 12, p. 4352, Jun. 2022, doi: 10.3390/en15124352.

[79] D. L. Nguyen, J. Luedtke, M. Nopens, and A. Krause, “Production of wood-based panel from recycled wood resource: a literature review,” *Eur. J. Wood Wood Prod.*, vol. 81, no. 3, pp. 557–570, Jun. 2023, doi: 10.1007/s00107-023-01937-4.

[80] A. N. Amenaghawon, C. L. Anyalewechi, C. O. Okieimen, and H. S. Kusuma, “Biomass pyrolysis technologies for value-added products: a state-of-the-art review,” *Environ. Dev. Sustain.*, vol. 23, no. 10, pp. 14324–14378, Oct. 2021, doi: 10.1007/s10668-021-01276-5.

[81] A. Saravanan, S. Karishma, P. S. Kumar, P. Thamarai, and P. R. Yaashikaa, “Recent insights into mechanism of modified bio-adsorbents for the remediation of environmental pollutants,” *Environ. Pollut.*, vol. 339, p. 122720, Dec. 2023, doi: 10.1016/j.envpol.2023.122720.

[82] D. Y. Hoo *et al.*, “Ultrasonic cavitation: An effective cleaner and greener intensification technology in the extraction and surface modification of nanocellulose,” *Ultrason. Sonochem.*, vol. 90, p. 106176, Nov. 2022, doi: 10.1016/j.ultsonch.2022.106176.

[83] Y. Gao, Q. Yue, B. Gao, and A. Li, “Insight into activated carbon from different kinds of chemical activating agents: A review,” *Sci. Total Environ.*, vol. 746, p. 141094, Dec. 2020, doi: 10.1016/j.scitotenv.2020.141094.

[84] D. Mangla, Annu, A. Sharma, and S. Ikram, “Critical review on adsorptive removal of antibiotics: Present situation, challenges and future perspective,” *J. Hazard. Mater.*, vol. 425, p. 127946, Mar. 2022, doi: 10.1016/j.jhazmat.2021.127946.

[85] Grand View Research, “Activated Carbon Market Size, Share & Trends Report, 2030,.” [Online]. Available: https://www.grandviewresearch.com/industry-analysis/activated-carbon-market

[86] S.-A. Sajjadi *et al.*, “Efficient mercury removal from wastewater by pistachio wood wastes-derived activated carbon prepared by chemical activation using a novel activating agent,” *J.*

Environ. Manage., vol. 223, pp. 1001–1009, Oct. 2018, doi: 10.1016/j.jenvman.2018.06.077.

[87] A. Elmouwahidi, J. F. Vivo-Vilches, A. F. Pérez-Cadenas, F. J. Maldonado-Hódar, and F. Carrasco-Marín, "Free metal oxygen-reduction electro-catalysts obtained from biomass residue of the olive oil industry," *Chem. Eng. J.*, vol. 306, pp. 1109–1115, Dec. 2016, doi: 10.1016/j.cej.2016.08.042.

[88] M. Şirazi and S. Aslan, "Comprehensive characterization of high surface area activated carbon prepared from olive pomace by KOH activation," *Chem. Eng. Commun.*, vol. 208, no. 10, pp. 1479–1493, Oct. 2021, doi: 10.1080/00986445.2020.1864628.

[89] H. Jiang, X. Li, and Y. Dai, "Phosphoric acid activation of cow dung biochar for adsorbing enrofloxacin in water: Icing on the cake," *Environ. Pollut.*, vol. 341, p. 122887, Jan. 2024, doi: 10.1016/j.envpol.2023.122887.

[90] N. A. Bakar *et al.*, "Nipah (Musa Acuminata Balbisiana) banana peel as a lignocellulosic precursor for activated carbon: characterization study after carbonization process with phosphoric acid impregnated activated carbon," *Biomass Convers. Biorefinery*, vol. 13, no. 12, pp. 11085–11098, Aug. 2023, doi: 10.1007/s13399-021-01937-5.

[91] L. S. Daniel, A. Rahman, M. N. Hamushembe, P. Kapolo, V. Uahengo, and S. B. Jonnalagadda, "The production of activated carbon from Acacia erioloba seedpods via phosphoric acid activation method for the removal of methylene blue from water," *Bioresour. Technol. Rep.*, vol. 23, p. 101568, Sep. 2023, doi: 10.1016/j.biteb.2023.101568.

[92] S.-A. Sajjadi *et al.*, "A novel route for preparation of chemically activated carbon from pistachio wood for highly efficient Pb(II) sorption," *J. Environ. Manage.*, vol. 236, pp. 34–44, Apr. 2019, doi: 10.1016/j.jenvman.2019.01.087.

[93] O. J. Al-sareji *et al.*, "A novel and sustainable composite of L@PSAC for superior removal of pharmaceuticals from different water matrices: Production, characterization, and application," *Environ. Res.*, vol. 251, p. 118565, Jun. 2024, doi: 10.1016/j.envres.2024.118565.

[94] A. C. Martins *et al.*, "Removal of tetracycline by NaOH-activated carbon produced from macadamia nut shells: Kinetic and equilibrium studies," *Chem. Eng. J.*, vol. 260, pp. 291–299, Jan. 2015, doi: 10.1016/j.cej.2014.09.017.

[95] O. J. Al-sareji *et al.*, “Removal of Pharmaceuticals from Water Using Laccase Immobilized on Orange Peels Waste-Derived Activated Carbon,” *Water*, vol. 15, no. 19, p. 3437, Sep. 2023, doi: 10.3390/w15193437.

[96] H. P. Boehm, “Surface oxides on carbon and their analysis: a critical assessment,” *Carbon*, vol. 40, no. 2, pp. 145–149, Feb. 2002, doi: 10.1016/S0008-6223(01)00165-8.

[97] ASTM, *ASTM International 2010 ASTM D3174-04 Standard Test Method for Ash in the Analysis Sample of Coal and Coke from Coal*.

[98] ASTM, “ASTM D3173-03; Standard Test Method for Moisture in the Analysis Sample of Coal and Coke,” West Conshohocken, PA, USA, 2012.

[99] ASTM, *ASTM International 2007 ASTM D 3175-07 Standard Test Method for Volatile Matter in the Analysis Sample of Coal and Coke*.

[100] ASTM, *ASTM D3176. 2015. Standard Practice for Ultimate Analysis of Coal and Coke, 1–2. United States:*

[101] R. A. Grmasha *et al.*, “A sustainable nano-hybrid system of laccase@M-MWCNTs for multifunctional PAHs and PhACs removal from water, wastewater, and lake water,” *Environ. Res.*, vol. 246, p. 118097, Apr. 2024, doi: 10.1016/j.envres.2024.118097.

[102] I. Langmuir, “THE CONSTITUTION AND FUNDAMENTAL PROPERTIES OF SOLIDS AND LIQUIDS. PART I. SOLIDS.,” *J. Am. Chem. Soc.*, vol. 38, no. 11, pp. 2221–2295, Nov. 1916, doi: 10.1021/ja02268a002.

[103] H. M. F. Freundlich, “Over the adsorption in solution,” *J. Phys. chem*, vol. 57, no. 385471, pp. 1100–1107, 1906.

[104] S. Lagergren, “Zur theorie der sogenannten adsorption geloster stoffe,” pp. 1–39, 1898.

[105] S. Endo and A. A. Koelmans, “Sorption of Hydrophobic Organic Compounds to Plastics in the Marine Environment: Equilibrium,” in *Hazardous Chemicals Associated with Plastics in the Marine Environment*, vol. 78, H. Takada and H. K. Karapanagioti, Eds., in The Handbook of Environmental Chemistry, vol. 78. , Cham: Springer International Publishing, 2016, pp. 185–204. doi: 10.1007/698_2016_11.

[106] Y. S. Ho and G. McKay, “Pseudo-second order model for sorption processes,” *Process Biochem.*, vol. 34, no. 5, pp. 451–465, Jul. 1999, doi: 10.1016/S0032-9592(98)00112-5.

[107] O. J. Al-sareji *et al.*, “A sustainable and highly efficient fossil-free carbon from olive stones for emerging contaminants removal from different water matrices,” *Chemosphere*, vol. 351, p. 141189, Mar. 2024, doi: 10.1016/j.chemosphere.2024.141189.

[108] C. Nguyen and D. D. Do, “The Dubinin–Radushkevich equation and the underlying microscopic adsorption description,” *Carbon*, vol. 39, no. 9, pp. 1327–1336, Aug. 2001, doi: 10.1016/S0008-6223(00)00265-7.

[109] F.-C. Wu, R.-L. Tseng, and R.-S. Juang, “Initial behavior of intraparticle diffusion model used in the description of adsorption kinetics,” *Chem. Eng. J.*, vol. 153, no. 1–3, pp. 1–8, Nov. 2009, doi: 10.1016/j.cej.2009.04.042.

[110] M. C. Ncibi and M. Sillanpää, “Optimized removal of antibiotic drugs from aqueous solutions using single, double and multi-walled carbon nanotubes,” *J. Hazard. Mater.*, vol. 298, pp. 102–110, Nov. 2015, doi: 10.1016/j.jhazmat.2015.05.025.

[111] I. Ghouma, M. Jeguirim, S. Dorge, L. Limousy, C. Matei Ghimbeu, and A. Ouederni, “Activated carbon prepared by physical activation of olive stones for the removal of NO2 at ambient temperature,” *Comptes Rendus Chim.*, vol. 18, no. 1, pp. 63–74, Jan. 2015, doi: 10.1016/j.crci.2014.05.006.

[112] T. Bohli, A. Ouederni, N. Fiol, and I. Villaescusa, “Single and binary adsorption of some heavy metal ions from aqueous solutions by activated carbon derived from olive stones,” *Desalination Water Treat.*, vol. 53, no. 4, pp. 1082–1088, Jan. 2015, doi: 10.1080/19443994.2013.859099.

[113] N. T. Abdel-Ghani, G. A. El-Chaghaby, M. H. ElGammal, and E.-S. A. Rawash, “Optimizing the preparation conditions of activated carbons from olive cake using KOH activation,” *New Carbon Mater.*, vol. 31, no. 5, pp. 492–500, Oct. 2016, doi: 10.1016/S1872-5805(16)60027-6.

[114] H. Annab, N. Fiol, I. Villaescusa, and A. Essamri, “A proposal for the sustainable treatment and valorisation of olive mill wastes,” *J. Environ. Chem. Eng.*, vol. 7, no. 1, p. 102803, Feb. 2019, doi: 10.1016/j.jece.2018.11.047.

[115] S. Larous and A.-H. Meniai, “Adsorption of Diclofenac from aqueous solution using activated carbon prepared from olive stones,” *Int. J. Hydrog. Energy*, vol. 41, no. 24, pp. 10380–10390, Jun. 2016, doi: 10.1016/j.ijhydene.2016.01.096.

[116] S. Aslan and M. Şirazi, “Adsorption of Sulfonamide Antibiotic onto Activated Carbon Prepared from an Agro-industrial By-Product as Low-Cost Adsorbent: Equilibrium, Thermodynamic, and Kinetic Studies,” *Water. Air. Soil Pollut.*, vol. 231, no. 5, p. 222, May 2020, doi: 10.1007/s11270-020-04576-0.

[117] Ş. Gülel and Y. Güvenilir, “Using Olive Stone Powder for Biodegradation of Bio-Based Polyamide 5.6,” in *The First International Conference on “Green” Polymer Materials 2020*, MDPI, Nov. 2020, p. 2. doi: 10.3390/CGPM2020-07214.

[118] T. Bohli, A. Ouederni, N. Fiol, and I. Villaescusa, “Evaluation of an activated carbon from olive stones used as an adsorbent for heavy metal removal from aqueous phases,” *Comptes Rendus Chim.*, vol. 18, no. 1, pp. 88–99, Nov. 2014, doi: 10.1016/j.crci.2014.05.009.

[119] M. Szymanska-Chargot and A. Zdunek, “Use of FT-IR Spectra and PCA to the Bulk Characterization of Cell Wall Residues of Fruits and Vegetables Along a Fraction Process,” *Food Biophys.*, vol. 8, no. 1, pp. 29–42, Mar. 2013, doi: 10.1007/s11483-012-9279-7.

[120] A. E. Hanandeh, R. A. Abu-Zurayk, I. Hamadneh, and A. H. Al-Dujaili, “Characterization of biochar prepared from slow pyrolysis of Jordanian olive oil processing solid waste and adsorption efficiency of Hg2+ ions in aqueous solutions,” *Water Sci. Technol.*, vol. 74, no. 8, pp. 1899–1910, Oct. 2016, doi: 10.2166/wst.2016.378.

[121] S. Gaspard, N. Passé-Coutrin, A. Durimel, T. Cesaire, and V. Jeanne-Rose, “CHAPTER 2. Activated Carbon from Biomass for Water Treatment,” in *Green Chemistry Series*, S. Gaspard and M. C. Ncibi, Eds., Cambridge: Royal Society of Chemistry, 2013, pp. 46–105. doi: 10.1039/9781849737142-00046.

[122] S. J. Parikh, F. N. D. Mukome, and X. Zhang, “ATR–FTIR spectroscopic evidence for biomolecular phosphorus and carboxyl groups facilitating bacterial adhesion to iron oxides,” *Colloids Surf. B Biointerfaces*, vol. 119, pp. 38–46, Jul. 2014, doi: 10.1016/j.colsurfb.2014.04.022.

[123] S. Brian, “The C=O Bond, Part III: Carboxylic Acids,” Spectroscopy. Accessed: Jan. 10, 2024. [Online]. Available: https://www.spectroscopyonline.com/view/co-bond-part-iii-carboxylic-acids

[124] T. F. Akinhanmi, E. A. Ofudje, A. I. Adeogun, P. Aina, and I. M. Joseph, “Orange peel as low-cost adsorbent in the elimination of Cd(II) ion: kinetics, isotherm, thermodynamic and

optimization evaluations," *Bioresour. Bioprocess.*, vol. 7, no. 1, p. 34, Dec. 2020, doi: 10.1186/s40643-020-00320-y.

[125] H. Demiral, İ. Demiral, F. Tümsek, and B. Karabacakoğlu, "Pore structure of activated carbon prepared from hazelnut bagasse by chemical activation," *Surf. Interface Anal.*, vol. 40, no. 3–4, pp. 616–619, Mar. 2008, doi: 10.1002/sia.2631.

[126] A. B. Fadhil and B. A. Kareem, "Co-pyrolysis of mixed date pits and olive stones: Identification of bio-oil and the production of activated carbon from bio-char," *J. Anal. Appl. Pyrolysis*, vol. 158, p. 105249, Sep. 2021, doi: 10.1016/j.jaap.2021.105249.

[127] R. A. Al-Juboori and N. Hilal, "Pharmaceuticals removal from wastewater: Ultrasound technology and its potential amalgamation with membrane processes," *J. Water Process Eng.*, vol. 53, p. 103810, Jul. 2023, doi: 10.1016/j.jwpe.2023.103810.

[128] S. Salvestrini, A. Fenti, S. Chianese, P. Iovino, and D. Musmarra, "Diclofenac sorption from synthetic water: Kinetic and thermodynamic analysis," *J. Environ. Chem. Eng.*, vol. 8, no. 5, p. 104105, Oct. 2020, doi: 10.1016/j.jece.2020.104105.

[129] C. E. Onu *et al.*, "Decolourization of bromocresol green dye solution by acid functionalized rice husk: Artificial intelligence modeling, GA optimization, and adsorption studies," *J. Hazard. Mater. Adv.*, vol. 9, p. 100224, Feb. 2023, doi: 10.1016/j.hazadv.2022.100224.

[130] C.-S. Chen and S.-T. Lin, "Prediction of pH Effect on the Octanol–Water Partition Coefficient of Ionizable Pharmaceuticals," *Ind. Eng. Chem. Res.*, vol. 55, no. 34, pp. 9284–9294, Aug. 2016, doi: 10.1021/acs.iecr.6b02040.

[131] T. X. Bui and H. Choi, "Adsorptive removal of selected pharmaceuticals by mesoporous silica SBA-15," *J. Hazard. Mater.*, vol. 168, no. 2–3, pp. 602–608, Sep. 2009, doi: 10.1016/j.jhazmat.2009.02.072.

[132] M. B. Ahmed, J. L. Zhou, H. H. Ngo, W. Guo, M. A. H. Johir, and K. Sornalingam, "Single and competitive sorption properties and mechanism of functionalized biochar for removing sulfonamide antibiotics from water," *Chem. Eng. J.*, vol. 311, pp. 348–358, Mar. 2017, doi: 10.1016/j.cej.2016.11.106.

[133] M. Turk Sekulic, N. Boskovic, A. Slavkovic, J. Garunovic, S. Kolakovic, and S. Pap, "Surface functionalised adsorbent for emerging pharmaceutical removal: Adsorption performance and mechanisms," *Process Saf. Environ. Prot.*, vol. 125, pp. 50–63, May 2019, doi: 10.1016/j.psep.2019.03.007.

[134] W. K. Wakejo, B. T. Meshasha, J. W. Kang, and Y. Chebude, “Enhanced Ciprofloxacin Removal from Aqueous Solution Using a Chemically Modified Biochar Derived from Bamboo Sawdust: Adsorption Process Optimization with Response Surface Methodology,” *Adsorpt. Sci. Technol.*, vol. 2022, p. 2699530, Jan. 2022, doi: 10.1155/2022/2699530.

[135] N. K. Soliman, H. S. Mohamed, S. A. Ahmed, F. H. Sayed, A. H. Elghandour, and S. A. Ahmed, “Cd 2 + and Cu 2 + removal by the waste of the marine brown macroalga Hydroclathrus clathratus,” *Environ. Technol. Innov.*, vol. 15, p. 100365, Aug. 2019, doi: 10.1016/j.eti.2019.100365.

[136] N. K. Soliman and A. F. Moustafa, “Industrial solid waste for heavy metals adsorption features and challenges; a review,” *J. Mater. Res. Technol.*, vol. 9, no. 5, pp. 10235–10253, Sep. 2020, doi: 10.1016/j.jmrt.2020.07.045.

[137] V. K. Gupta, C. K. Jain, I. Ali, M. Sharma, and V. K. Saini, “Removal of cadmium and nickel from wastewater using bagasse fly ash—a sugar industry waste,” *Water Res.*, vol. 37, no. 16, pp. 4038–4044, Sep. 2003, doi: 10.1016/S0043-1354(03)00292-6.

[138] B. S. Yadav and S. Dasgupta, “Effect of time, pH, and temperature on kinetics for adsorption of methyl orange dye into the modified nitrate intercalated MgAl LDH adsorbent,” *Inorg. Chem. Commun.*, vol. 137, p. 109203, Mar. 2022, doi: 10.1016/j.inoche.2022.109203.

[139] J. Vievard *et al.*, “Bio-Based Adsorption as Ecofriendly Method for Wastewater Decontamination: A Review,” *Toxics*, vol. 11, no. 5, p. 404, Apr. 2023, doi: 10.3390/toxics11050404.

[140] M. A. M. Salleh, D. K. Mahmoud, W. A. W. A. Karim, and A. Idris, “Cationic and anionic dye adsorption by agricultural solid wastes: A comprehensive review,” *Desalination*, vol. 280, no. 1–3, pp. 1–13, Oct. 2011, doi: 10.1016/j.desal.2011.07.019.

[141] T. A. Saleh, “Kinetic models and thermodynamics of adsorption processes: classification,” in *Interface Science and Technology*, vol. 34, Elsevier, 2022, pp. 65–97. doi: 10.1016/B978-0-12-849876-7.00003-8.

[142] I. Salahshoori, M. Namayandeh Jorabchi, S. Ghasemi, S. M. S. Mirnezami, M. A. L. Nobre, and H. A. Khonakdar, “Assessing cationic dye adsorption mechanisms on MIL-53 (Al) nanostructured MOF materials using quantum chemical and molecular simulations: Toward environmentally sustainable wastewater treatment,” *J. Water Process Eng.*, vol. 55, p. 104081, Oct. 2023, doi: 10.1016/j.jwpe.2023.104081.

[143] F. Karadeniz and F. Güzel, “Adsorptive performance of Melia Azedarach fruit-derived biochar in removing methylene blue, diclofenac, and copper(II) from aqueous solution,” *Biomass Convers. Biorefinery*, vol. 13, no. 3, pp. 2429–2447, Feb. 2023, doi: 10.1007/s13399-022-02864-9.

[144] N. Thi Minh Tam, Y. Liu, H. Bashir, Z. Yin, Y. He, and X. Zhou, “Efficient Removal of Diclofenac from Aqueous Solution by Potassium Ferrate-Activated Porous Graphitic Biochar: Ambient Condition Influences and Adsorption Mechanism,” *Int. J. Environ. Res. Public. Health*, vol. 17, no. 1, p. 291, Dec. 2019, doi: 10.3390/ijerph17010291.

[145] J. Iqbal *et al.*, “Exploring the potential of nano-zerovalent copper modified biochar for the removal of ciprofloxacin from water,” *Environ. Nanotechnol. Monit. Manag.*, vol. 16, p. 100604, Dec. 2021, doi: 10.1016/j.enmm.2021.100604.

[146] M. El-Azazy, I. Nabil, S. S. Hassan, and A. S. El-Shafie, “Adsorption Characteristics of Pristine and Magnetic Olive Stones Biochar with Respect to Clofazimine,” *Nanomaterials*, vol. 11, no. 4, p. 963, Apr. 2021, doi: 10.3390/nano11040963.

[147] L. Limousy, I. Ghouma, A. Ouederni, and M. Jeguirim, “Amoxicillin removal from aqueous solution using activated carbon prepared by chemical activation of olive stone,” *Environ. Sci. Pollut. Res.*, vol. 24, no. 11, pp. 9993–10004, Apr. 2017, doi: 10.1007/s11356-016-7404-8.

[148] H. El Bakouri, J. Usero, J. Morillo, and A. Ouassini, “Adsorptive features of acid-treated olive stones for drin pesticides: Equilibrium, kinetic and thermodynamic modeling studies,” *Bioresour. Technol.*, vol. 100, no. 18, pp. 4147–4155, Sep. 2009, doi: 10.1016/j.biortech.2009.04.003.

[149] F. Medjdoub, K. Louhab, and A. Hamouche, “Comparative study of the adsorption of paracetamol from aqueous solution on olive stones and date pits,” *Desalination Water Treat.*, vol. 104, pp. 225–233, Feb. 2018, doi: 10.5004/dwt.2018.21835.

[150] O. S. Agboola and O. S. Bello, “Enhanced adsorption of ciprofloxacin from aqueous solutions using functionalized banana stalk,” *Biomass Convers. Biorefinery*, vol. 12, no. 12, pp. 5463–5478, Dec. 2022, doi: 10.1007/s13399-020-01038-9.

[151] O. A. Hussain, A. S. Hathout, Y. E. Abdel-Mobdy, M. M. Rashed, E. A. Abdel Rahim, and A. S. M. Fouzy, “Preparation and characterization of activated carbon from agricultural

wastes and their ability to remove chlorpyrifos from water," *Toxicol. Rep.*, vol. 10, pp. 146–154, 2023, doi: 10.1016/j.toxrep.2023.01.011.

[152] P. Singh, A. Sarswat, C. U. Pittman, T. Mlsna, and D. Mohan, "Sustainable Low-Concentration Arsenite [As(III)] Removal in Single and Multicomponent Systems Using Hybrid Iron Oxide–Biochar Nanocomposite Adsorbents—A Mechanistic Study," *ACS Omega*, vol. 5, no. 6, pp. 2575–2593, Feb. 2020, doi: 10.1021/acsomega.9b02842.

[153] W. Yang *et al.*, "Removal of Pb(II) from Aqueous Solution and Adsorption Kinetics of Corn Stalk Biochar," *Separations*, vol. 10, no. 8, p. 438, Aug. 2023, doi: 10.3390/separations10080438.

[154] N. A. Baharum, H. M. Nasir, M. Y. Ishak, N. M. Isa, M. A. Hassan, and A. Z. Aris, "Highly efficient removal of diazinon pesticide from aqueous solutions by using coconut shell-modified biochar," *Arab. J. Chem.*, vol. 13, no. 7, pp. 6106–6121, Jul. 2020, doi: 10.1016/j.arabjc.2020.05.011.

[155] D. Mohan, A. Sarswat, V. K. Singh, M. Alexandre-Franco, and C. U. Pittman, "Development of magnetic activated carbon from almond shells for trinitrophenol removal from water," *Chem. Eng. J.*, vol. 172, no. 2–3, pp. 1111–1125, Aug. 2011, doi: 10.1016/j.cej.2011.06.054.

[156] D. Qu, "Studies of the activated carbons used in double-layer supercapacitors," *J. Power Sources*, vol. 109, no. 2, pp. 403–411, Jul. 2002, doi: 10.1016/S0378-7753(02)00108-8.

[157] W. Tong, Q. Liu, S. Ren, J. Zhou, T. Zhang, and C. Yang, "Effect of pyrolysis temperature on pine sawdust chars and their gasification reactivity mechanism with CO_2," *Asia-Pac. J. Chem. Eng.*, vol. 13, no. 6, p. e2256, Nov. 2018, doi: 10.1002/apj.2256.

[158] M. Patel, R. Kumar, C. U. Pittman, and D. Mohan, "Ciprofloxacin and acetaminophen sorption onto banana peel biochars: Environmental and process parameter influences," *Environ. Res.*, vol. 201, p. 111218, Oct. 2021, doi: 10.1016/j.envres.2021.111218.

[159] Universitas Sebelas Maret Surakarta, Indonesia, I. H. Pusponegoro, Kementerian Pertanian, M. Mujiyo, Universitas Sebelas Maret Surakarta, Indonesia, and S. Suntoro, "Planning of banana plant development based on the land conservation aspect in Jenawi District," *J. Degraded Min. Lands Manag.*, vol. 5, no. 4, pp. 1319–1326, Jul. 2018, doi: 10.15243/jdmlm.2018.054.1319.

[160] S. Ben-Ali, I. Jaouali, S. Souissi-Najar, and A. Ouederni, “Characterization and adsorption capacity of raw pomegranate peel biosorbent for copper removal,” *J. Clean. Prod.*, vol. 142, pp. 3809–3821, Jan. 2017, doi: 10.1016/j.jclepro.2016.10.081.

[161] J. L. Guimarães, E. Frollini, C. G. Da Silva, F. Wypych, and K. G. Satyanarayana, “Characterization of banana, sugarcane bagasse and sponge gourd fibers of Brazil,” *Ind. Crops Prod.*, vol. 30, no. 3, pp. 407–415, Nov. 2009, doi: 10.1016/j.indcrop.2009.07.013.

[162] M. Farahani, S. R. S. Abdullah, S. Hosseini, S. Shojaeipour, and M. Kashisaz, “Adsorption-based Cationic Dyes using the Carbon Active Sugarcane Bagasse,” *Procedia Environ. Sci.*, vol. 10, pp. 203–208, 2011, doi: 10.1016/j.proenv.2011.09.035.

[163] P. D. Pathak and S. A. Mandavgane, “Preparation and characterization of raw and carbon from banana peel by microwave activation: Application in citric acid adsorption,” *J. Environ. Chem. Eng.*, vol. 3, no. 4, pp. 2435–2447, Dec. 2015, doi: 10.1016/j.jece.2015.08.023.

[164] A. Selvarajoo, D. Muhammad, and S. K. Arumugasamy, “An experimental and modelling approach to produce biochar from banana peels through pyrolysis as potential renewable energy resources,” *Model. Earth Syst. Environ.*, vol. 6, no. 1, pp. 115–128, Mar. 2020, doi: 10.1007/s40808-019-00663-2.

[165] H. Çelebi, İ. Şimşek, T. Bahadir, and Ş. Tulun, “Use of banana peel for the removal of boron from aqueous solutions in the batch adsorption system,” *Int. J. Environ. Sci. Technol.*, vol. 20, no. 1, pp. 161–176, Jan. 2023, doi: 10.1007/s13762-022-04566-1.

[166] A. H. Jawad, R. A. Rashid, M. A. M. Ishak, and K. Ismail, “Adsorptive removal of methylene blue by chemically treated cellulosic waste banana (*Musa sapientum*) peels,” *J. Taibah Univ. Sci.*, vol. 12, no. 6, pp. 809–819, Nov. 2018, doi: 10.1080/16583655.2018.1519893.

[167] R. S. D. Castro *et al.*, “Banana Peel Applied to the Solid Phase Extraction of Copper and Lead from River Water: Preconcentration of Metal Ions with a Fruit Waste,” *Ind. Eng. Chem. Res.*, vol. 50, no. 6, pp. 3446–3451, Mar. 2011, doi: 10.1021/ie101499e.

[168] Z. Shao, Shuangbao, S. Wu, Y. Gao, X. Liu, and Y. Dai, “Two-step pyrolytic preparation of biochar for the adsorption study of tetracycline in water,” *Environ. Res.*, vol. 242, p. 117566, Feb. 2024, doi: 10.1016/j.envres.2023.117566.

[169] M. E. Fernandez, B. Ledesma, S. Román, P. R. Bonelli, and A. L. Cukierman, “Development and characterization of activated hydrochars from orange peels as potential adsorbents for

emerging organic contaminants," *Bioresour. Technol.*, vol. 183, pp. 221–228, May 2015, doi: 10.1016/j.biortech.2015.02.035.

[170] P. Yang *et al.*, "Effective removal of methylene blue and crystal violet by low-cost biomass derived from eucalyptus: Characterization, experiments, and mechanism investigation," *Environ. Technol. Innov.*, vol. 33, p. 103459, Feb. 2024, doi: 10.1016/j.eti.2023.103459.

[171] H. S. Mohamed, N. K. Soliman, D. A. Abdelrheem, A. A. Ramadan, A. H. Elghandour, and S. A. Ahmed, "Adsorption of Cd2+ and Cr3+ ions from aqueous solutions by using residue of Padina gymnospora waste as promising low-cost adsorbent," *Heliyon*, vol. 5, no. 3, p. e01287, Mar. 2019, doi: 10.1016/j.heliyon.2019.e01287.

[172] C. Hodúr, N. Bellahsen, E. Mikó, V. Nagypál, Z. Šereš, and S. Kertész, "The Adsorption of Ammonium Nitrogen from Milking Parlor Wastewater Using Pomegranate Peel Powder for Sustainable Water, Resources, and Waste Management," *Sustainability*, vol. 12, no. 12, p. 4880, Jun. 2020, doi: 10.3390/su12124880.

[173] M. Ghaedi, A. Hassanzadeh, and S. N. Kokhdan, "Multiwalled Carbon Nanotubes as Adsorbents for the Kinetic and Equilibrium Study of the Removal of Alizarin Red S and Morin," *J. Chem. Eng. Data*, vol. 56, no. 5, pp. 2511–2520, May 2011, doi: 10.1021/je2000414.

[174] S. Dawood and T. K. Sen, "Removal of anionic dye Congo red from aqueous solution by raw pine and acid-treated pine cone powder as adsorbent: Equilibrium, thermodynamic, kinetics, mechanism and process design," *Water Res.*, vol. 46, no. 6, pp. 1933–1946, Apr. 2012, doi: 10.1016/j.watres.2012.01.009.

[175] M. Sathishkumar, A. Binupriya, D. Kavitha, and S. Yun, "Kinetic and isothermal studies on liquid-phase adsorption of 2,4-dichlorophenol by palm pith carbon," *Bioresour. Technol.*, vol. 98, no. 4, pp. 866–873, Mar. 2007, doi: 10.1016/j.biortech.2006.03.002.

[176] M. C. Ncibi and M. Sillanpää, "Optimizing the removal of pharmaceutical drugs Carbamazepine and Dorzolamide from aqueous solutions using mesoporous activated carbons and multi-walled carbon nanotubes," *J. Mol. Liq.*, vol. 238, pp. 379–388, Jul. 2017, doi: 10.1016/j.molliq.2017.05.028.

[177] M. Naghdi *et al.*, "Pine-wood derived nanobiochar for removal of carbamazepine from aqueous media: Adsorption behavior and influential parameters," *Arab. J. Chem.*, vol. 12, no. 8, pp. 5292–5301, Dec. 2019, doi: 10.1016/j.arabjc.2016.12.025.

[178] P. Chakraborty, S. Show, S. Banerjee, and G. Halder, “Mechanistic insight into sorptive elimination of ibuprofen employing bi-directional activated biochar from sugarcane bagasse: Performance evaluation and cost estimation,” *J. Environ. Chem. Eng.*, vol. 6, no. 4, pp. 5287–5300, Aug. 2018, doi: 10.1016/j.jece.2018.08.017.

[179] A. B. Azzam, Y. A. Tokhy, F. M. El Dars, and A. A. Younes, “Construction of porous biochar decorated with NiS for the removal of ciprofloxacin antibiotic from pharmaceutical wastewaters,” *J. Water Process Eng.*, vol. 49, p. 103006, Oct. 2022, doi: 10.1016/j.jwpe.2022.103006.

[180] Y. S. Ho, C. T. Huang, and H. W. Huang, “Equilibrium sorption isotherm for metal ions on tree fern,” *Process Biochem.*, vol. 37, no. 12, pp. 1421–1430, Jul. 2002, doi: 10.1016/S0032-9592(02)00036-5.

[181] K. Jafari, M. Heidari, and O. Rahmanian, “Wastewater treatment for Amoxicillin removal using magnetic adsorbent synthesized by ultrasound process,” *Ultrason. Sonochem.*, vol. 45, pp. 248–256, Jul. 2018, doi: 10.1016/j.ultsonch.2018.03.018.

[182] S. X. Zha, Y. Zhou, X. Jin, and Z. Chen, “The removal of amoxicillin from wastewater using organobentonite,” *J. Environ. Manage.*, vol. 129, pp. 569–576, Nov. 2013, doi: 10.1016/j.jenvman.2013.08.032.

[183] H. Laksaci, B. Belhamdi, O. Khelifi, A. Khelifi, and M. Trari, “Elimination of amoxicillin by adsorption on coffee waste based activated carbon,” *J. Mol. Struct.*, vol. 1274, p. 134500, Feb. 2023, doi: 10.1016/j.molstruc.2022.134500.

[184] G. Moussavi, A. Alahabadi, K. Yaghmaeian, and M. Eskandari, “Preparation, characterization and adsorption potential of the NH4Cl-induced activated carbon for the removal of amoxicillin antibiotic from water,” *Chem. Eng. J.*, vol. 217, pp. 119–128, Feb. 2013, doi: 10.1016/j.cej.2012.11.069.

[185] Q. Qin, X. Wu, L. Chen, Z. Jiang, and Y. Xu, “Simultaneous removal of tetracycline and Cu(II) by adsorption and coadsorption using oxidized activated carbon,” *RSC Adv.*, vol. 8, no. 4, pp. 1744–1752, 2018, doi: 10.1039/C7RA12402C.

[186] R. S. Ingole, D. H. Lataye, and P. T. Dhorabe, “Adsorption of phenol onto Banana Peels Activated Carbon,” *KSCE J. Civ. Eng.*, vol. 21, no. 1, pp. 100–110, Jan. 2017, doi: 10.1007/s12205-016-0101-9.

[187] C. R. Silva *et al.*, “Banana Peel as an Adsorbent for Removing Atrazine and Ametryne from Waters,” *J. Agric. Food Chem.*, vol. 61, no. 10, pp. 2358–2363, Mar. 2013, doi: 10.1021/jf304742h.

[188] A. Firas Saeed, “Thorium removal from waste water using Banana peel and employment of Waste Residue,” *Advances in Natural and Applied Sciences*, vol. 7, no. 3.

[189] S. Chaturvedi and P. N. Dave, “Review on Thermal Decomposition of Ammonium Nitrate,” *J. Energ. Mater.*, vol. 31, no. 1, pp. 1–26, Jan. 2013, doi: 10.1080/07370652.2011.573523.

[190] Z. Liu *et al.*, “A study of nitrogen conversion and polycyclic aromatic hydrocarbon (PAH) emissions during hydrochar–lignite co-pyrolysis,” *Appl. Energy*, vol. 108, pp. 74–81, Aug. 2013, doi: 10.1016/j.apenergy.2013.03.012.

[191] X. He *et al.*, “Effects of pyrolysis temperature on the physicochemical properties of gas and biochar obtained from pyrolysis of crop residues,” *Energy*, vol. 143, pp. 746–756, Jan. 2018, doi: 10.1016/j.energy.2017.11.062.

[192] J.-H. Park *et al.*, “Cadmium adsorption characteristics of biochars derived using various pine tree residues and pyrolysis temperatures,” *J. Colloid Interface Sci.*, vol. 553, pp. 298–307, Oct. 2019, doi: 10.1016/j.jcis.2019.06.032.

[193] X. Zhang, P. Zhang, X. Yuan, Y. Li, and L. Han, “Effect of pyrolysis temperature and correlation analysis on the yield and physicochemical properties of crop residue biochar,” *Bioresour. Technol.*, vol. 296, p. 122318, Jan. 2020, doi: 10.1016/j.biortech.2019.122318.

[194] J.-H. Kwak *et al.*, “Biochar properties and lead(II) adsorption capacity depend on feedstock type, pyrolysis temperature, and steam activation,” *Chemosphere*, vol. 231, pp. 393–404, Sep. 2019, doi: 10.1016/j.chemosphere.2019.05.128.

[195] A. Zubrik *et al.*, “Preparation of chemically activated carbon from waste biomass by single-stage and two-stage pyrolysis,” *J. Clean. Prod.*, vol. 143, pp. 643–653, Feb. 2017, doi: 10.1016/j.jclepro.2016.12.061.

[196] A. M. Puziy, O. I. Poddubnaya, A. Martínez-Alonso, F. Suárez-García, and J. M. D. Tascón, “Synthetic carbons activated with phosphoric acid,” *Carbon*, vol. 40, no. 9, pp. 1493–1505, Aug. 2002, doi: 10.1016/S0008-6223(01)00317-7.

[197] P. S. Pauletto, S. F. Lütke, G. L. Dotto, and N. P. G. Salau, “Adsorption mechanisms of single and simultaneous removal of pharmaceutical compounds onto activated carbon:

Isotherm and thermodynamic modeling," *J. Mol. Liq.*, vol. 336, p. 116203, Aug. 2021, doi: 10.1016/j.molliq.2021.116203.

[198] C. H. Pimentel, M. S. Freire, D. Gómez-Díaz, and J. González-Álvarez, "Preparation of activated carbon from pine (Pinus radiata) sawdust by chemical activation with zinc chloride for wood dye adsorption," *Biomass Convers. Biorefinery*, vol. 13, no. 18, pp. 16537–16555, Dec. 2023, doi: 10.1007/s13399-023-04138-4.

[199] V. N. Scheverin, M. F. Horst, and V. L. Lassalle, "Novel hydroxyapatite-biomass nanocomposites for fluoride adsorption," *Results Eng.*, vol. 16, p. 100648, Dec. 2022, doi: 10.1016/j.rineng.2022.100648.

[200] M. Fatih Dilekoglu and M. Yapici, "Adsorption of naproxen pharmaceutical micropollutant from aqueous solutions on superior activated carbon synthesized from sheep manure: Kinetics, thermodynamics, and mechanism," *J. Mol. Liq.*, vol. 381, p. 121839, Jul. 2023, doi: 10.1016/j.molliq.2023.121839.

[201] M. Zhou *et al.*, "Pinewood outperformed bamboo as feedstock to prepare biochar-supported zero-valent iron for Cr6+ reduction," *Environ. Res.*, vol. 187, p. 109695, Aug. 2020, doi: 10.1016/j.envres.2020.109695.

[202] O. J. Al-sareji *et al.*, "Efficient removal of pharmaceutical contaminants from water and wastewater using immobilized laccase on activated carbon derived from pomegranate peels," *Sci. Rep.*, vol. 13, no. 1, p. 11933, Jul. 2023, doi: 10.1038/s41598-023-38821-3.

[203] O. Tomin and M. R. Yazdani, "Production and characterization of porous magnetic biochar: before and after phosphate adsorption insights," *J. Porous Mater.*, vol. 29, no. 3, pp. 849–859, Jun. 2022, doi: 10.1007/s10934-022-01217-1.

[204] Y. Wongmat and D. R. Wagner, "Effect of Potassium Salts on Biochar Pyrolysis," *Energies*, vol. 15, no. 16, p. 5779, Aug. 2022, doi: 10.3390/en15165779.

[205] N. PubChem, "National Center for Biotechnology Information. "PubChem Compound Summary for CID 3033, Diclofenac." [Online]. Available: https://pubchem.ncbi.nlm.nih.gov/compound/Diclofenac.

[206] N. PubChem, "National Center for Biotechnology Information. "PubChem Compound Summary for CID 2764, Ciprofloxacin." [Online]. Available: https://pubchem.ncbi.nlm.nih.gov/compound/Ciprofloxacin

[207] C. Lara-Pérez, E. Leyva, B. Zermeño, I. Osorio, C. Montalvo, and E. Moctezuma, "Photocatalytic degradation of diclofenac sodium salt: adsorption and reaction kinetic studies," *Environ. Earth Sci.*, vol. 79, no. 11, p. 277, Jun. 2020, doi: 10.1007/s12665-020-09017-z.

[208] X. Xing *et al.*, "Adsorption Mechanism of Ciprofloxacin from Water by Synthesized Birnessite," *Adv. Mater. Sci. Eng.*, vol. 2015, pp. 1–7, 2015, doi: 10.1155/2015/148423.

[209] W. Plazinski, W. Rudzinski, and A. Plazinska, "Theoretical models of sorption kinetics including a surface reaction mechanism: A review," *Adv. Colloid Interface Sci.*, vol. 152, no. 1–2, pp. 2–13, Nov. 2009, doi: 10.1016/j.cis.2009.07.009.

[210] L. Largitte and R. Pasquier, "A review of the kinetics adsorption models and their application to the adsorption of lead by an activated carbon," *Chem. Eng. Res. Des.*, vol. 109, pp. 495–504, May 2016, doi: 10.1016/j.cherd.2016.02.006.

[211] Y. Lu *et al.*, "Adsorption Characteristics and Mechanism of Methylene Blue in Water by NaOH-Modified Areca Residue Biochar," *Processes*, vol. 10, no. 12, p. 2729, Dec. 2022, doi: 10.3390/pr10122729.

[212] E. Al-Hetlani, B. D'Cruz, M. O. Amin, and M. Madkour, "An effective magnetic nanoadsorbent based on a carbonaceous/spinel ferrite nanocomposite for the removal of pharmaceutical pollutants from wastewater," *Environ. Sci. Water Res. Technol.*, vol. 8, no. 5, pp. 998–1010, 2022, doi: 10.1039/D1EW00495F.

[213] M. Abdullah *et al.*, "Removal of ceftriaxone sodium antibiotic from pharmaceutical wastewater using an activated carbon based TiO2 composite: Adsorption and photocatalytic degradation evaluation," *Chemosphere*, vol. 317, p. 137834, Mar. 2023, doi: 10.1016/j.chemosphere.2023.137834.

[214] A. O. Dada, A. A. Inyinbor, O. S. Bello, and B. E. Tokula, "Novel plantain peel activated carbon–supported zinc oxide nanocomposites (PPAC-ZnO-NC) for adsorption of chloroquine synthetic pharmaceutical used for COVID-19 treatment," *Biomass Convers. Biorefinery*, vol. 13, no. 10, pp. 9181–9193, Jul. 2023, doi: 10.1007/s13399-021-01828-9.

[215] S. Xu *et al.*, "Macro- and micro-algae-based carbon composite for pharmaceutical wastewater treatment: Batch adsorption and mechanism study," *Process Saf. Environ. Prot.*, vol. 176, pp. 641–652, Aug. 2023, doi: 10.1016/j.psep.2023.06.020.

[216] N. Magesh, A. A. Renita, R. Siva, N. Harirajan, and A. Santhosh, “Adsorption behavior of fluoroquinolone(ciprofloxacin) using zinc oxide impregnated activated carbon prepared from jack fruit peel: Kinetics and isotherm studies,” *Chemosphere*, vol. 290, p. 133227, Mar. 2022, doi: 10.1016/j.chemosphere.2021.133227.

[217] O. J. Al-sareji *et al.*, “A novel two stages chemical activation of pinewood waste for removing organic micropollutants from water and wastewater,” *Chemosphere*, vol. 363, p. 142974, Sep. 2024, doi: 10.1016/j.chemosphere.2024.142974.

[218] C. Ng, W. E. Marshall, R. M. Rao, R. R. Bansode, and J. N. Losso, “Activated carbon from pecan shell: process description and economic analysis,” *Ind. Crops Prod.*, vol. 17, no. 3, pp. 209–217, May 2003, doi: 10.1016/S0926-6690(03)00002-5.

[219] J. Y. Lai and L. H. Ngu, “The production cost analysis of oil palm waste activated carbon: a pilot-scale evaluation,” *Greenh. Gases Sci. Technol.*, vol. 10, no. 5, pp. 999–1026, Oct. 2020, doi: 10.1002/ghg.2020.

[220] M. Nowrouzi, H. Younesi, and N. Bahramifar, “High efficient carbon dioxide capture onto as-synthesized activated carbon by chemical activation of Persian Ironwood biomass and the economic pre-feasibility study for scale-up,” *J. Clean. Prod.*, vol. 168, pp. 499–509, Dec. 2017, doi: 10.1016/j.jclepro.2017.09.080.

[221] I. M. Lima, A. McAloon, and A. A. Boateng, “Activated carbon from broiler litter: Process description and cost of production,” *Biomass Bioenergy*, vol. 32, no. 6, pp. 568–572, Jun. 2008, doi: 10.1016/j.biombioe.2007.11.008.

Acknowledgement

I would like to express my deepest gratitude to Dr. Mónika Meiczinger and Dr. Viola Somogyi for their invaluable guidance, patience, and encouragement throughout my PhD journey. I am sincerely thankful for their dedication and support, which have greatly contributed to both my academic and personal growth. I am truly honored to have had them as my supervisors.

I wish to express my sincere gratitude to Prof. Dr. Csilla Stenger-Kovács, Dr. Miklós Jakab, Dr. Adrienn Boros, Dr. Raed A. Al-Juboori, Dr. Norbert Miskolczi, and Ruqayah Ali Grmasha for their invaluable assistance during my PhD journey. Their support was crucial in enhancing my research and enriching my comprehension of the topic. I am deeply thankful for the time and commitment they have devoted to my work. This achievement would not have been feasible without their input, and I am honored to have had their support throughout this endeavor.